

NACA

RESEARCH MEMORANDUM

CLASSIFICATION CHANGED
UNCLASSIFIED

Declassified by authority of NASA
Classification Change Notices No. 187
Dated ** 11-30-69

TO NASA TR #69-326
By Authority of Sept 25, 1969

AN INVESTIGATION OF EJECTION RELEASES OF SUBMERGED AND
SEMISUBMERGED DYNAMICALLY SCALED STORES FROM A
SIMULATED BOMB BAY OF A FIGHTER-BOMBER

AIRPLANE AT SUPERSONIC SPEEDS

By John B. Lee and Howard S. Carter

Langley Aeronautical Laboratory
Langley Field, Va.

CLASSIFIED DOCUMENT

This material contains information affecting the National Defense of the United States within the meaning of the espionage laws, Title 18, U.S.C., Secs. 793 and 794, the transmission or revelation of which in any manner to an unauthorized person is prohibited by law.

**NATIONAL ADVISORY COMMITTEE
FOR AERONAUTICS**

WASHINGTON

December 26, 1956

CONFIDENTIAL

N70-72633

(ACCESSION NUMBER)

78

(PAGES)

(NASA CR OR TNX OR AD NUMBER)

(THRU)

NONE

(CODE)

(CATEGORY)

NATIONAL ADVISORY COMMITTEE FOR AERONAUTICS

RESEARCH MEMORANDUM

AN INVESTIGATION OF EJECTION RELEASES OF SUBMERGED AND

SEMISUBMERGED DYNAMICALLY SCALED STORES FROM A

SIMULATED BOMB BAY OF A FIGHTER-BOMBER


AIRPLANE AT SUPERSONIC SPEEDS

By John B. Lee and Howard S. Carter

SUMMARY

An investigation has been conducted in the 27- by 27-inch preflight jet of the Langley Pilotless Aircraft Research Station at Wallops Island, Va. on the release characteristics of several dynamically scaled store shapes from a simulated bomb bay at Mach numbers of 1.39, 1.60, and 1.98. A model of a typical fighter-bomber airplane with high sweptback wings was used. It had a box-type bomb bay for internally carried or submerged stores and a cavity for a semisubmerged store. A streamline store, a blunt-nose store with wedge-type fins of low aspect ratio, and a bluff store with a skirt were tested. The altitudes simulated were 3,400 feet at a Mach number of 1.39, 16,400 feet at a Mach number of 1.60, and 29,000 feet at a Mach number of 1.98.

The results of this investigation indicate that interference effects of the fuselage and bomb bay on the store release may be adverse, but satisfactory releases may be made at supersonic speeds at low altitudes. An increase in altitude (or a decrease in dynamic pressure) is beneficial, however, to the release characteristics of the store. The store pitch oscillations depend on the relationship of the disturbances of the flow field to the natural free-pitching period of the store as it moves along its drop path. Store ejection velocity, store stability, and moment of inertia are three variables that may be used to control the motion of the store, to oppose the disturbances in the flow field, and to produce low-amplitude disturbances. Tests should be made of actual scale models including the bomb-bay configuration and ejection equipment to obtain the most favorable ejection velocity and trajectory for a specific airplane and store configuration.



INTRODUCTION

The problem of obtaining successful store releases at supersonic speeds is of primary concern. The nonuniform flow field surrounding the airplane and in the bomb bay can cause store release motions that endanger the airplane. In addition, it is desired that the oscillations of the store be minimized for accurate trajectories and to obtain low aerodynamic loadings on the store. Ejection tests of two stores, similar in length, weight, moment of inertia, and static stability but different in frontal area and fineness ratio, are shown in reference 1. A large difference is shown in their release characteristics and trajectories. The results of store release drop tests in reference 2 also show that serious troubles may be encountered. The foregoing tests were of an exploratory nature and were made to determine the interference effects that might be involved and to ascertain, in some cases, the modifications that may be used.

A definite interest has been shown in a wide variety of stores and store shapes that may be carried in the same airplane with little or no change in the airplane. It is generally advantageous to carry as small a store as possible, but the type of mission may dictate the type of store to be used. Three stores that would cover a wide variety of store shapes were chosen. The store models were dynamically scaled from specific stores, but the results of the tests may be scaled to any size.

Tests were conducted by using a model of a typical fighter-bomber airplane with high sweptback wings in the 27- by 27-inch preflight jet of the Langley Pilotless Aircraft Research Station at Wallops Island, Va. (ref. 3). The dynamically scaled stores simulated altitudes of 3,400, 16,400, and 29,000 feet at Mach numbers of 1.39, 1.60, and 1.98, respectively, and at Reynolds numbers per foot from 10×10^6 to 14×10^6 . These altitudes and Mach numbers were chosen as typical for fighter-bomber performance.

SYMBOLS

$b/2$	fin half span, in.
d	store diameter, in.
h_p	simulated altitude, ft
\bar{c}	mean aerodynamic chord, in.

i_0	preset store incidence angle at start of ejection, deg
I_y	moment of inertia of store in pitch plane, lb-in. ²
l	store length, in.
L	characteristic length
m	mass, lb
M_0	free-stream Mach number
N	number of cycles
P	pitching period
p	static pressure, lb/sq ft
r	body radius, in.
k_1	ratio of flare length to store diameter
R	gas constant
S	store frontal area, sq in.
t	time, milliseconds
v	velocity, ft/sec
W	store weight, lb
x	body length from nose, in.
$\frac{x}{d}$	horizontal distance in terms of store diameter
$\frac{z}{d}$	vertical distance in terms of store diameter
\dot{z}_0	store ejection velocity, ft/sec
ρ	air density, slugs/cu ft
D	store density, lb/cu in.

α_F	airplane fuselage angle of attack with tunnel free-stream direction, deg
θ_s	store pitch angle in reference to free-stream direction, positive for nose up, deg
Δt	time interval of Strobolight pictures, milliseconds
ΔV	velocity change, ft/sec
C_D	drag coefficient
C_m	pitching-moment coefficient
C_L	lift coefficient
$C_{m_\alpha} = \frac{dC_m}{d\alpha}$	
$C_{m_{\dot{\alpha}}} = \frac{dC_m}{\frac{d\alpha}{dt} \frac{\bar{c}}{2V}}$	
$C_{m_q} = \frac{dC_m}{\frac{d\theta}{dt} \frac{\bar{c}}{2V}}$	

Subscripts:

m	model
p	prototype
b	base diameter

MODELS AND APPARATUS

Stores

Ordinates of all stores tested are given in table I, and drawings of the stores are shown in figure 1. Figure 2 shows photographs of the models.

Store A was a streamline store with a fineness ratio of 8.6. Three modifications of the standard fin were made: (1) by decreasing the fin span, (2) by increasing the fin span, and (3) by increasing the fin chord (fig. 3).

Store B was a blunt-nose store with a fineness ratio of 4.66. The fins were of low aspect ratio and had a wedge plan form (fig. 3(b)).

Bluff store C was tested with fineness ratios of 3.75 and 4.40, with skirt lengths of $\frac{1}{2}d$ and $\frac{3}{4}d$, respectively, and with a skirt base diameter of $1.2d$ (fig. 1(c)). Modifications of the bluff store were made by the use of a spike or a plate on the nose of the store.

In order to scale the weights and inertias properly to simulate the different altitudes, the store bodies were made of various materials including balsa, mahogany, plastic, magnesium, aluminum, brass, and steel. In order to obtain the proper inertia and center-of-gravity location, the cores were made of lead, brass, steel, or tungsten. The fins of stores A and B were made of magnesium. The method of simulation used is described in the appendix.

Airplane and Bomb Bay

A model of a typical fighter-bomber airplane with a circular cross section and a streamlined nose (fig. 4) was used for this investigation and for that of reference 3. The high wing was swept back 45° along the quarter-chord line. A box-type bomb bay was used for the tests. Photographs of the model with store A are shown in figure 5. The store was carried in the bomb bay with its fins at 45° to the horizontal. For the semisubmerged stores, most of the bomb bay was filled with a high-strength quick-setting plastic except for a cavity the shape of the upper half of the store. The cavity was formed by placing the store in the plastic before it hardened. The fins were placed 90° to the horizontal for the semisubmerged tests (fig. 5(c)). The airplane model was attached by two struts to an extension of the top plate of the nozzle.

Ejection Mechanism

Store ejection was accomplished through the use of a mechanism which was mounted on the tunnel end support directly above the bomb-bay center line. A photograph of an exploded view of the ejection mechanism with its sway braces is shown in figure 6. During the ejection stroke the rotational motion of the store was prevented by a sway brace which held the store firmly until the release point was reached. The ejection force

was applied through the center of gravity of the store. The ejection device operates as follows: A predetermined pressure is applied to the pressure cylinder in order to obtain the desired ejection velocity. The solenoid is actuated by an electrical impulse that pulls the rod assembly release pin. A model sway brace is pinned to the rod assembly. The model is held firmly against the sway braces by a small pin in the top of the store that is locked into the rod assembly by two ball bearings (fig. 6(b)). At the bottom of the ejection stroke, the rod assembly is unlocked by the store release latch; thus, the ball bearings are released from the store pin. The store is then free to move away from the sway brace which has stopped.

The sway braces were made interchangeable in order to give preset incidence angles of $i_0 = 0^\circ$ and $i_0 = -6^\circ$. Results showed, however, that the actual release incidence angle changed because of the high aerodynamic loads on the store as it was guided into the airstream. The actual store incidence angle at release may be obtained from the time-history plots. The point of store release was taken as zero time. The preset incidence angle was 0° unless otherwise noted.

The length of the ejection stroke was 1.76 inches for the submerged tests and 0.76 inch for the semisubmerged tests. The release point of the store was the same in all cases.

Photography

For the present series of tests, two methods were used to obtain Strobolight pictures. For the first method, a bank of 20 electronic flash lights that were fired in sequence by a 1000-cycle-per-second timer at 2-millisecond intervals were synchronized with the shutter of an 8 by 10 camera. The camera was set at one-twentieth of a second and was synchronized with the electrical impulse that released the model by means of the solenoid. For the second method, a disk with slits cut in it was mounted in front of the camera. The desired number of revolutions per minute of the disk was set before the test was started. The camera shutter was synchronized with the electrical impulse that released the model by means of the solenoid and fired a no. 30 focal plane bulb. The voltage output of the motor required to obtain the desired number of revolutions per minute of the disk was previously calibrated and was recorded for each test. The time interval of the Strobolight pictures for each test is given in table II. The picture obtained is thus a Strobolight picture of a scaled time trajectory on one sheet of 8- by 10-inch film. The store pitch angle and trajectory were read directly from the Strobolight picture. The Strobolight system used in each test is given in table II.

Preflight Jet

All tests were made in the 27- by 27-inch preflight jet of the Langley Pilotless Aircraft Research Station at Wallops Island, Va. (ref. 4) in which the stagnation pressures and temperatures could be varied. The test setup is shown in figure 7. The Mach number of the test was changed by the use of interchangeable nozzle blocks. The store was held inside the bomb bay until the tunnel pressure was adjusted to give sea-level static pressure.

DYNAMIC SIMILARITY

For dynamic testing, exact simulation of prototype conditions is desirable, but this is not always possible. The usual procedure is to match the similarity parameters that have the greatest influence on test data. Corrections may then be attempted to account for the effect of those parameters which are not duplicated or, if it can be shown that the probable differences are small, they may be neglected.

The Mach numbers for the model tests were the same as for the airplane. Dynamic scaling was obtained: (1) by maintaining the ratio of store density to dynamic pressure the same for the model as for the prototype store, and (2) by maintaining the mass distribution of the store model the same as that in the store prototype. This scaling results in the following equations:

$$\left(\frac{\rho l^3}{m}\right)_m = \left(\frac{\rho l^3}{m}\right)_p \quad (1)$$

$$\left(\frac{\rho l^5}{I_y}\right)_m = \left(\frac{\rho l^5}{I_y}\right)_p \quad (2)$$

The basis for this similarity is given in the appendix and in references 1 and 5.

Since the acceleration due to gravity cannot be altered, the vertical acceleration due to gravity for the model tests is too small for dynamic similarity by the scale factor. The effect when gravity is not properly simulated has been shown in reference 1. These tests were made with an ejection velocity of from 10 to 34 feet per second, and the effect of gravity on the vertical motion of the model becomes smaller

~~CONFIDENTIAL~~

as this velocity is increased. A 17-percent error in model position at $\dot{z}_0 = 15$ feet per second and approximately 8.5 percent error at $\dot{z}_0 = 30$ feet per second is shown in reference 1.

Except as affected by the vertical-position error as noted, all aerodynamic forces and moments, the resulting pitching angles, the vertical and horizontal displacements due to aerodynamic forces, and all damping effects are faithfully represented.

RESULTS AND DISCUSSION

Table II gives the pertinent conditions of each test. Figures 8 to 16 are Strobolight pictures of tests of the streamline store A with $\frac{l}{d} = 8.6$, blunt-nose store B with $\frac{l}{d} = 4.66$, and bluff store C with $\frac{l}{d} = 3.75$ and $\frac{l}{d} = 4.40$. In order to obtain a closer comparison of the release characteristics, the store pitch-angle time history and trajectory are shown in figures 17 to 36. Zero time is the release point of the store, and $i_0 = 0^\circ$ unless otherwise noted. The plots of some tests were repeated where it was deemed necessary for comparison.

Streamline Store A

Effect of fin geometry.— A comparison of the fin changes in figure 17 at $M_0 = 1.39$ and $\alpha_F = 0^\circ$ indicates a small difference in the pitch oscillations and trajectories of the stores for the standard fin and for fins having an increase in span or an increase in chord. The standard fin gave the smallest pitch oscillations, whereas increasing the span gave the shortest pitch period; however, a decrease in fin span (that is, a smaller fin area) caused the store to have higher amplitude pitch oscillations and a longer pitch period. These conditions, in turn, caused a change in the store trajectory because of the increased lift and drag.

At a fuselage angle of attack of 4° (fig. 18), a favorable trajectory was obtained with the standard fin. By decreasing the fin span, a similar trajectory was obtained for the first 20 milliseconds, but then the store began to diverge from the standard fin model (fig. 8(g), test 6). When the store with a decreased fin span was ejected at a negative incidence angle (test 7), it pitched back to a positive pitch angle of 10° .

Tests of fin changes at $M_0 = 1.98$, $h_p = 29,000$ feet, and $\alpha_f = 4^\circ$ (fig. 19) also showed little changes in the store oscillations and trajectories for the standard fins, increased span, or increased chord. The store with decreased span again showed higher pitch amplitude oscillations and a longer pitch period. For all cases tested, it appears, in general, that the fins having the greater exposed area (or perhaps, more accurately, the greater stability) produce a reduced pitch amplitude and a shorter period. However, it is likely that the relationship of the natural frequency of isolated store to the pattern of the disturbances as the store follows its path is an important consideration and that different results may be obtained under other conditions.

When the store was ejected at a negative incidence angle (fig. 20), it immediately pitched nose up and followed essentially the same pitch oscillations and trajectories as the store ejected at $i_0 = 0^\circ$ (fig. 19). In all cases the store had a nose-up pitching tendency at release at both Mach numbers and altitudes.

Effect of inertia.— Tests were made of the store with standard fins to study the effect of inertia on the pitch oscillations of the store. At $M_0 = 1.39$ and $\alpha_f = 0^\circ$ (fig. 21) as the inertia of the store was increased, the pitch amplitudes increased. Since the store had a nose-up pitching moment at release and was at a positive pitch angle, the inertia increase caused an increase in the pitch amplitude of the store, whereas, at $\alpha_f = 4^\circ$ (fig. 22), the store was released near an angle of 0° with the bomb bay and fuselage, and the store pitch amplitudes did not increase. The higher inertia subsequently resisted disturbances to a greater degree, probably because the moments due to the additional angle of attack opposed the influence of the airplane flow field. It thus appears that the inertia of the store may be used advantageously if the proper release conditions are chosen.

Simulation check.— In order to check the method of simulation, a store was made 6.2 times as heavy as a standard model. In order to simulate the same altitude, the ejection velocity was made equal to the square root of the ratio of static pressure to model density.

($\Delta V \approx \sqrt{\frac{P}{D}}$. See appendix.) The pitch-amplitude time curve was converted to the standard store time curve ($t \approx \frac{D}{P} L$). The corresponding trajectories showed excellent agreement (fig. 23).

Semisubmerged position.— Because of the present-day interest in the carriage of stores in a cavity or semisubmerged position, tests of the release characteristics of stores from such a position were made with store A. As noted previously, the stroke length was shortened for

the semisubmerged ejections, but the release point of the store was the same for both the submerged and semisubmerged ejections. A lower ejection velocity of from 20 to 24 feet per second was used for the ejections from the cavity, and it is very probable that this would be the case for the full-scale airplane for a shorter ejection stroke.

In figure 24, the effect of the store ejection velocity and the store trajectory can be seen. For tests at $\alpha_f = 0^\circ$, small changes in ejection velocity show significant changes in the store trajectory. The store had a nose-down tendency at release, and the pitch oscillations were essentially the same for the first 10 milliseconds after release. As the store trajectory changed, the pitch oscillations began to change. It appeared that the pitch oscillations of the store were affected by the relative position of the store to the bomb bay. A more complete study would possibly show the most ideal ejection velocity needed in order to obtain the minimum pitch amplitudes. A favorable pitch trajectory was also obtained at $\alpha_f = 4^\circ$.

At an increased Mach number and altitude, $M_o = 1.98$ and $h_p = 29,000$ feet (fig. 25), the store had a nose-up tendency at release for both $\alpha_f = 0^\circ$ and $\alpha_f = 4^\circ$.

A comparison of ejections at $M_o = 1.39$, $h_p = 3,400$ feet (fig. 26) from submerged and semisubmerged positions shows opposite pitching motions at release. Smaller pitch oscillations were obtained from the submerged ejections. At $M_o = 1.98$, $h_p = 29,000$ feet, and $\alpha_f = 4^\circ$ (fig. 27), ejections from both types of bomb bays show a nose-up tendency at release, and the most favorable release conditions were made from a submerged position. Figure 27 also shows the excellent repeatability of an identical ejection (tests 16 and 24).

It appears from these tests that the disturbances encountered by the store as it traverses the flow field under the mother ship may be either in or out of phase with the natural aerodynamic period of the store. Thus it appears advisable to make tests of an actual scale model, including the bomb-bay configuration and ejection equipment, to obtain the most favorable ejection velocity and trajectory for a specific airplane.

Blunt-Nose Store B

$M_o = 1.39$, $h_p = 3,400$ feet. Ejection tests of the blunt-nose store B at $M_o = 1.39$, $h_p = 3,400$ feet, $\alpha_f = 0^\circ$, and $\alpha_f = 4^\circ$ (fig. 28) show a shift in their pitch-time curve of only approximately 4°

for the major portion of their trajectories. The store pitched nose up soon after release at a negative incidence angle and at $\alpha_f = 4^\circ$ and followed similar pitch oscillations of the ejection at $\alpha_f = 4^\circ$ and $i_0 = 0^\circ$.

$M_0 = 1.60$, $h_p = 16,400$ feet.- There appears to be no correlation in the store pitching motion with a change in fuselage angle of attack (fig. 29) at $M_0 = 1.60$ and $h_p = 16,400$ feet except for the first portion of the trajectory of the store. No improvement is shown by ejecting the store at a negative incidence angle.

$M_0 = 1.98$, $h_p = 29,000$ feet.- Figure 30 shows that only inconsequential pitching motions were obtained in the tests made at $M_0 = 1.98$ and $h_p = 29,000$ feet for both fuselage angles of attack. A comparison of trajectories (fig. 31) shows that more favorable release conditions were obtained with store B at high altitude and Mach number. In all cases, successful release characteristics with store B were obtained for all Mach numbers, altitudes, and angles of attack of the fuselage. Ejections at a negative incidence angle did not appear to improve the release characteristics, but the releases were still considered good.

Bluff Store C

Effect of ejection velocity \dot{z}_0 .- Bluff store C with $\frac{l}{d} = 3.75$ and with a $\frac{1}{2} d$ flare was ejected over a range of ejection velocities of 10, 21, and 34 feet per second (fig. 32). Test 38 for $\dot{z}_0 = 21$ feet per second showed a large change in the store pitching motion from tests 37 and 39 with ejections at 34 and 10 feet per second, respectively. The store pitch oscillations thus appeared to be a function of both the store trajectory and ejection velocity through a nonuniform flow field rather than of the ejection velocity alone. A more extensive test program would probably show the most desirable ejection velocity to use in order to obtain the most satisfactory pitch trajectory.

High negative pitch angles of 21° to 25° were obtained in all cases. The pitch-time curve appeared to have been shifted with changes in ejection velocity. The store motions appeared to be damping.

There is also a large change in the store trajectory due to the ejection velocity. It should be noted, however, that the error in simulation is increased with the decrease in ejection velocity, as was stated previously. Repeatability of the bluff store C (tests 36 and 37) was

not as good as that obtained with store A (tests 16 and 24); however, at nine store diameters from the fuselage, the store trajectory had changed by only one-half a store diameter.

Effect of spike and plate.- Reference 6 showed that a large decrease in drag was caused by the application of a conical windshield on a round nose. Tests were made with a spike and a plate in order to study their effects on a bluff-type store nose. The use of a spike or plate (fig. 33) on the nose of the store with $\frac{l}{d} = 3.75$ decreased the drag of the store but increased the pitch amplitude of the store by 5° . The spike (test 40) appeared to have a destabilizing effect on the store, whereas the store with the plate remained stable.

A spike or a plate on the nose of a higher fineness-ratio store ($\frac{l}{d} = 4.40$, fig. 34) gave the same results as shown above, the spike having a destabilizing effect on the store. A decrease in ejection velocity to 26 feet per second (fig. 35) also showed similar results and a shift in the pitch-time curve and trajectory.

Effect of fineness ratio and flare length.- A change in fineness ratio and flare length from 3.75 and $\frac{1}{2}d$ to 4.40 and $\frac{3}{4}d$, respectively, (fig. 36) caused only a small change in the pitch-time curve, the maximum pitch amplitude -24° being the same in both cases. Their trajectories were similar.

CONCLUSIONS

As a result of the store ejection tests at Mach numbers of 1.39, 1.60, and 1.98, the following conclusions are indicated:

1. All stores tested were successfully released, in that all cleared the airplane and all showed only modest pitching motions, except the bluff stores which experienced pitching amplitudes as high as 25° .

2. It appears that the pitch oscillations of the store depend on the relationship of the disturbances of the flow field to the natural free-pitching period of the store as it moves along its drop path. Store ejection velocity, store stability, and moment of inertia are three variables that may be used to control these effects so that they oppose and produce a low-amplitude pitch oscillation.

3. An increase in altitude (or decrease in dynamic pressure) is beneficial to the release characteristics of the store.

4. Tests should be made of actual scale models, including the bomb-bay configuration and ejection equipment, to obtain the most favorable ejection velocity and trajectory for a specific airplane and store configuration.

5. The addition of either a plate or a spike to the nose of a bluff store decreased the store drag; however, the spike appeared to have a destabilizing effect on the store.

Langley Aeronautical Laboratory,
National Advisory Committee for Aeronautics,
Langley Field, Va., August 23, 1956.

APPENDIX A

SIMILARITY RELATIONSHIP

In order to discuss the effects of scale on the store motion properly, some simplified equations relating to the translational and rotary motion of the store are first derived. Only translational motion resulting from drag forces and rotary motion in pitch are determined; however, the other translational and rotary motions will follow the same relationships.

The analysis is made with the assumption that the aerodynamic coefficients do not vary with scale (no Reynolds number effect). In addition, the free-stream Mach number is the same for the model and the full-scale airplane. If these factors are held constant, the variables defining the model motion can be reduced to three which are store density D , dynamic pressure q , and characteristic length L . The characteristic length is an arbitrary length, such as store diameter, which will define the model scale in relation to the full-size store. Other variables can then be stated in terms of the fundamental variables as follows:

$$\bar{c} \propto L$$

$$K \propto L$$

$$S \propto L^2$$

$$p \propto \rho T \propto q$$

$$\rho = \frac{2q}{\gamma R T M_0^2} \propto \frac{q}{T}$$

$$m \propto D L^3$$

$$V \propto \sqrt{T}$$

$$I_y \propto D L^5$$

$$I' \propto \frac{D L^2}{p}$$

$$m' \propto \frac{D L \sqrt{T}}{p}$$

where

\bar{c} mean aerodynamic chord, in.

K radius of gyration, in.

S area, in.

T static temperature, deg

p static pressure, lb/sq ft

ρ air density, slugs/cu ft

m mass, lb

V velocity, ft/sec

I_y moment of inertia

$$I' = \frac{I_y}{Sq\bar{c}} \propto \frac{DL^5}{L^2qL} \propto \frac{DL^2}{q}$$

$$m' = \frac{mV}{sq} \propto \frac{DL^3\sqrt{T}}{L^2q}$$

The store motion parameters to be found are: the translational acceleration from aerodynamic drag forces a , the time t to be accelerated by aerodynamic force an incremental distance proportional to L , the change in velocity ΔV during time t , the pitching period P , the time to damp to one-half amplitude $T_{1/2}$.

The relationship existing between the store motion parameters and the fundamental variables is next derived.

$$a = \frac{C_D Sq}{m} \propto \frac{L^2 q}{DL^3} \propto \frac{q}{DL}$$

$$a \propto \frac{p}{DL} \quad (A1)$$

$$t^2 = \frac{2L}{a} \propto \frac{2L}{q/DL} \propto \frac{DL^2}{q}$$

$$t \propto \sqrt{\frac{D}{p}} L \quad (A2)$$

$$\Delta V = at \propto \frac{q}{DL} \sqrt{\frac{D}{q}} L \propto \sqrt{\frac{q}{D}}$$

$$\Delta V \propto \sqrt{\frac{p}{D}} \quad (A3)$$

$$P = \frac{2\pi}{\sqrt{\frac{-57.3C_{m\alpha}}{I'}}} \approx \sqrt{I'} \propto \sqrt{\frac{D}{q}} L$$

$$P \propto \sqrt{\frac{D}{p}} L \quad (A4)$$

$$\frac{1}{T_{1/2}} = \frac{57.3}{2(\ln 2)} \frac{1}{m'} \left[(C_{mq} + C_{m\alpha}) \frac{1}{2} \left(\frac{\bar{c}}{K} \right) - C_{L\alpha} \right]$$

$$\frac{1}{T_{1/2}} \propto \frac{1}{m'}$$

$$T_{1/2} \propto m' \propto \frac{DL\sqrt{T}}{q}$$

$$T_{1/2} \propto \frac{DL\sqrt{T}}{p} \quad (A5)$$

The relationships for P and $\frac{1}{T_{1/2}}$ were obtained from reference 7.

By making the ratio of static pressure to store density $\frac{p}{D}$ constant, the period and the time to accelerate under aerodynamic forces to a

characteristics distance L are proportional to the characteristic length L (eqs. (A2) and (A4)). If the tunnel temperature can be varied to obtain the simulated-altitude static temperature, the time to damp to one-half amplitude also becomes proportional to L (eq. (A5)). Thus, if the motion is considered in terms of the position of the store with respect to the mother ship in units of L , these motions will be the same regardless of scale size, provided that the flow pattern over the store is not appreciably changed because of Reynolds number. In addition, the amount the velocity has changed during the time the model moves an increment of L is independent of scale (eq. (A3)). The translational velocity therefore is always duplicated. The number of cycles N required to damp to one-half an amplitude will be the same for the model as for the prototype, that is,

$$N = \frac{T_{1/2}}{P}$$

or

$$\left(\frac{T_{1/2}}{P} \right)_m = \left(\frac{T_{1/2}}{P} \right)_p = \frac{L}{L}$$

Therefore,

$$N_m = N_p$$

It can be shown from this relationship that, when the ratio of store density to static pressure is held constant, the model moves a scaled distance in length of time proportional to the scale factor. Thus, the Strobolight pictures obtained from these tests are scale representations with the time between store positions that are equal to one-seventeenth of full scale.

In order for the vertical translational motion to be correct, the gravitational acceleration required for the model must vary in the same manner as the aerodynamic acceleration. From equation (A1) it can be seen that the aerodynamic acceleration is inversely proportional to L . Thus, the proper gravitational acceleration should vary inversely with model size; that is, it should become larger for the model. However, the error because gravity is not properly simulated becomes smaller as the initial ejection velocity is increased. This effect is discussed in reference 1. Ejection velocities from 10 feet per second to 34 feet per second were used for these tests.

With a constant ratio of the store static pressure to store density, the proper scaling parameters become

$$\left(\frac{p}{D}\right)_m = \left(\frac{p}{D}\right)_p$$

Since $m = DL^3$ or $D = \frac{m}{L^3}$,

$$\left(\frac{pL^3}{m}\right)_m = \left(\frac{pL^3}{m}\right)_p \quad (A6)$$

Since, $I_y = DL^5$ or $D = \frac{I_y}{L^5}$,

$$\left(\frac{pL^5}{I_y}\right)_m = \left(\frac{pL^5}{I_y}\right)_p \quad (A7)$$

REFERENCES

1. Faget, Maxime A., and Carlson, Harry W.: Experimental Techniques for Predicting Store Motions During Release or Ejection. NACA RM L55L20b, 1956.
2. Rainey, Robert W.: A Wind-Tunnel Investigation of Bomb Release at a Mach Number of 1.62. NACA RM L53L29, 1954.
3. Smith, Norman F., and Carlson, Harry W.: Measurements of Static Forces on Internally Carried Bombs of Three Fineness Ratios in Flow Field of a Swept-Wing Fighter-Bomber Configuration at a Mach Number of 1.61 With Illustrative Drop-Path Calculations. NACA RM L56118, 1956.
4. Faget, Maxime A., Watson, Raymond S., and Bartlett, Walter A., Jr.: Free-Jet Tests of a 6.5-Inch-Diameter Ram-Jet Engine at Mach Numbers of 1.81 and 2.00. NACA RM L50L06, 1951.
5. Murphy, Glenn: Similitude in Engineering. The Ronald Press Co., 1950.
6. Jones, Jim J.: Experimental Drag Coefficients of Round Noses With Conical Windshields at Mach Number 2.72. NACA RM L55E10, 1955.
7. Gillis, Clarence L., Peck, Robert F., and Vitale, A. James: Preliminary Results From a Free-Flight Investigation at Transonic and Supersonic Speeds of the Longitudinal Stability and Control Characteristics of an Airplane Configuration With a Thin Straight Wing of Aspect Ratio 3. NACA RM L9K25a, 1950.

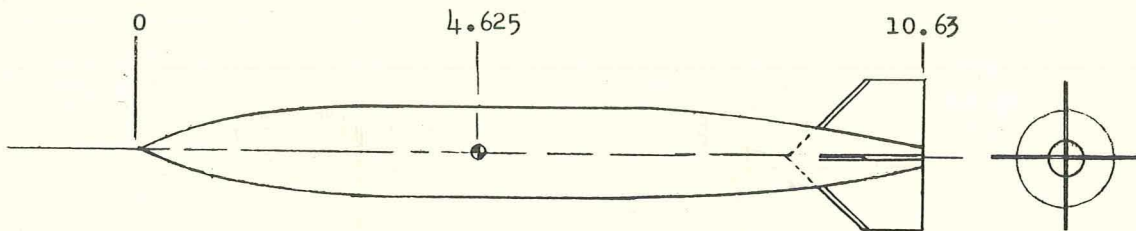
TABLE I.- STORE ORDINATES

Store A		Store B	
Fineness ratio, $l/d = 8.6$		Fineness ratio, $l/d = 4.66$	
x, in.	r, in.	x, in.	r, in.
0	0	0	0.375
.375	.194	.406	.605
.688	.291	.656	.615
1.000	.365	.969	.622
1.938	.505	1.281	.625
2.875	.586	2.781	.625
3.500	.620	3.094	.619
3.813	.625	3.406	.606
5.313	.625	3.718	.586
5.625	.623	4.031	.568
6.250	.602	4.344	.535
6.879	.565	4.656	.504
7.500	.511	4.969	.467
8.125	.445	5.281	.422
8.750	.370	5.594	.365
9.375	.288	5.828	.311
10.000	.205		
10.625	.123		
Nose radius, $1/16$ in.			

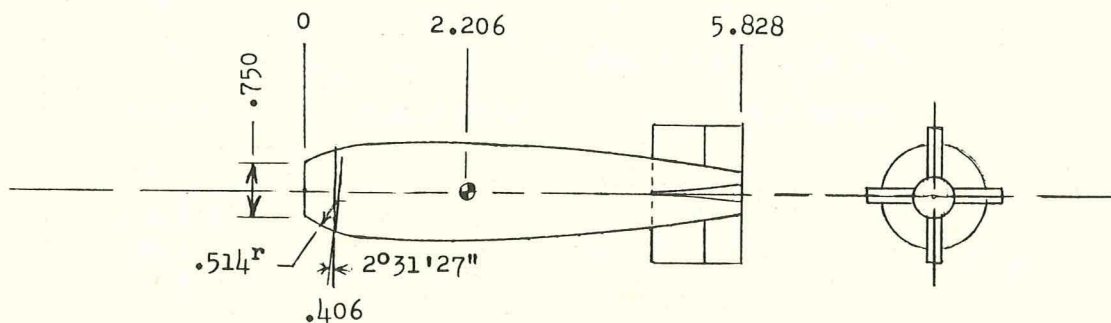
Store C					
l/d	d, in.	l, in.	$k_1 d$	d_b , in.	Center of gravity, percent
3.75	1.0	3.75	$\frac{1}{2} d$	1.20	38.0
4.40	1.0	4.40	$\frac{3}{4} d$	1.20	38.0

TABLE II.- TESTING CONDITIONS

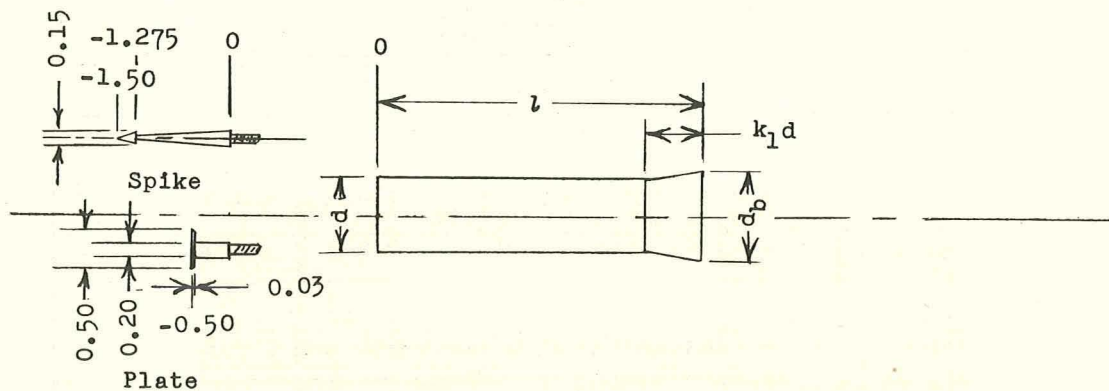
Test	Model	Figure	M ₀	hp, ft	Model conditions				Ejections				Δt, milliseconds	Strobolight system	Remarks
					W _m , lb	I _y , lb-in. ²	Center of gravity, % l	l/d	$\frac{\dot{z}_0}{\dot{r}}$, ft/sec	α _r , deg	α _o , deg	Bomb bay			
1	A, standard	8(a)	1.39	3,400	0.474	1.610	43.5	8.5	27.0	0	0	Submerged	2.0	20 Electronic flash lights	
2	A-1	8(b), 8(c)	1.39	3,400	.476	1.610	43.5	8.5	27.5	0	0	Submerged	2.0	20 Electronic flash lights	
3	A-2	8(d)	1.39	3,400	.476	1.610	43.5	8.5	27.0	0	0	Submerged	2.0	20 Electronic flash lights	
4	A-3	8(e)	1.39	3,400	.475	1.610	43.5	8.5	27.0	0	0	Submerged	2.0	20 Electronic flash lights	
5	A, standard	8(f)	1.39	3,400	.475	1.570	43.5	8.5	26.5	4	0	Submerged	2.0	20 Electronic flash lights	
6	A-1	8(g)	1.39	3,400	.476	1.610	43.5	8.5	26.5	4	0	Submerged	2.0	20 Electronic flash lights	
7	A-1	8(h)	1.39	3,400	.472	1.500	43.5	8.5	26.5	4	-6	Submerged	2.0	20 Electronic flash lights	
8	A, standard	8(i)	1.39	45,000	2.942	13.680	43.8	8.5	10.7	4	0	Submerged	3.8	20 Electronic flash lights	1.37I _y
9	A, standard	8(j)	1.39	3,400	.481	2.080	43.7	8.5	26.0	0	0	Submerged	2.0	20 Electronic flash lights	1.28I _y
10	A, standard	8(k)	1.39	3,400	.482	3.020	43.5	8.5	27.0	0	0	Submerged	2.0	20 Electronic flash lights	1.88I _y
11	A, standard	8(l)	1.39	3,400	.482	3.020	43.5	8.5	26.5	4	0	Submerged	2.0	20 Electronic flash lights	1.88I _y
12	A, standard	9(a), 9(b)	1.39	3,400	.474	1.550	43.8	8.5	23.0	4	0	Semisubmerged	2.0	20 Electronic flash lights	
13	A, standard	9(c)	1.39	3,400	.474	1.550	43.8	8.5	20.5	0	0	Semisubmerged	2.0	20 Electronic flash lights	
14	A, standard	9(d)	1.39	3,400	.474	1.550	43.8	8.5	23.0	0	0	Semisubmerged	2.0	20 Electronic flash lights	
15	A, standard	9(e)	1.39	3,400	.474	1.550	43.8	8.5	24.0	0	0	Semisubmerged	2.0	20 Electronic flash lights	
16	A, standard	10(a)	1.98	29,000	1.365	4.250	43.5	8.5	29.5	4	0	Submerged	2.0	20 Electronic flash lights	Condensation
17	A-1	10(b)	1.98	29,000	1.355	4.200	43.5	8.5	29.5	4	0	Submerged	2.0	20 Electronic flash lights	
18	A-2	10(c)	1.98	29,000	1.360	4.300	43.5	8.5	29.5	4	0	Submerged	2.0	20 Electronic flash lights	
19	A-3	10(d)	1.98	29,000	1.355	4.250	43.5	8.5	29.5	4	0	Submerged	2.0	20 Electronic flash lights	
20	A, standard	10(e)	1.98	29,000	1.350	4.200	43.5	8.5	32.5	4	-6	Submerged	2.0	20 Electronic flash lights	
21	A-1	10(f)	1.98	29,000	1.360	4.260	43.5	8.5	32.5	4	-6	Submerged	2.0	20 Electronic flash lights	
22	A-2	10(g)	1.98	29,000	1.355	4.200	43.5	8.5	32.5	4	-6	Submerged	2.0	20 Electronic flash lights	
23	A-3	10(h)	1.98	29,000	1.370	4.280	43.5	8.5	32.5	4	-6	Submerged	2.0	20 Electronic flash lights	
24	A, standard	10(i)	1.98	29,000	1.365	4.250	43.5	8.5	29.5	4	0	Submerged	2.0	20 Electronic flash lights	Repeat of test 16
25	A, standard	11(a)	1.98	29,000	1.365	4.250	43.5	8.5	24.0	4	0	Semisubmerged	2.0	20 Electronic flash lights	
26	A, standard	11(b)	1.98	29,000	1.350	4.200	43.5	8.5	24.0	0	0	Semisubmerged	2.0	20 Electronic flash lights	
27	B	12(a)	1.39	3,400	.467	1.100	37.9	4.7	32.0	0	0	Submerged	2.03	Spinning disk	
28	B	12(b)	1.39	3,400	.472	1.100	37.9	4.7	30.0	4	0	Submerged	2.0	Spinning disk	
29	B	12(c)	1.39	3,400	.474	1.100	37.9	4.7	32.0	4	-6	Submerged	1.99	Spinning disk	
30	B	13(a)	1.60	16,400	.769	1.726	37.9	4.7	29.5	0	0	Submerged	1.99	Spinning disk	
31	B	13(b)	1.60	16,400	.781	1.701	37.9	4.7	29.5	4	0	Submerged	2.0	Spinning disk	
32	B	13(c)	1.60	16,400	.772	1.584	37.9	4.7	29.5	4	-6	Submerged	2.0	Spinning disk	
33	B	14(a)	1.98	29,000	1.321	2.960	37.9	4.7	31.0	0	0	Submerged	2.03	Spinning disk	
34	B	14(b)	1.98	29,000	1.321	3.020	37.9	4.7	30.0	4	0	Submerged	2.08	Spinning disk	
35	B	14(c)	1.98	29,000	1.321	3.160	37.9	4.7	30.0	4	-6	Submerged	2.03	Spinning disk	
36	C	15(a)	1.39	3,400	.248	0.252	38.5	3.8	34.0	0	0	Submerged	1.97	Spinning disk	Flare $\frac{1}{2}$ d
37	C	15(b)	1.39	3,400	.241	0.259	38.0	3.8	34.0	0	0	Submerged	2.0	Spinning disk	Flare $\frac{1}{2}$ d
38	C	15(c)	1.39	3,400	.248	0.252	38.5	3.8	21.0	0	0	Submerged	2.0	Spinning disk	Flare $\frac{1}{2}$ d
39	C	15(d), 15(e)	1.39	3,400	.249	0.257	38.4	3.8	10.0	0	0	Submerged	2.0	Spinning disk	Flare $\frac{1}{2}$ d
40	C, spike	15(f)	1.39	3,400	.242	0.259	38.0	3.8	34.0	0	0	Submerged	2.01	Spinning disk	Flare $\frac{1}{2}$ d
41	C, plate	15(g)	1.39	3,400	.242	0.259	38.0	3.8	34.0	0	0	Submerged	1.99	Spinning disk	Flare $\frac{1}{2}$ d
42	C	16(a)	1.39	3,400	.266	0.402	38.0	4.4	34.0	0	0	Submerged	1.99	Spinning disk	Flare $\frac{3}{4}$ d
43	C, spike	16(b)	1.39	3,400	.265	0.402	38.0	4.4	33.0	0	0	Submerged	2.02	Spinning disk	Flare $\frac{3}{4}$ d
44	C, plate	16(c)	1.39	3,400	.265	0.412	38.0	4.4	35.0	0	0	Submerged	2.0	Spinning disk	Flare $\frac{3}{4}$ d
45	C	16(d)	1.39	3,400	.266	0.402	38.0	4.4	26.0	0	0	Submerged	1.99	Spinning disk	Flare $\frac{3}{4}$ d
46	C, spike	16(e)	1.39	3,400	.262	0.409	38.0	4.4	26.0	0	0	Submerged	1.97	Spinning disk	Flare $\frac{3}{4}$ d
47	c, plate	16(f)	1.39	3,400	.265	0.413	38.0	4.4	26.0	0	0	Submerged	2.0	Spinning disk	Flare $\frac{3}{4}$ d



(a) Streamline store A; $l/d = 8.6$.



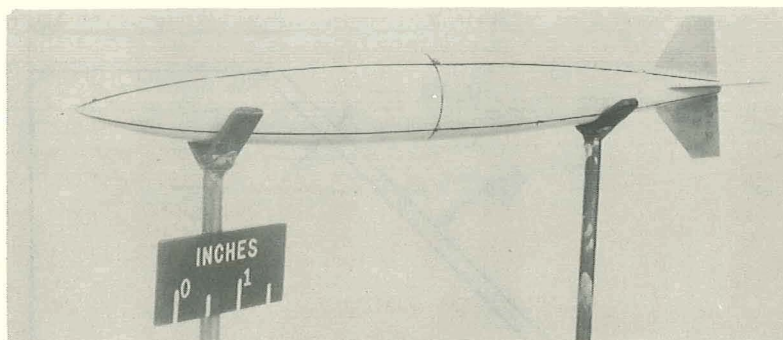
(b) Blunt nose store B; $l/d = 4.66$.



(c) Bluff store C.

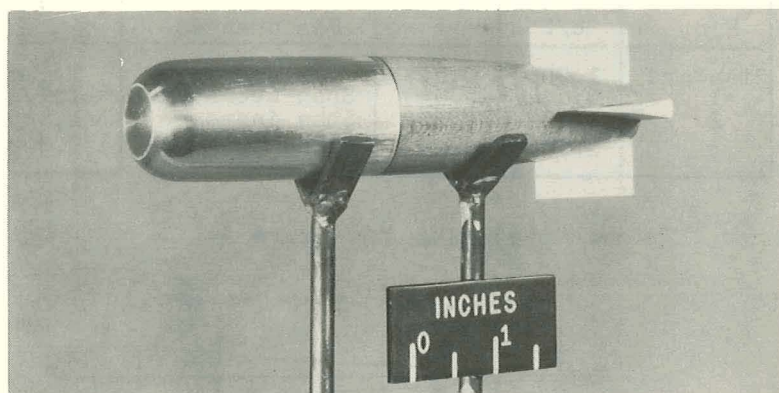
Figure 1.- Store model dimensions and designations. (All dimensions are in inches.)

CONFIDENTIAL



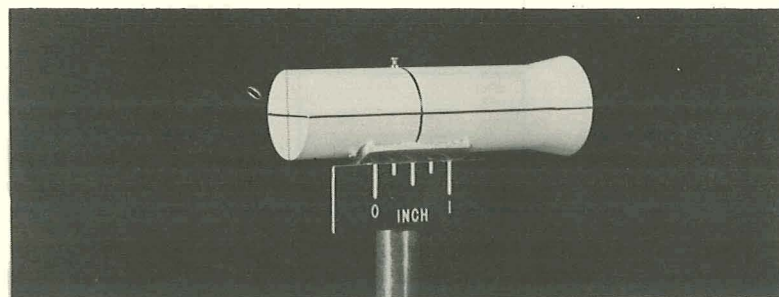
(a) Store A; $l/d = 8.6$.

L-90934



(b) Store B; $l/d = 4.66$.

L-93277

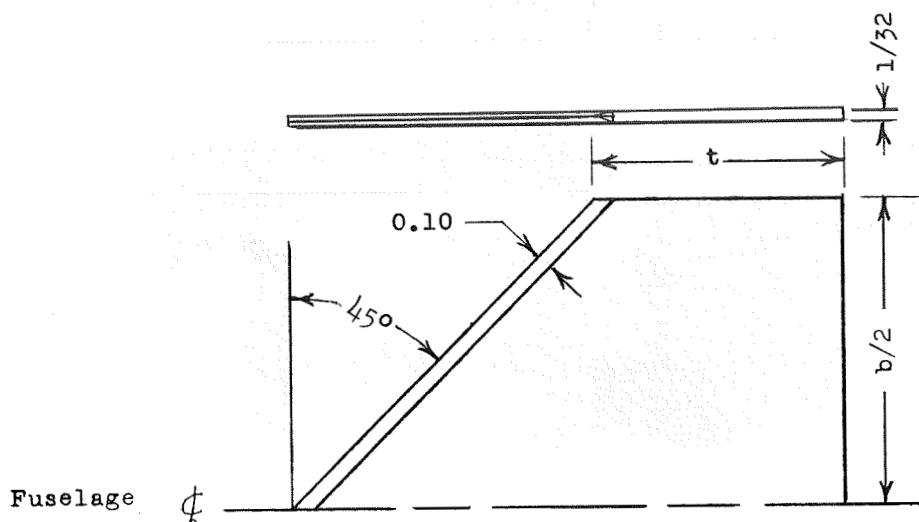


(c) Store C.

L-91599

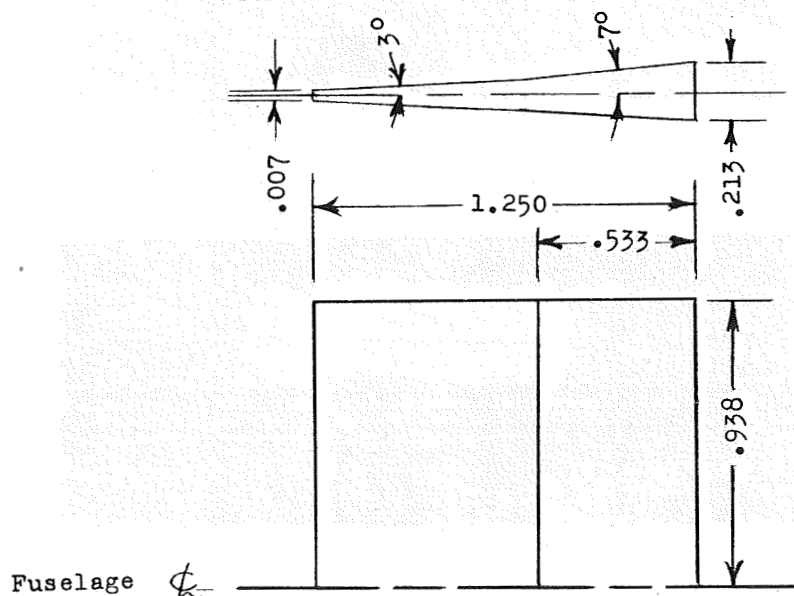
Figure 2.- Store photographs.

CONFIDENTIAL



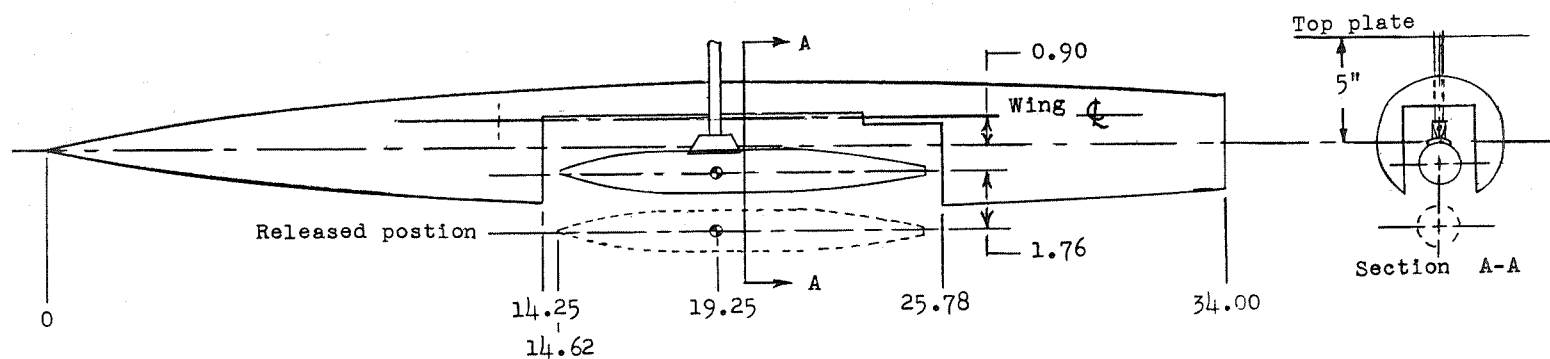
Fin dimensions and designations				
Fin	$b/2$	t	Fin changes	Fin area, Sq. in.
Standard	1.000	0.813		1.314
1	0.844	0.969	Span decrease	1.175
2	1.157	0.656	Span increase	1.429
3	1.000	0.969	Chord increase	1.392

(a) Fins for store A.



(b) Fins for store B.

Figure 3.- Dimensions and designations of store fins. (All dimensions are in inches.)



Fuselage station numbers

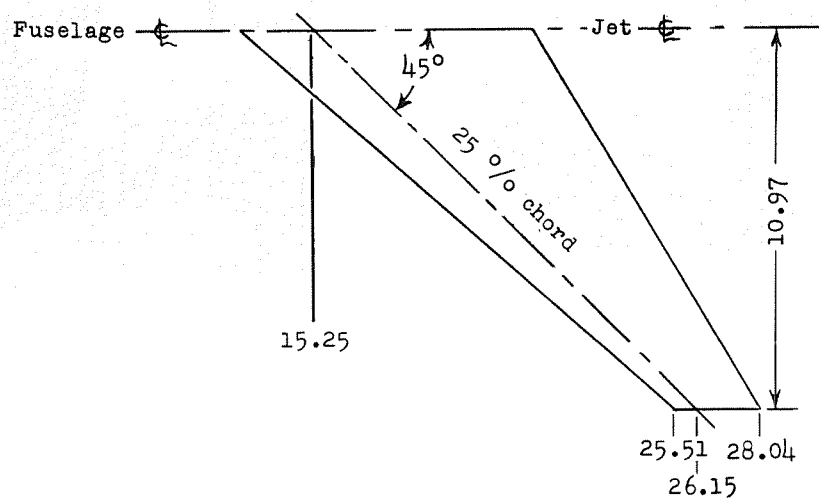
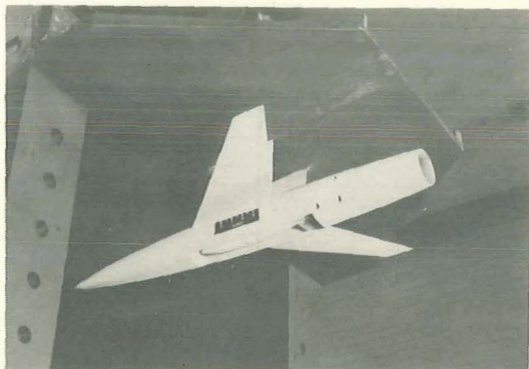


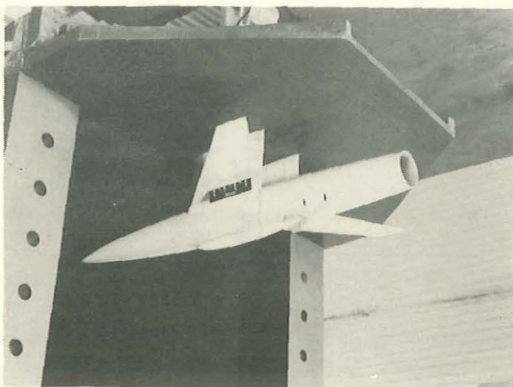
Figure 4.- Model layout. (All dimensions are in inches.)



(a) Store in bomb bay. L-91196

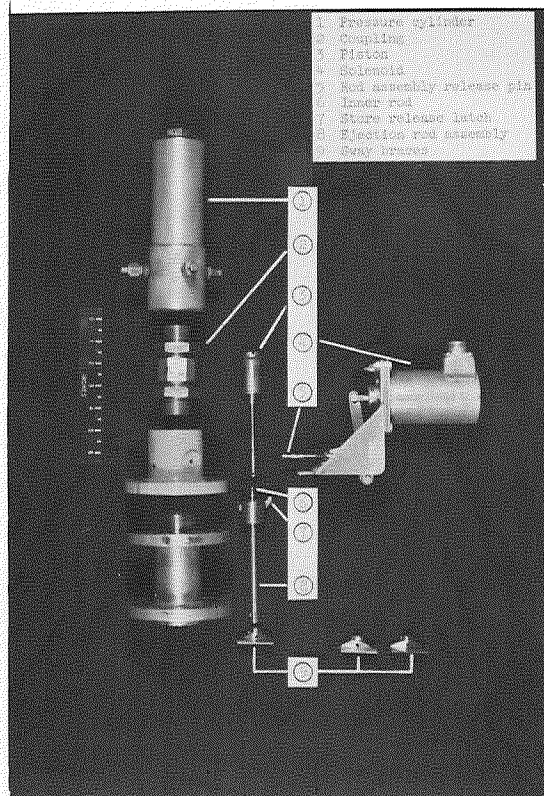


(b) Store extended to release point. L-91199

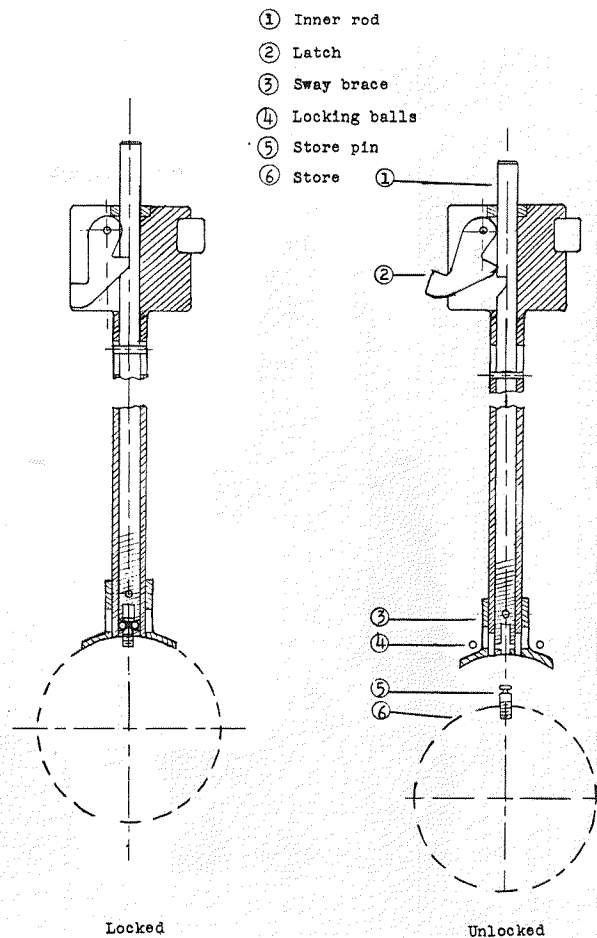


(c) Store in semisubmerged position. L-91203

Figure 5.- Model installation in the 27- by 27-inch preflight jet of the Langley Pilotless Aircraft Research Station at Wallops Island, Va.

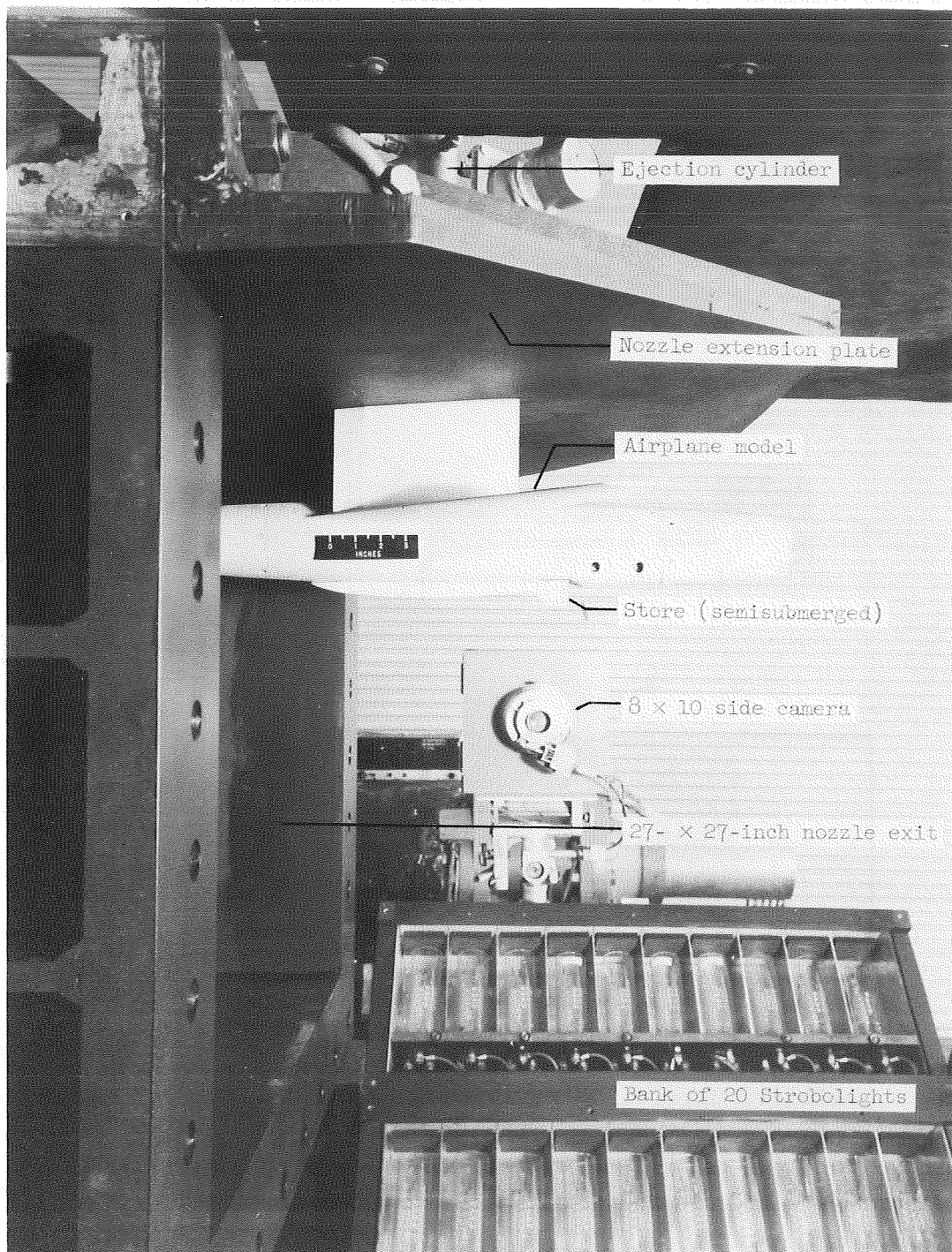


L-89034.1
(a) Exploded view of ejection cylinder
with sway braces.



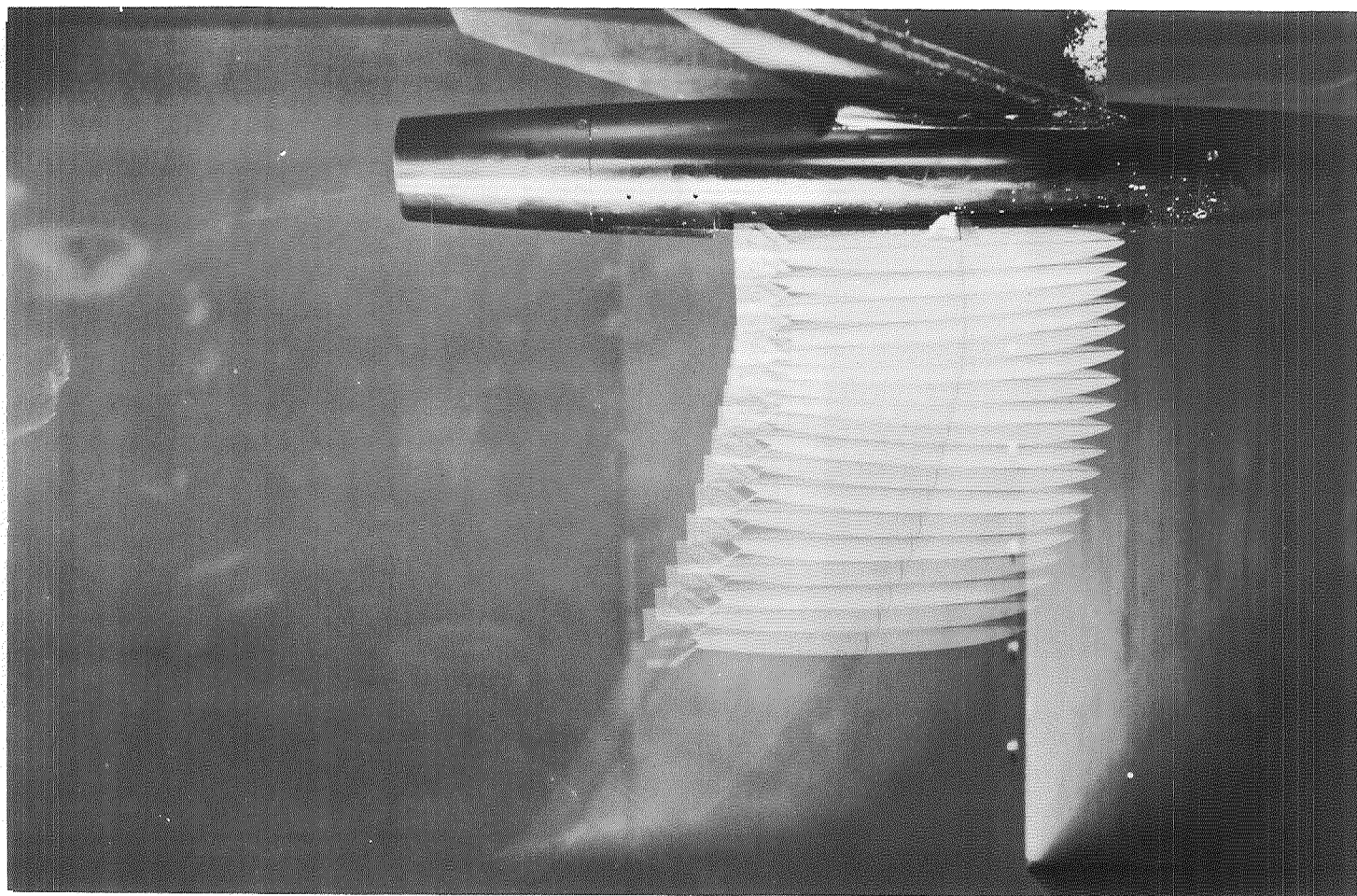
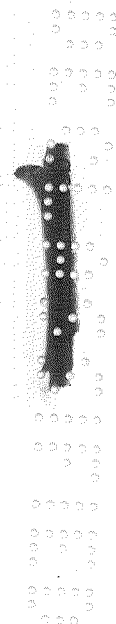
(b) Ejection rod assembly.

Figure 6.- Ejection mechanism.



L-91198.1

Figure 7.- Model and equipment installation in 27- by 27-inch preflight jet.

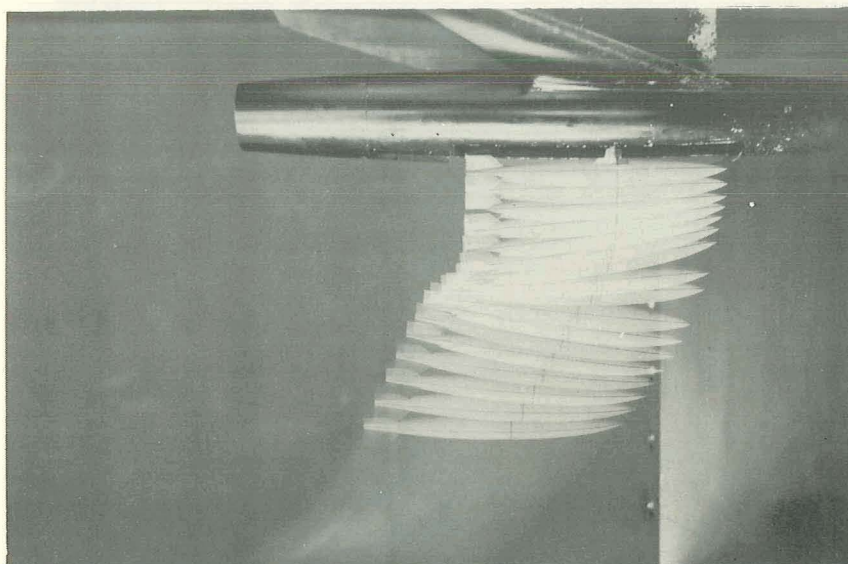


(a) Test 1; standard fin; $\alpha_f = 0^\circ$.

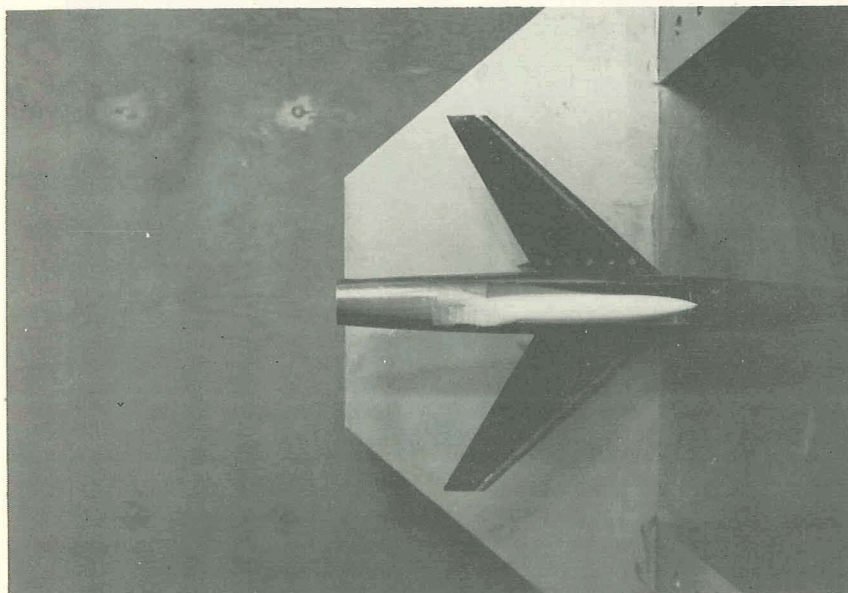
L-91133

Figure 8.- Ejection tests from a submerged position. Store A; $M_0 = 1.39$;
 $h_p = 3,400$ feet.

CONFIDENTIAL



(b) Test 2; fin 1; $\alpha_f = 0^\circ$. L-91127

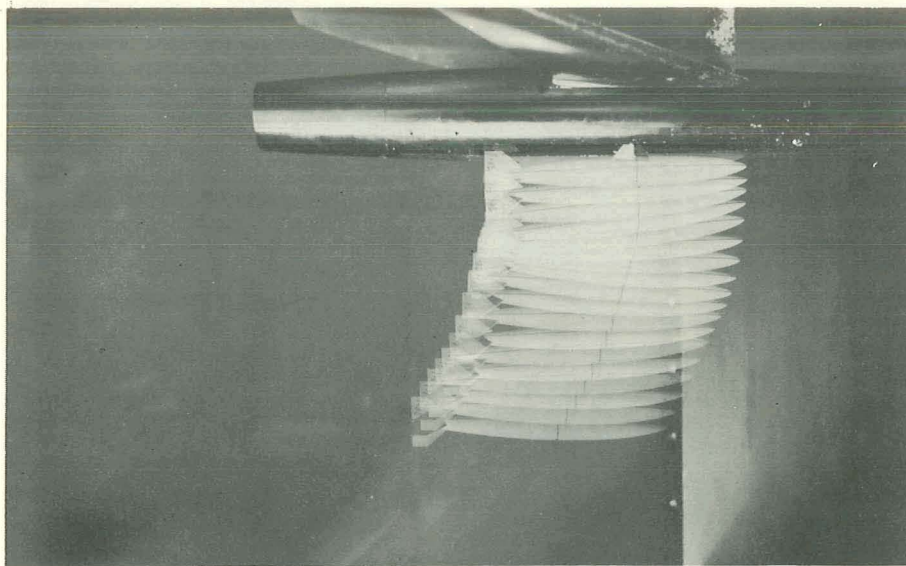


(c) Test 2; bottom view of model. L-91113

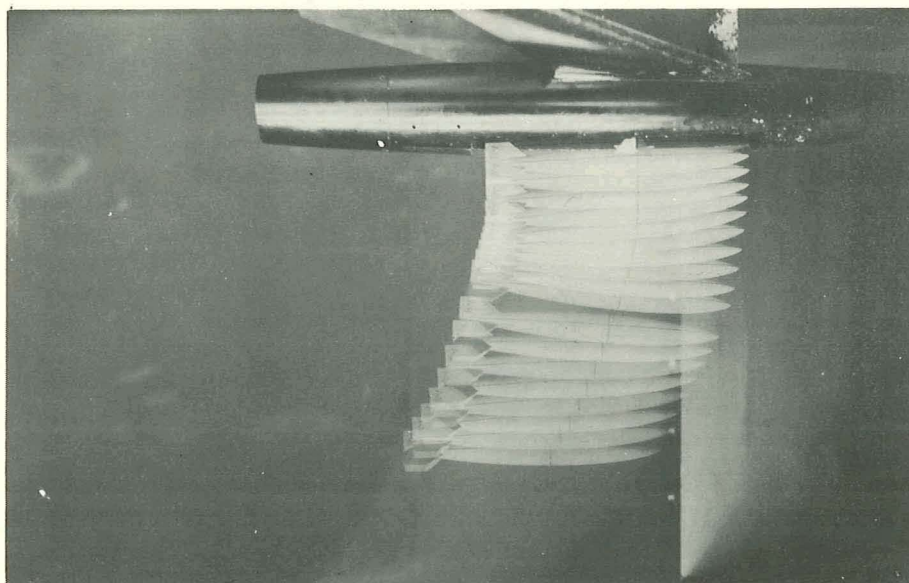
Figure 8.- Continued.

CONFIDENTIAL

CONFIDENTIAL



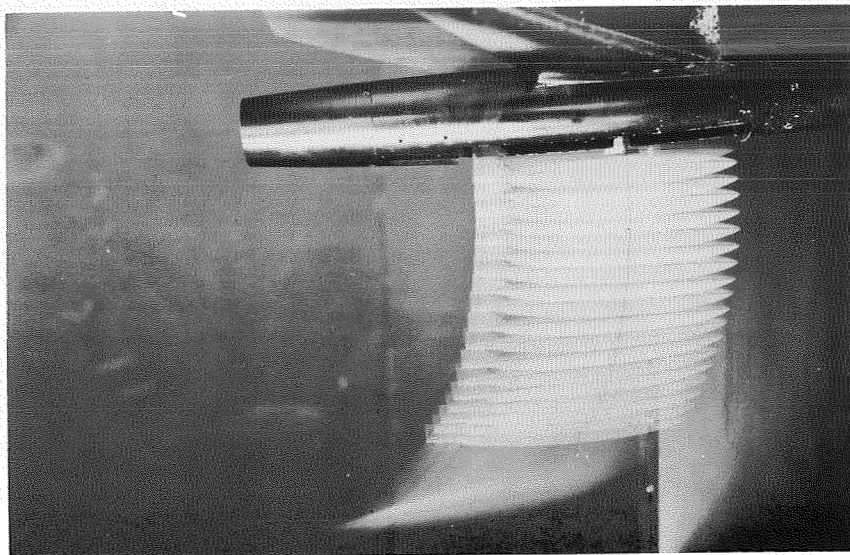
(d) Test 3; fin 2; $\alpha_F = 0^\circ$. L-91131



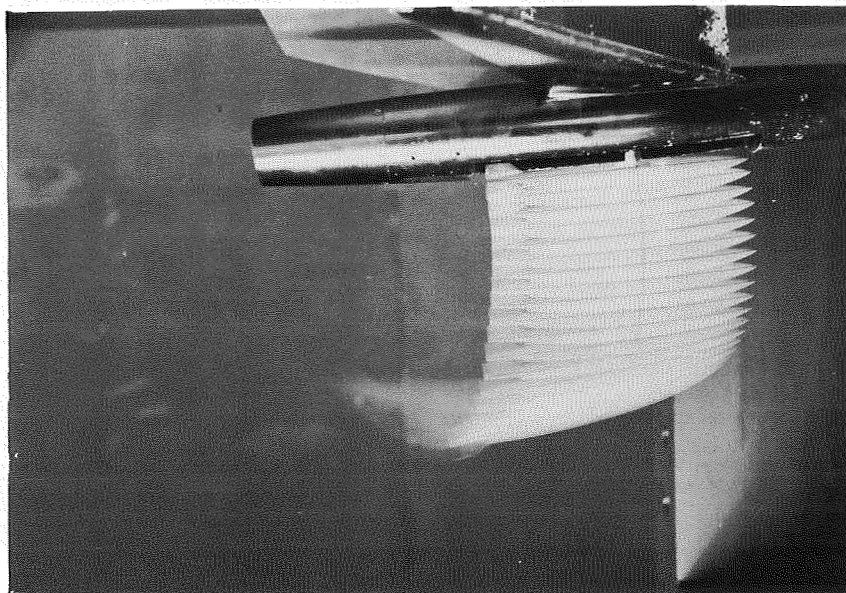
(e) Test 4; fin 3; $\alpha_F = 0^\circ$. L-91130

Figure 8.- Continued.

CONFIDENTIAL



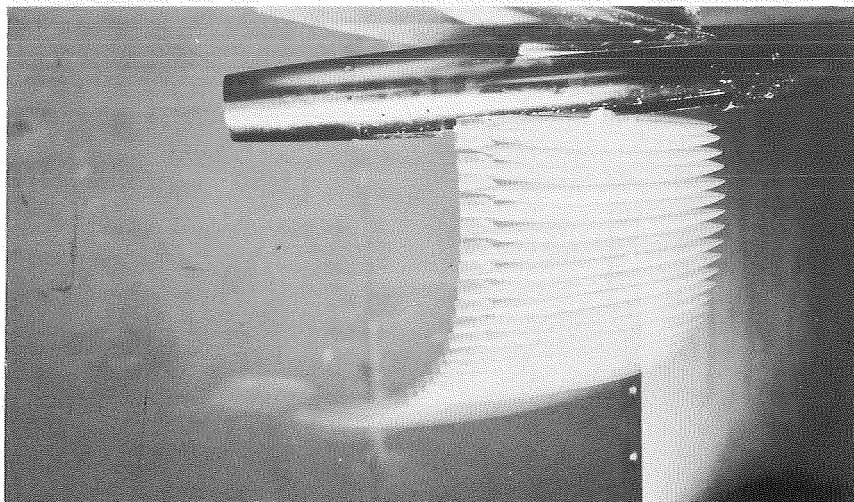
(f) Test 5; standard fin; $\alpha_F = 4^\circ$. L-91126



(g) Test 6; fin 1; $\alpha_F = 4^\circ$.

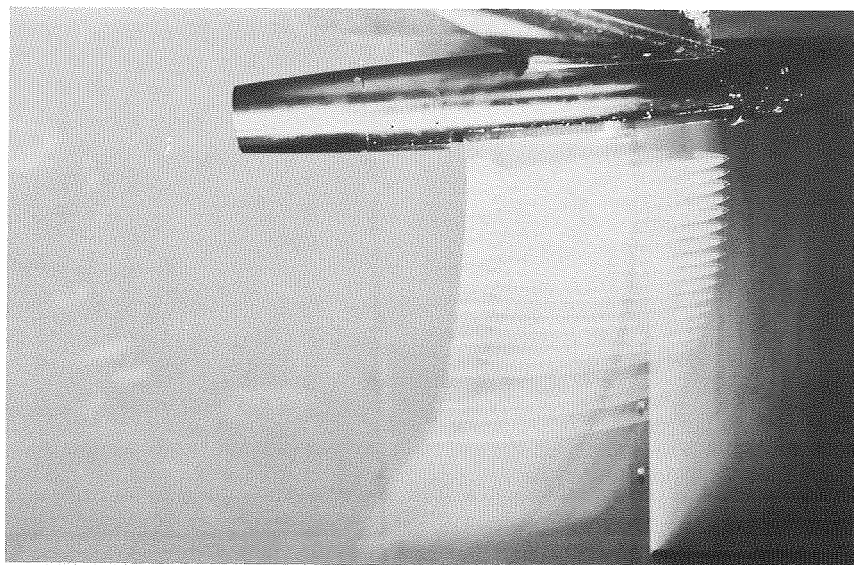
L-91125

Figure 8.- Continued.



(h) Test 7; fin 1; $\alpha_f = 4^\circ$; $i_o = -6^\circ$.

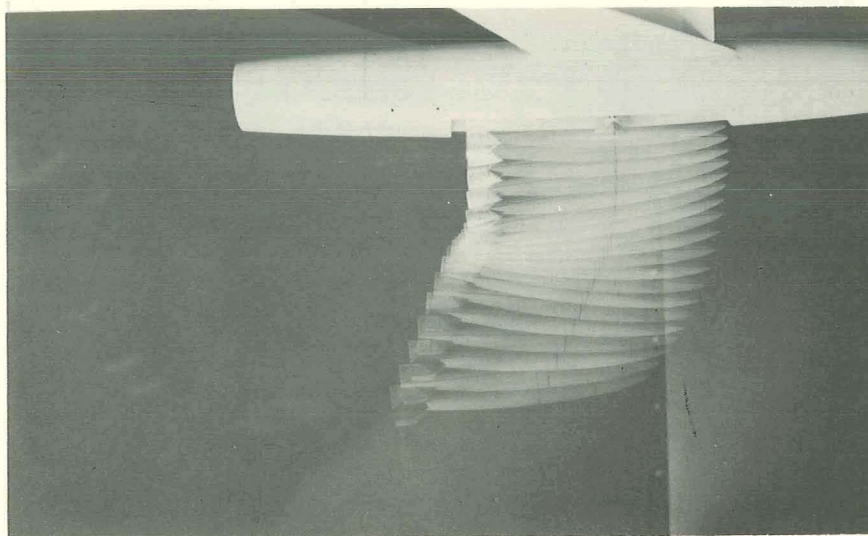
L-91282



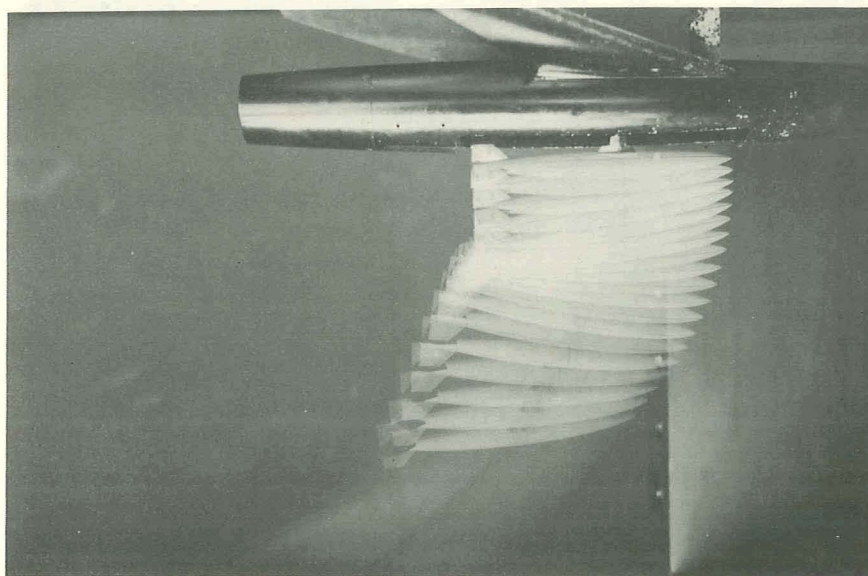
(i) Test 8; standard fin; $\alpha_f = 4^\circ$; similitude check.

L-91284

Figure 8.- Continued.



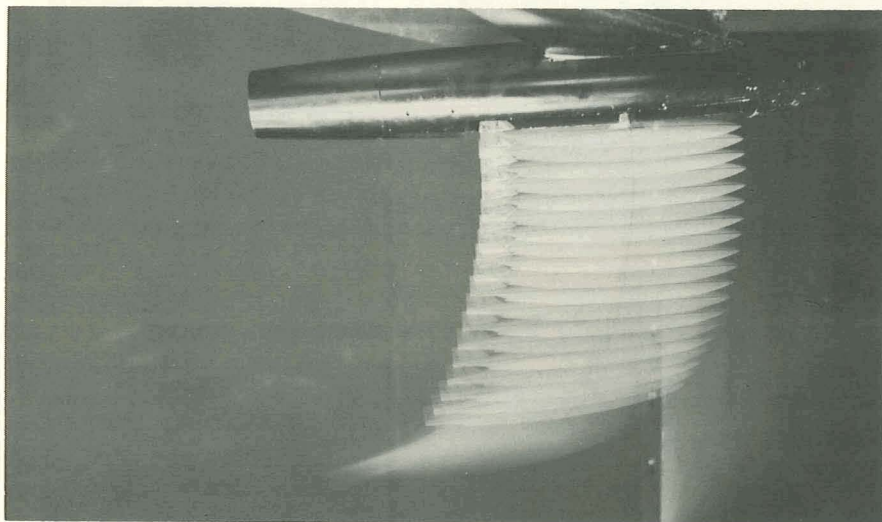
(j) Test 9; standard fins; $\alpha_f = 0^\circ$; $1.28I_y$. L-91293



(k) Test 10; standard fin; $\alpha_f = 0^\circ$; $1.88I_y$. L-91129

Figure 8.- Continued.

CONFIDENTIAL

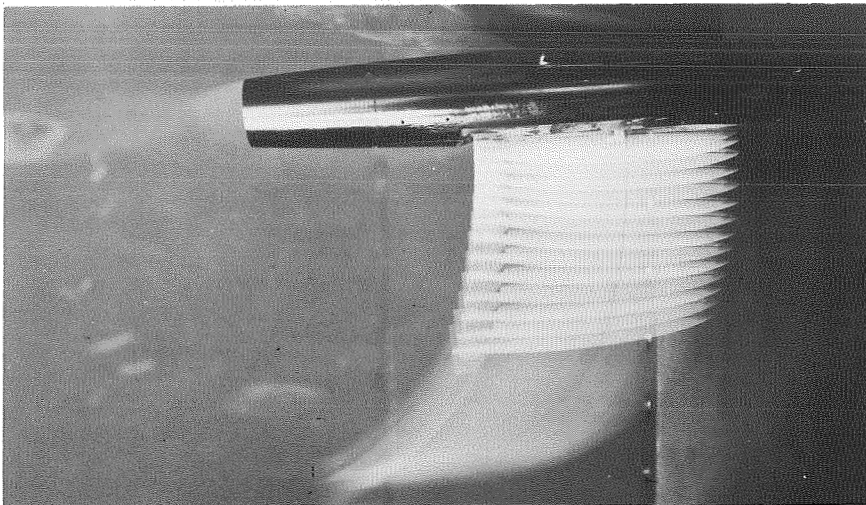


(1) Test 11; standard fin; $\alpha_f = 4^\circ$; $1.88I_y$.

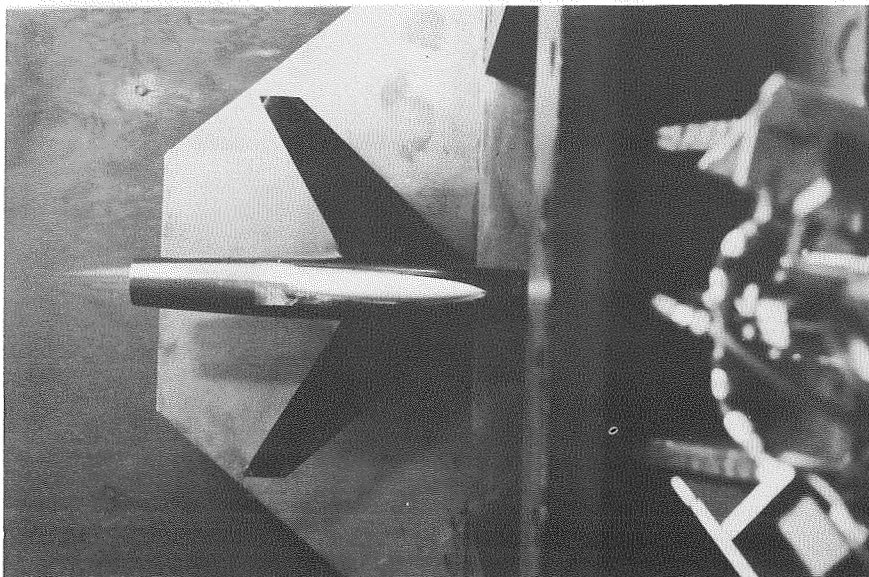
L-91280

Figure 8.- Concluded.

CONFIDENTIAL

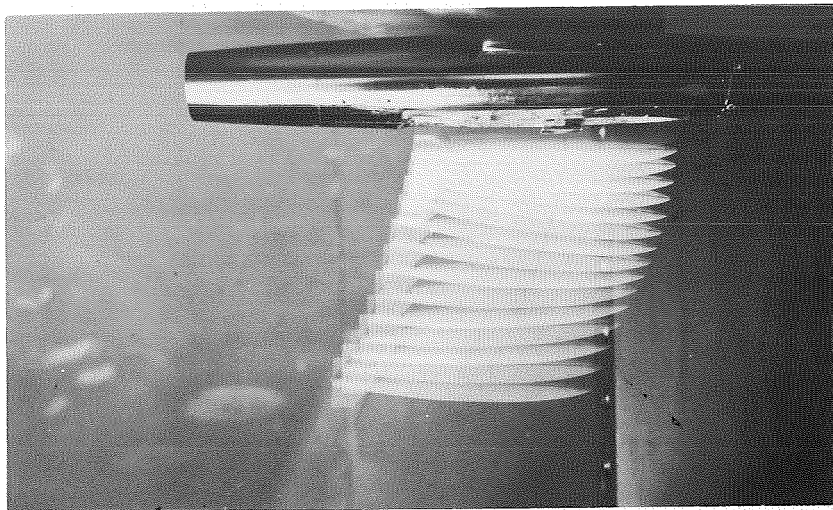


(a) Test 12; $\alpha_F = 4^\circ$; $\dot{z}_O = 23.0$ feet per second. L-91286



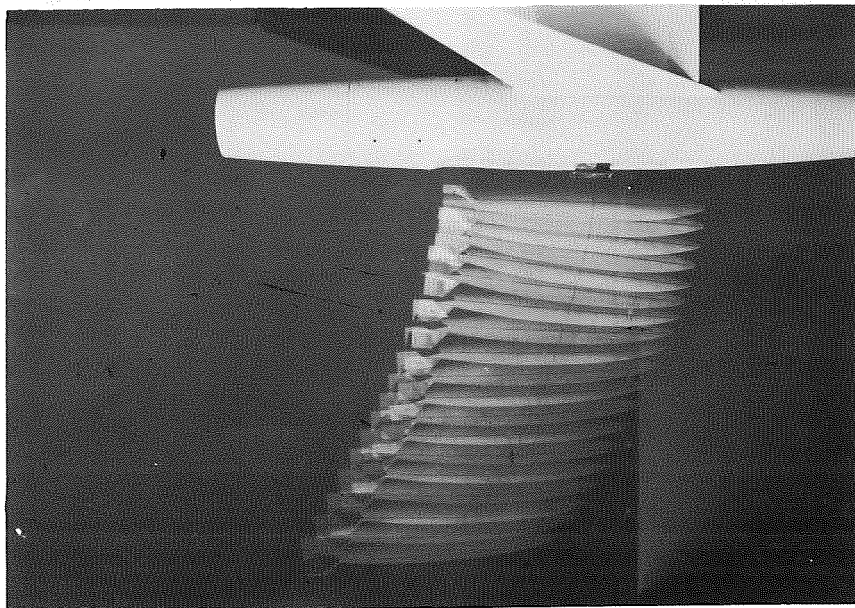
(b) Test 12; bottom view of model. L-91287

Figure 9.- Ejection tests from a semisubmerged position. Store A;
 $l/d = 8.6$; $M_O = 1.39$; $h_p = 3,400$ feet; standard fin.



L-91288

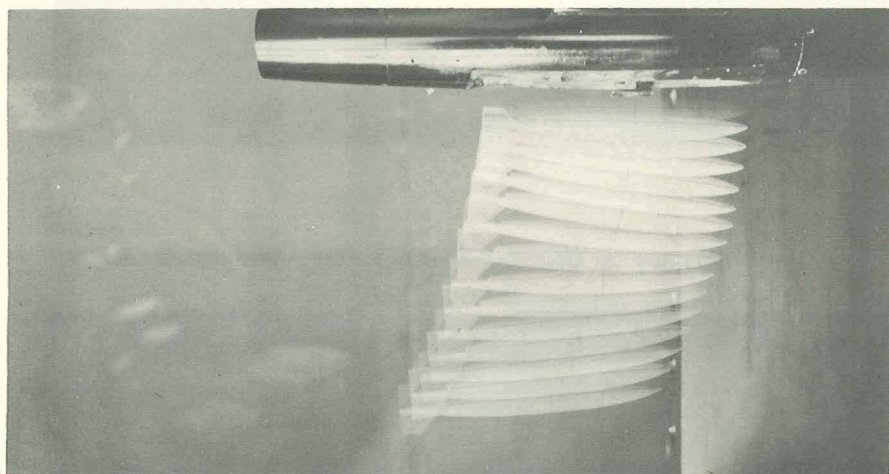
(c) Test 13; $\alpha_f = 0^\circ$; $\dot{z}_0 = 20.5$ feet per second.



L-91291

(d) Test 14; $\alpha_f = 0^\circ$; $\dot{z}_0 = 23.0$ feet per second.

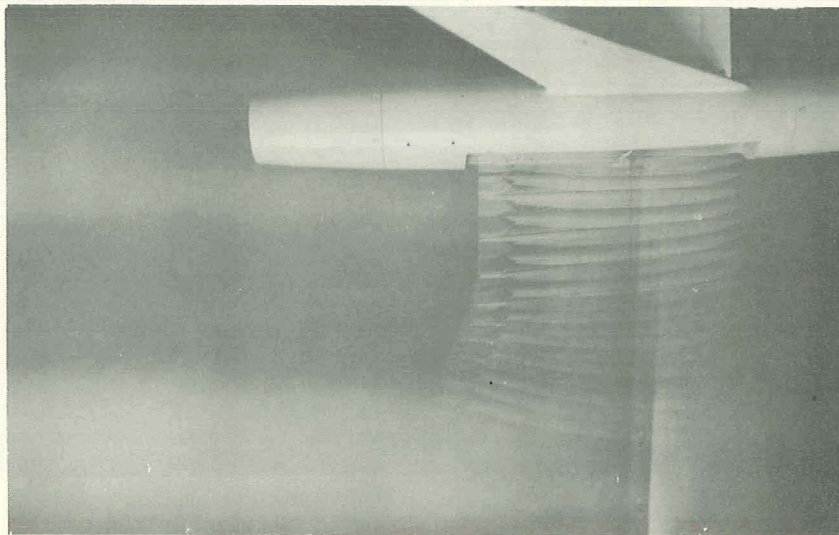
Figure 9.- Continued.



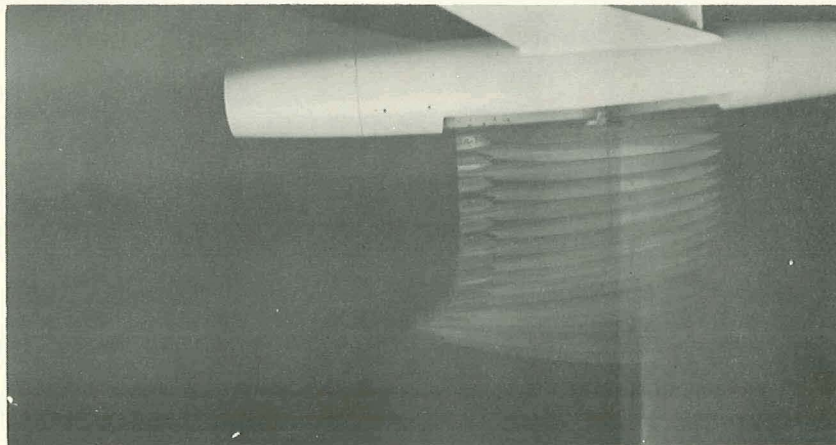
L-91289

(e) Test 15; $\alpha_f = 0^\circ$; $\dot{z}_0 = 24.0$ feet per second.

Figure 9.- Concluded.

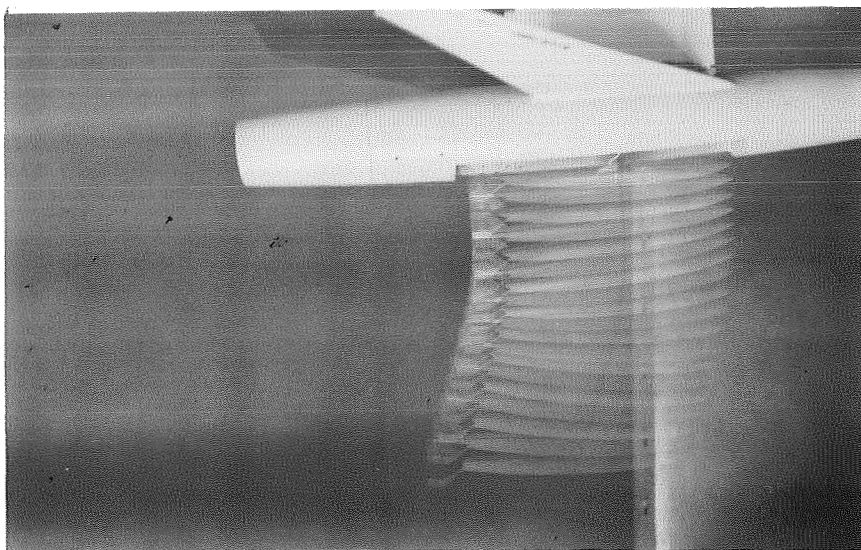


(a) Test 16; standard fin; $\alpha_f = 4^\circ$; $\dot{z}_0 = 29.5$ feet per second. L-91311

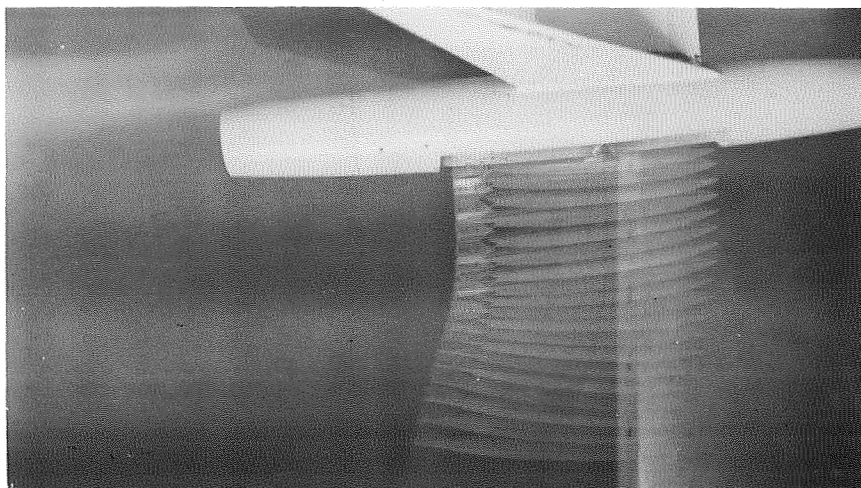


(b) Test 17; fin 1; $\alpha_f = 4^\circ$; $\dot{z}_0 = 29.5$ feet per second. L-91313

Figure 10.- Ejection tests from a submerged position. Store A; $l/d = 8.6$;
 $M_0 = 1.98$; $h_p = 29,000$ feet.

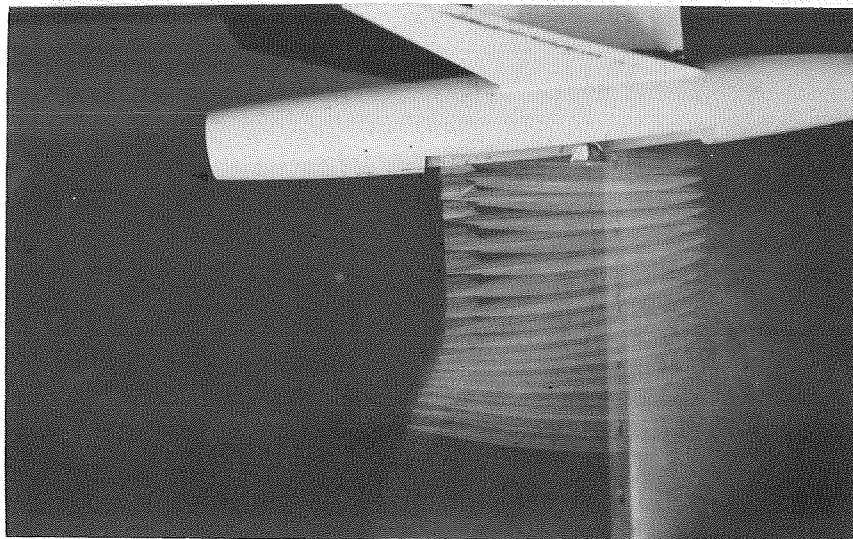


(c) Test 18; fin 2; $\alpha_f = 4^\circ$; $\dot{z}_0 = 29.5$ feet per second. L-91316

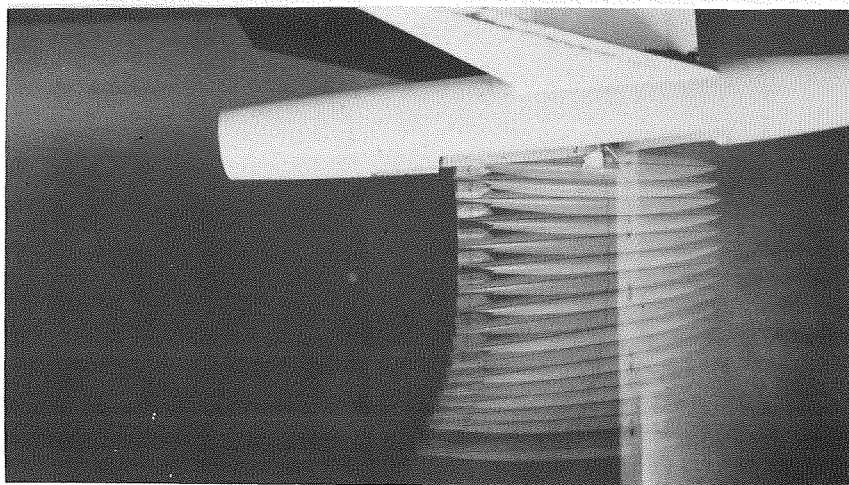


(d) Test 19; fin 3; $\alpha_f = 4^\circ$; $\dot{z}_0 = 29.5$ feet per second. L-91500

Figure 10.- Continued.

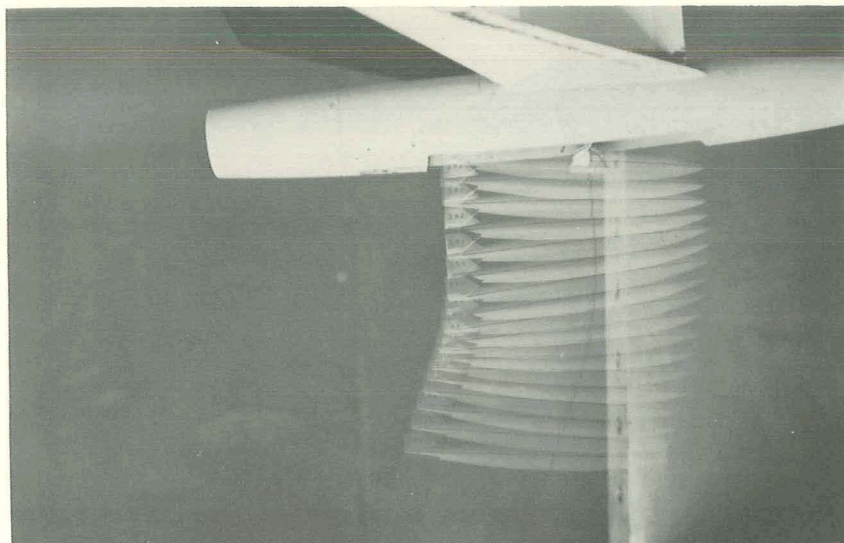


(e) Test 20; standard fin; $\alpha_F = 4^\circ$; $i_O = -6^\circ$; $\dot{z}_O = 32.5$ feet per second. L-91503



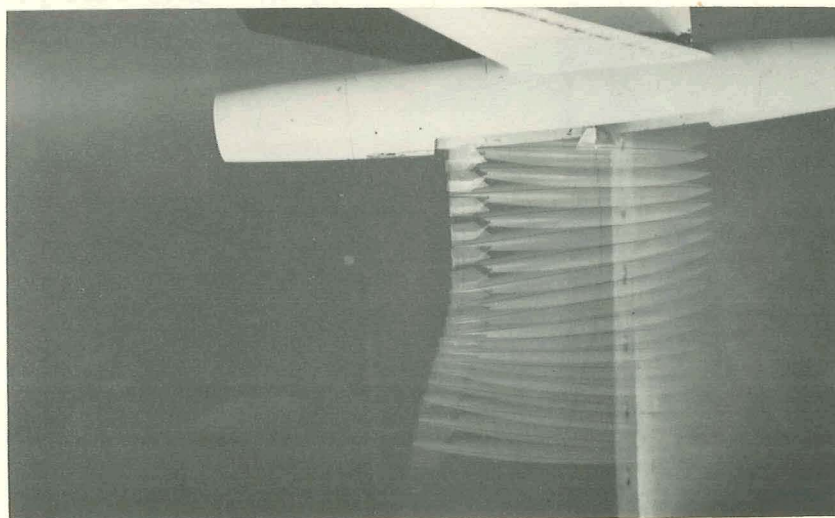
(f) Test 21; fin 1; $\alpha_F = 4^\circ$; $i_O = -6^\circ$; $\dot{z}_O = 32.5$ feet per second. L-91505

Figure 10.- Continued.



L-91507

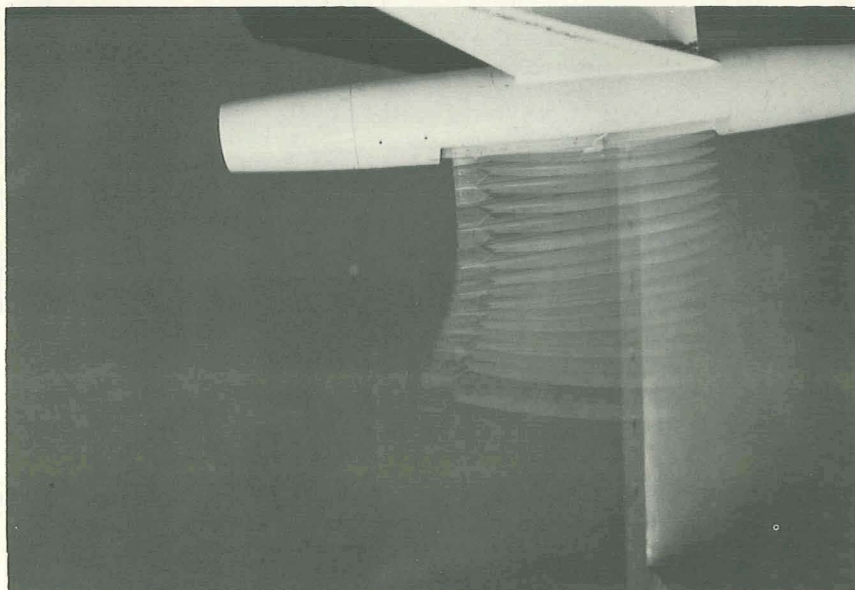
(g) Test 22; fin 2; $\alpha_F = 4^\circ$; $i_O = -6^\circ$; $\dot{z}_O = 32.5$ feet per second.



L-91509

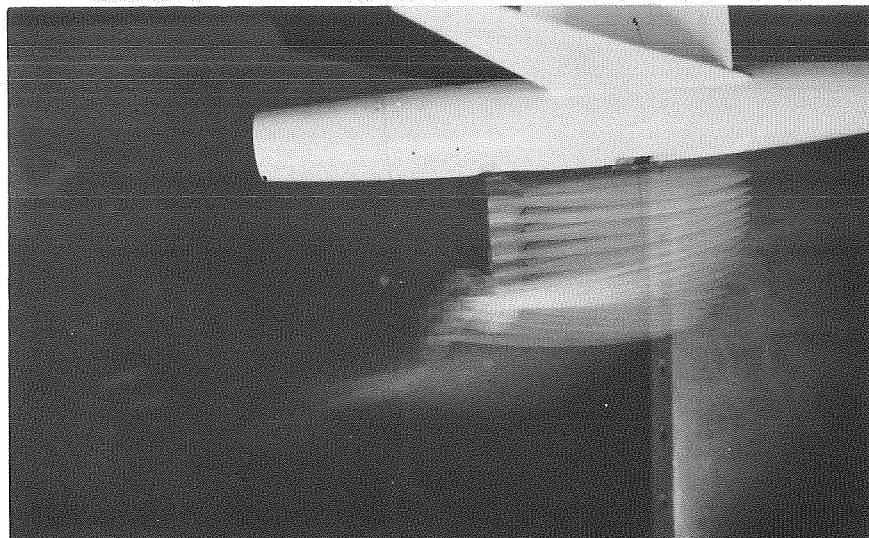
(h) Test 23; fin 3; $\alpha_F = 4^\circ$; $i_O = -6^\circ$; $\dot{z}_O = 32.5$ feet per second.

Figure 10.- Continued.

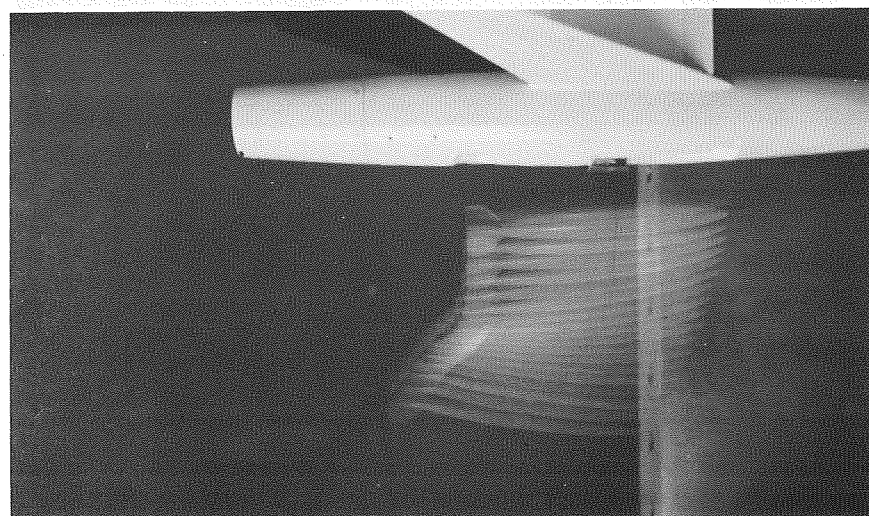


(1) Test 24; standard fin; repeat of test 16. L-91501

Figure 10.- Concluded.

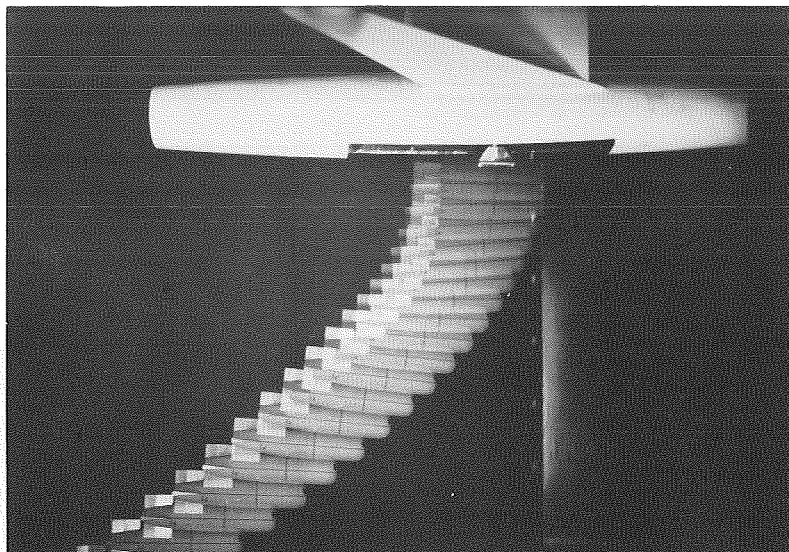
(a) Test 25; $\alpha_f = 4^\circ$.

L-91516

(b) Test 26; $\alpha_f = 0^\circ$.

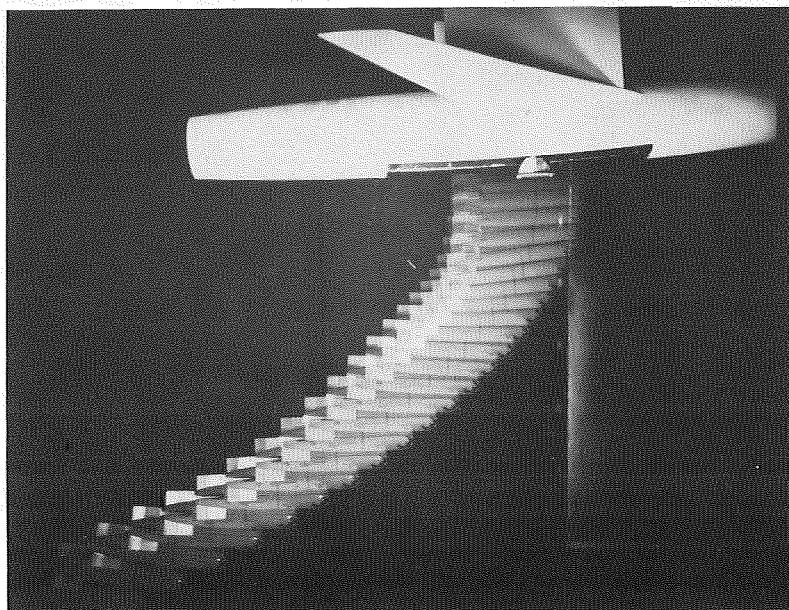
L-91517

Figure 11.- Ejection tests from a semisubmerged position. Store A;
 $l/d = 8.6$; $M_0 = 1.98$; $h_p = 29,000$ feet; $\dot{z}_0 = 24$ feet per second;
standard fin.



(a) Test 27; $\alpha_f = 0^\circ$.

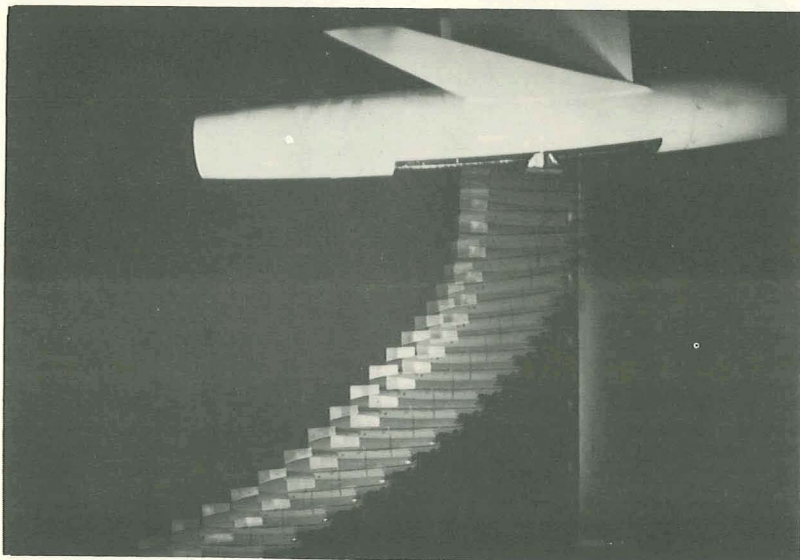
L-95781



(b) Test 28; $\alpha_f = 4^\circ$.

L-95782

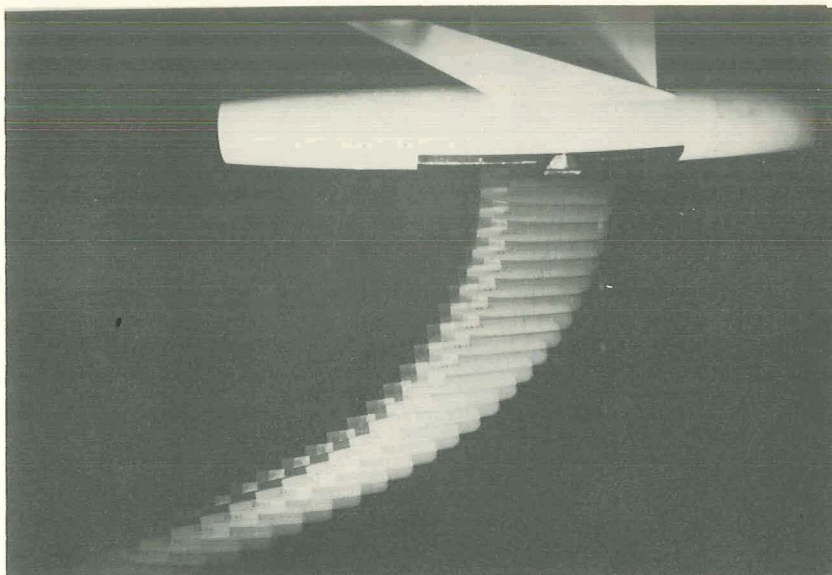
Figure 12.- Ejection tests. Store B; $l/d = 4.66$; $M_0 = 1.39$;
 $h_p = 3,400$ feet; $\dot{z}_0 = 31$ feet per second.



(c) Test 29; $\alpha_F = 4^\circ$; $i_0 = -6^\circ$.

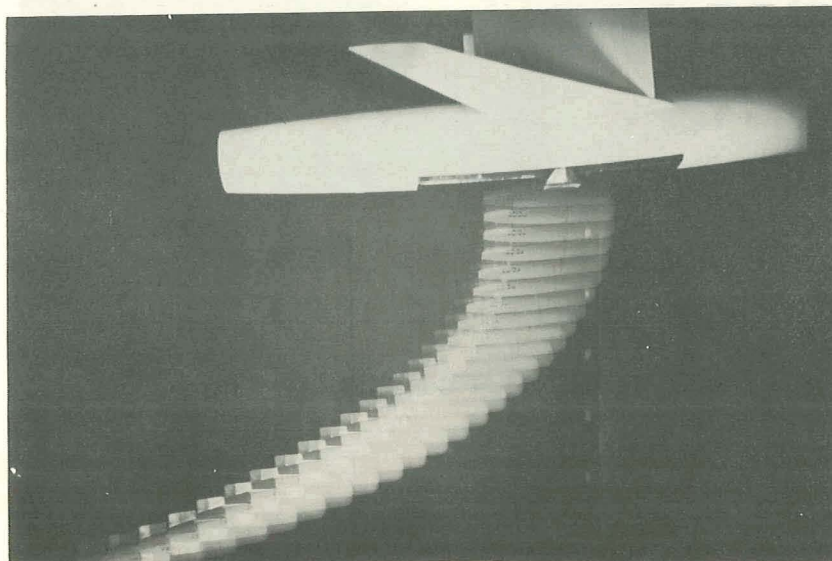
L-95783

Figure 12.- Concluded.



(a) Test 30; $\alpha_F = 0^\circ$.

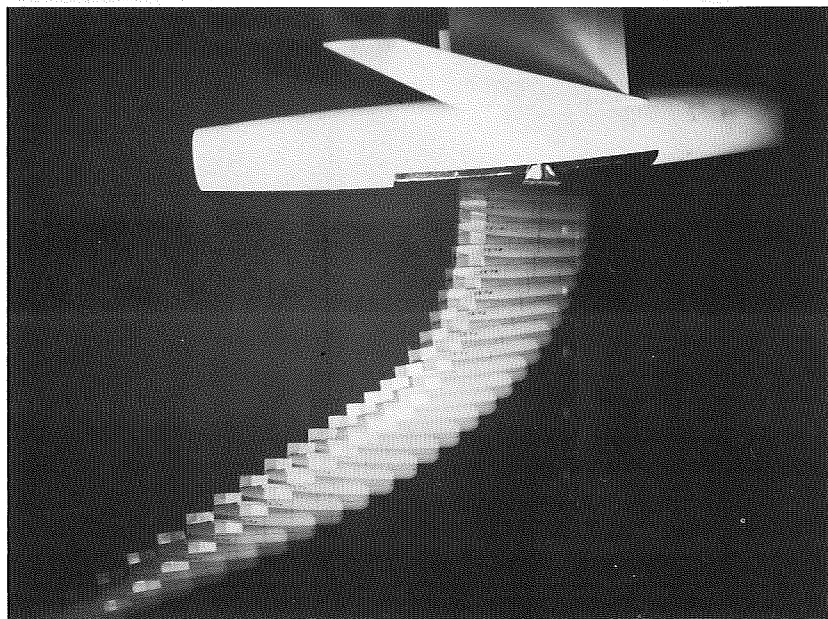
L-95784



(b) Test 31; $\alpha_F = 4^\circ$.

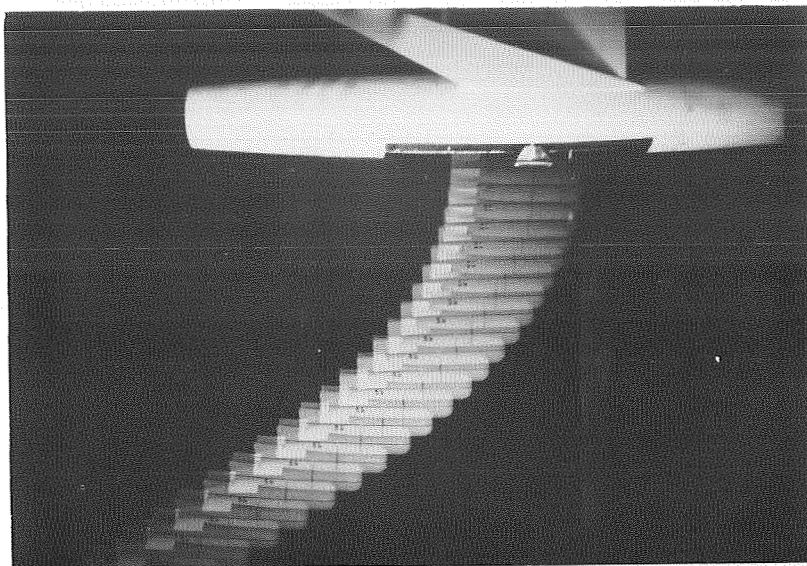
L-95785

Figure 13.- Ejection tests. Store B; $l/d = 4.66$; $M_0 = 1.60$;
 $h_p = 16,400$ feet; $\dot{z}_0 = 29.5$ feet per second.



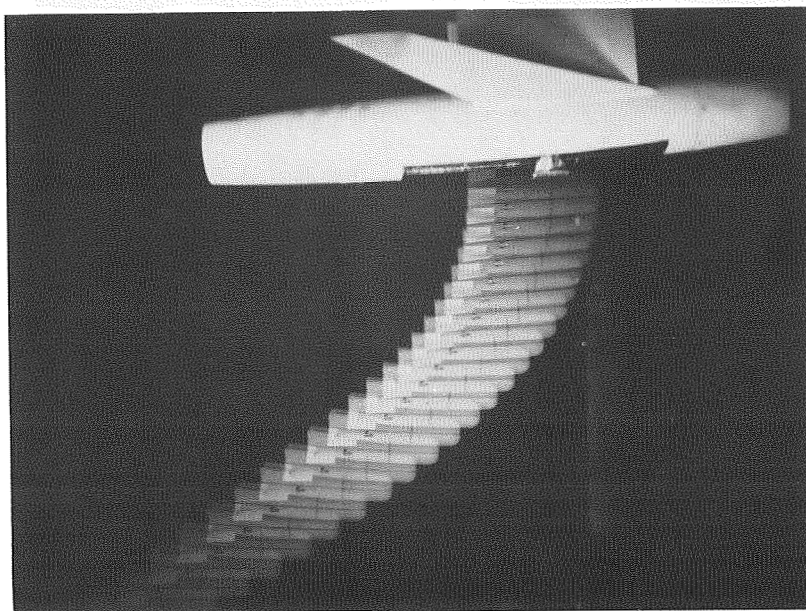
(c) Test 32; $\alpha_f = 4^\circ$; $i_o = -6^\circ$. L-95786

Figure 13.- Concluded.



(a) Test 33; $\alpha_F = 0^\circ$.

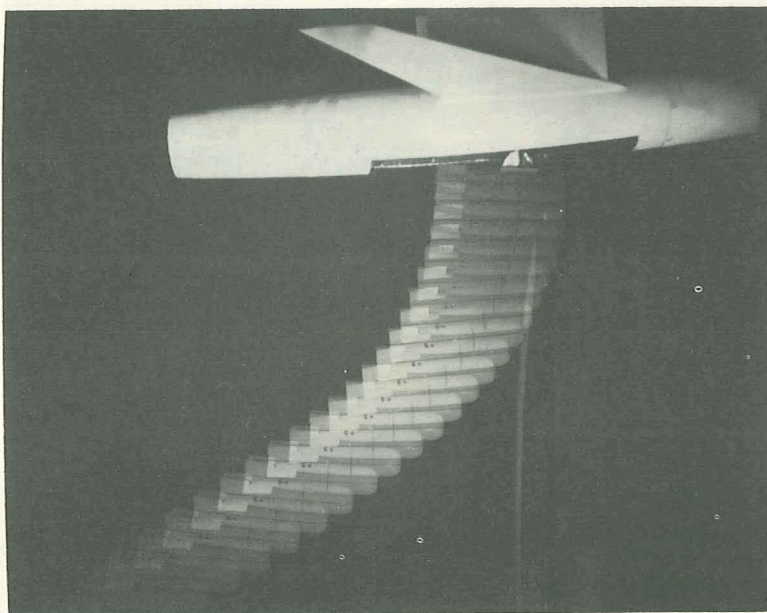
L-95787



(b) Test 34; $\alpha_F = 4^\circ$.

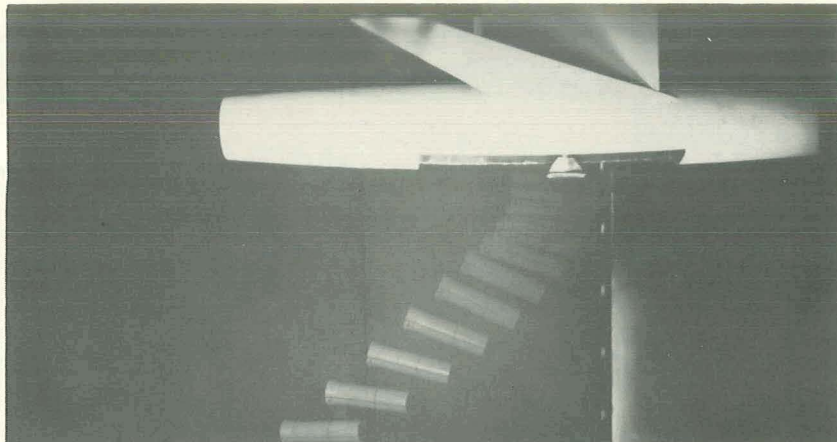
L-95788

Figure 14.- Ejection tests. Store B; $l/d = 4.66$; $M_0 = 1.98$;
 $h_p = 29,000$ feet; $\dot{z}_0 = 30$ feet per second.

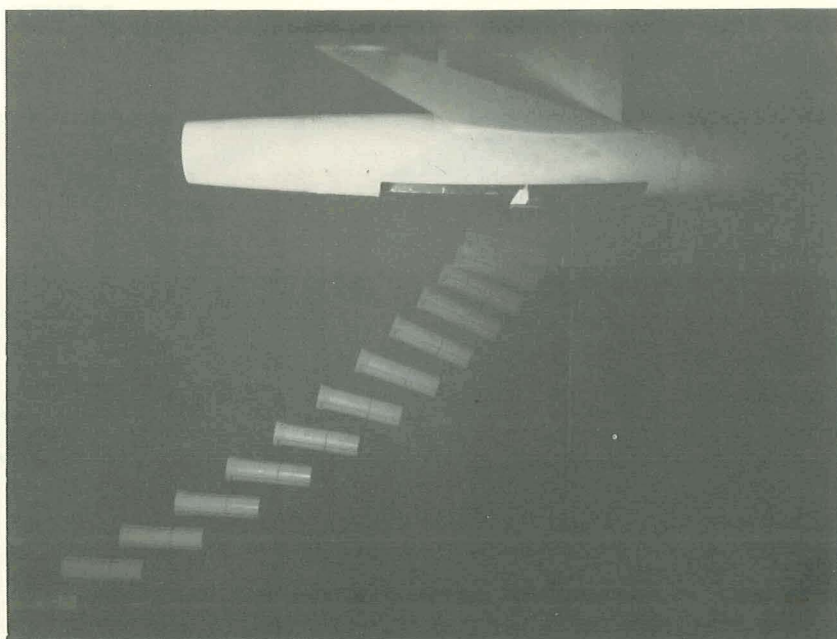


(c) Test 35; $\alpha_f = 4^\circ$; $i_o = -6^\circ$. L-95789

Figure 14.- Concluded.

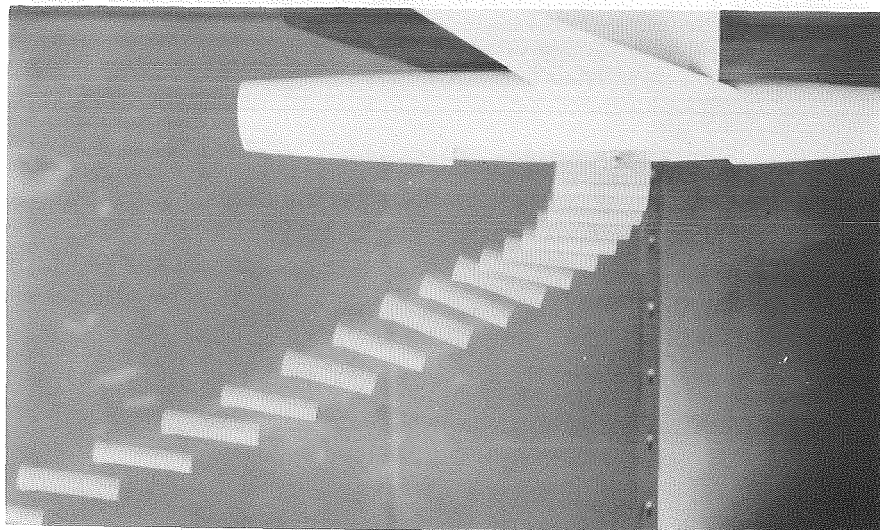


(a) Test 36; $\dot{z}_0 = 34$ feet per second. L-95790

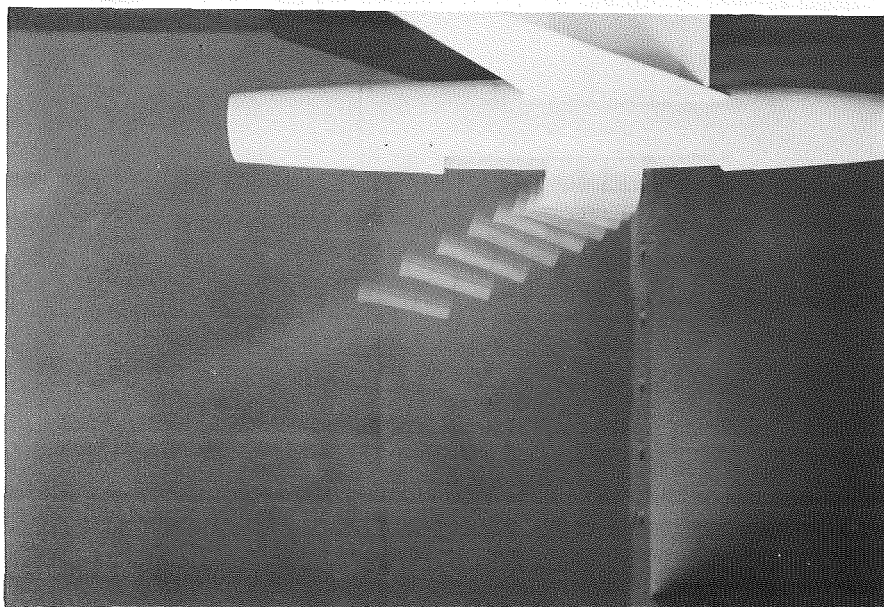


(b) Test 37; repeat of test 36. L-95791

Figure 15.- Ejection tests. Store C; $l/d = 3.75$; $M_0 = 1.39$;
 $h_p = 3,400$ feet; $\alpha_F = 0^\circ$.

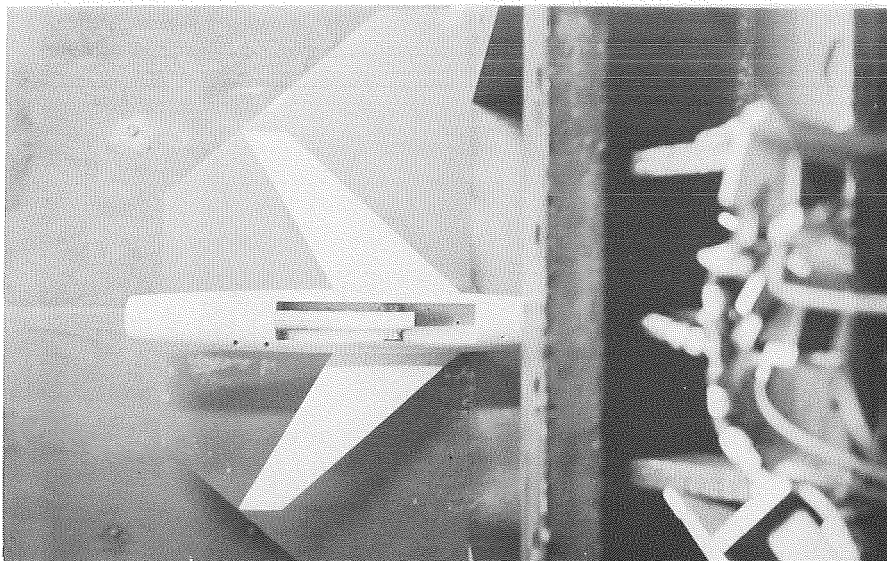


(c) Test 38; $\dot{z}_0 = 21$ feet per second. L-91295



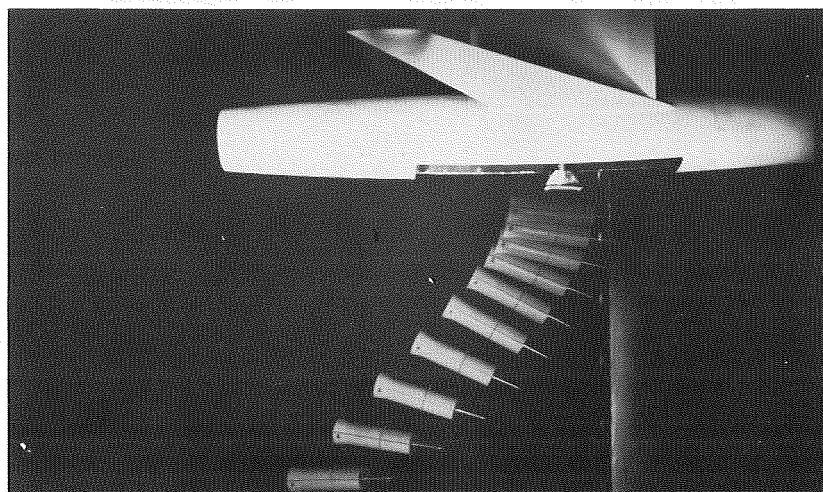
(d) Test 39; $\dot{z}_0 = 10$ feet per second. L-91297

Figure 15.- Continued.



(e) Test 39; bottom view of model.

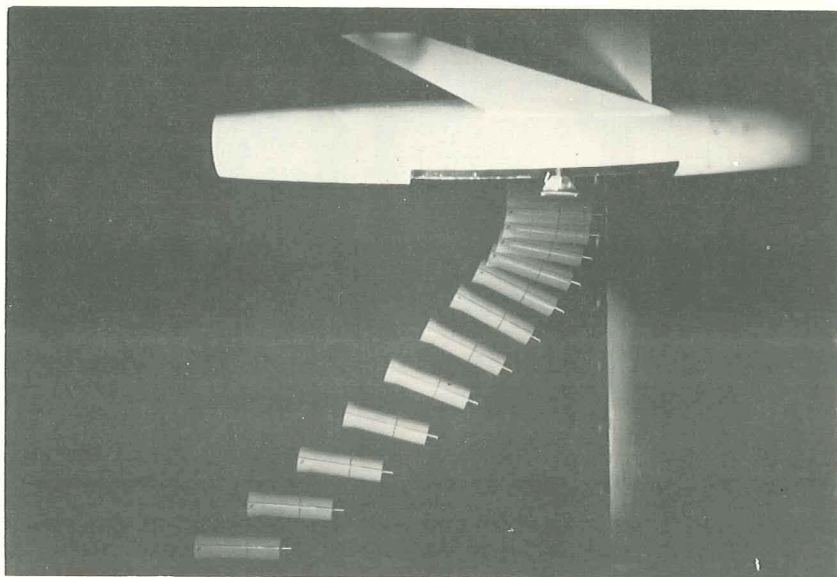
L-91298



(f) Test 40; $\dot{z}_0 = 34$ feet per second; spike.

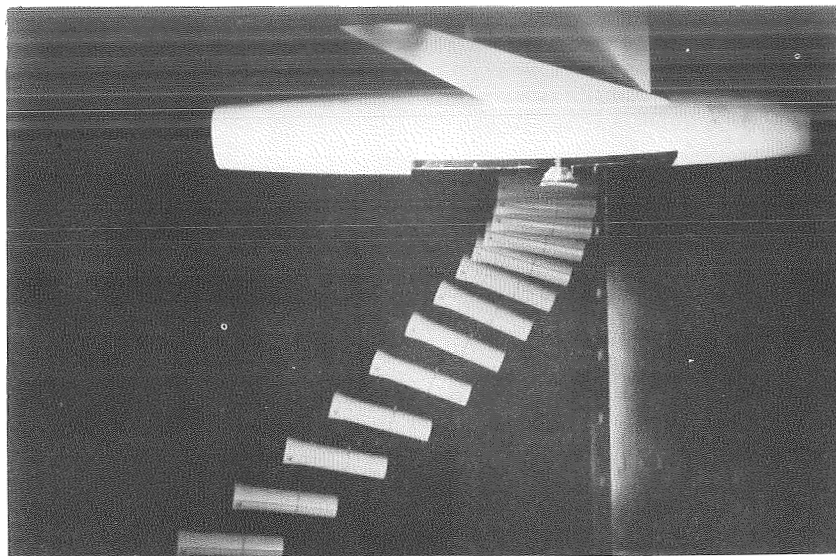
L-95792

Figure 15.- Continued.



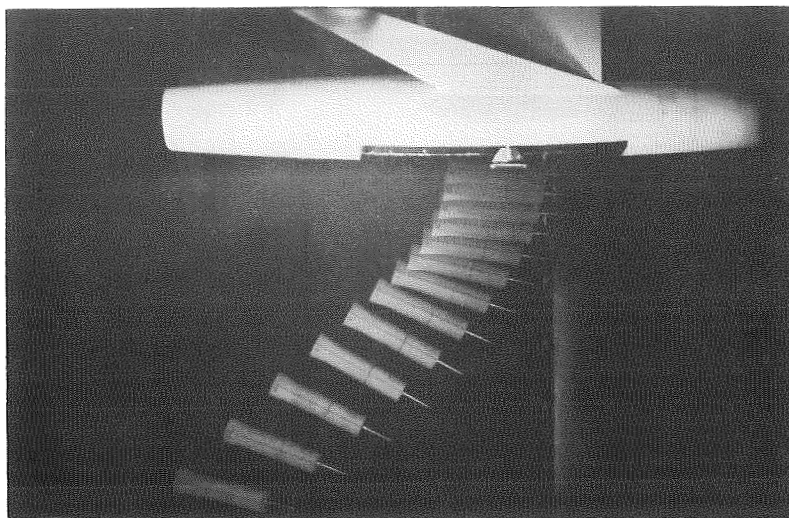
(g) Test 41; $\dot{z}_0 = 34$ feet per second; plate. L-95793

Figure 15.- Concluded.



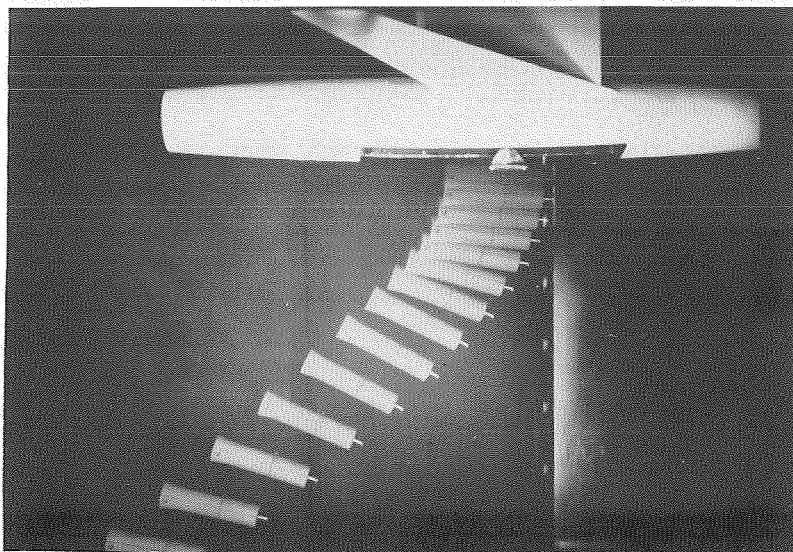
(a) Test 42; $\dot{z}_0 = 34$ feet per second.

L-95794

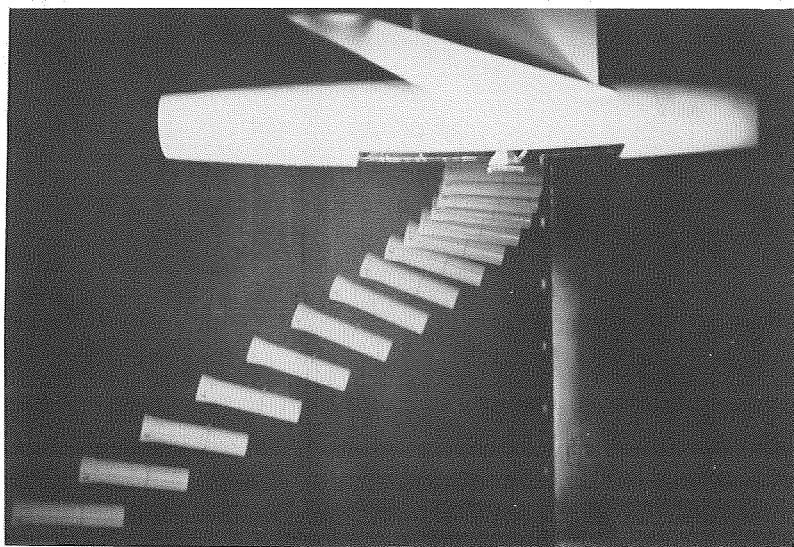


(b) Test 43; $\dot{z}_0 = 33$ feet per second; spike. L-95795

Figure 16.- Ejection tests. Store C; $l/d = 4.40$; $M_0 = 1.39$;
 $h_p = 3,400$ feet; $\alpha_F = 0^\circ$.

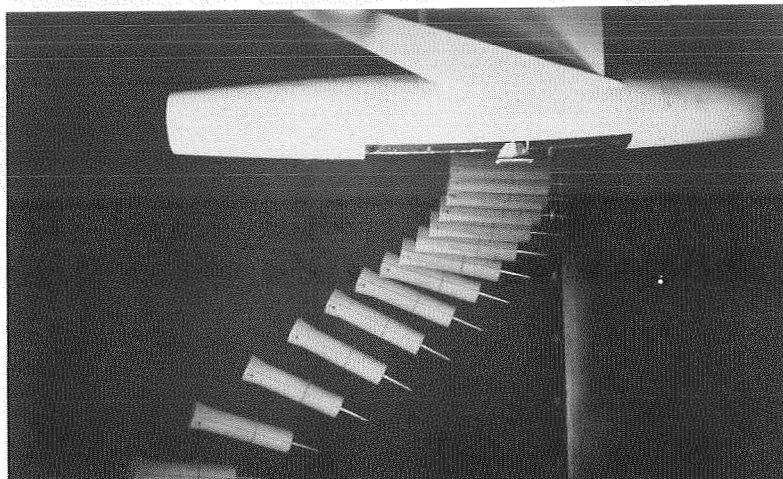


(c) Test 44; $\dot{z}_0 = 35$ feet per second; plate. L-95796

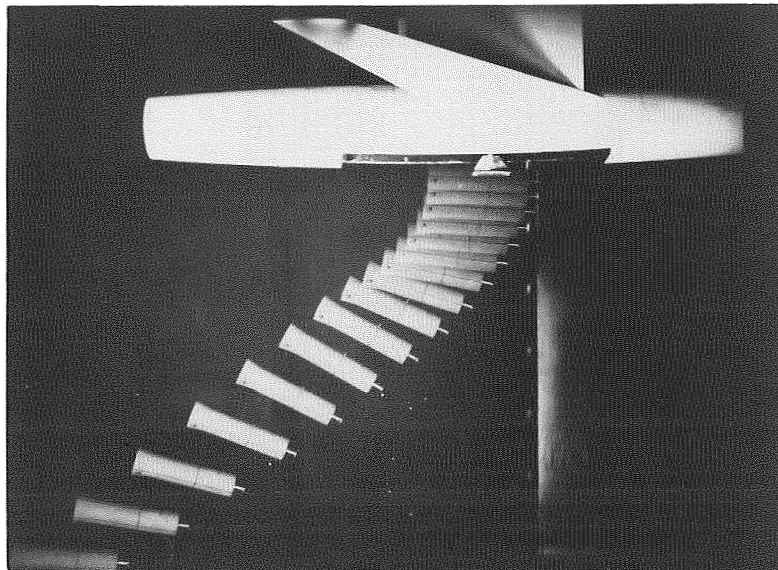


(d) Test 45; $\dot{z}_0 = 26$ feet per second. L-95797

Figure 16.- Continued.

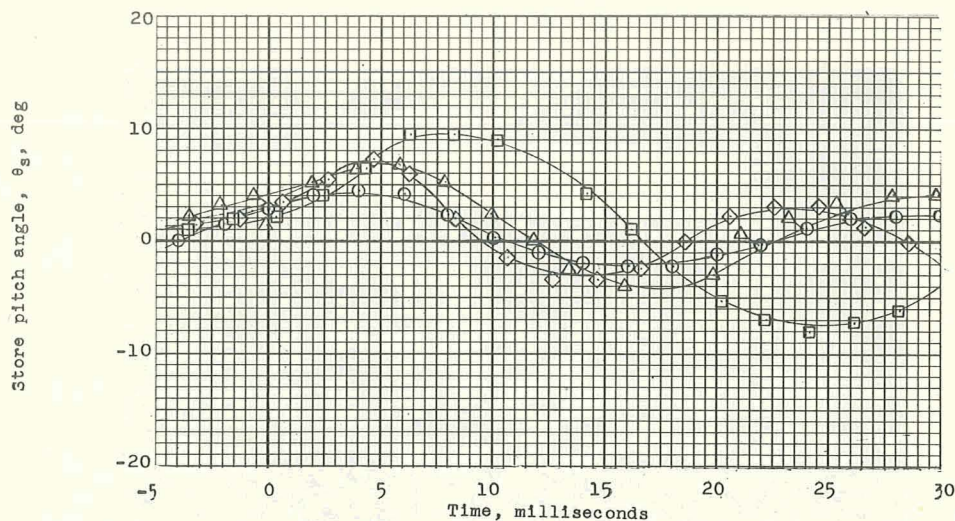


(e) Test 46; $\dot{z}_0 = 26$ feet per second; spike. L-95798

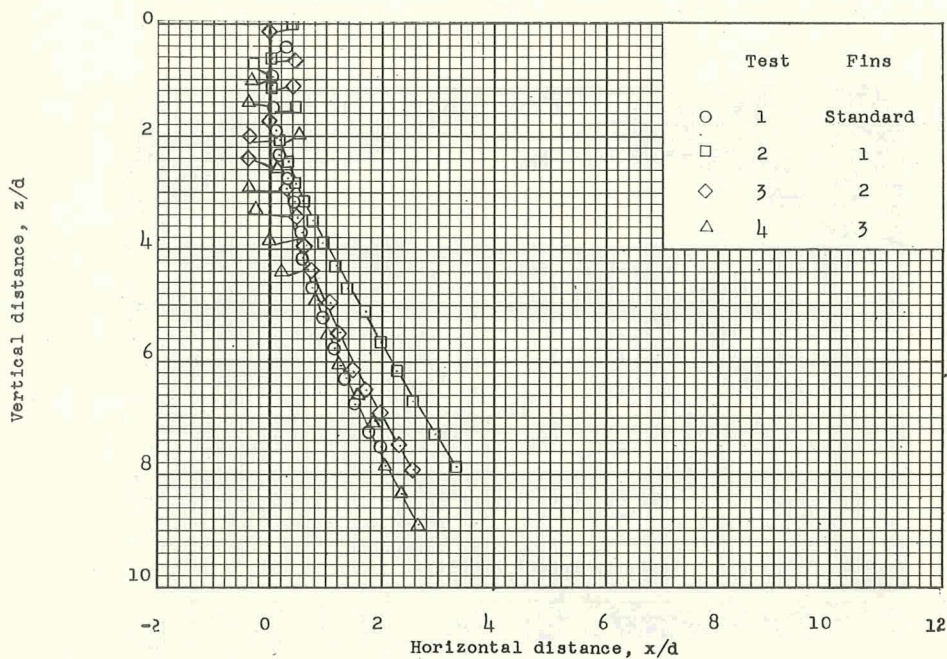


(f) Test 47; $\dot{z}_0 = 26$ feet per second; plate. L-95799

Figure 16.- Concluded.

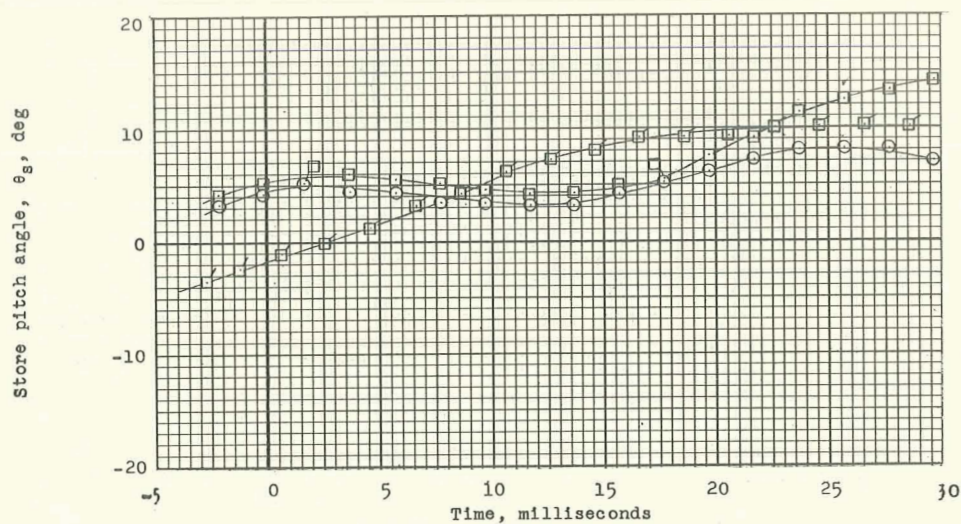


(a) Time history.

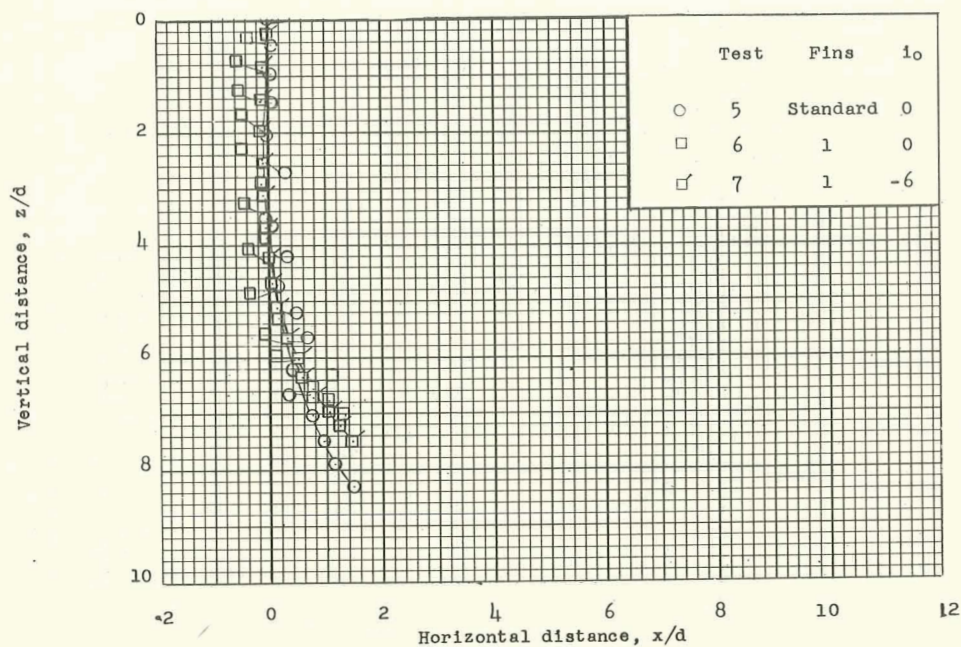


(b) Trajectory.

Figure 17.- Time history and trajectories for streamline store A with fin modifications. $M_0 = 1.39$; $h_p = 3,400$ feet; $\alpha_f = 0^\circ$; and $\dot{z}_0 = 27.0$ feet per second.

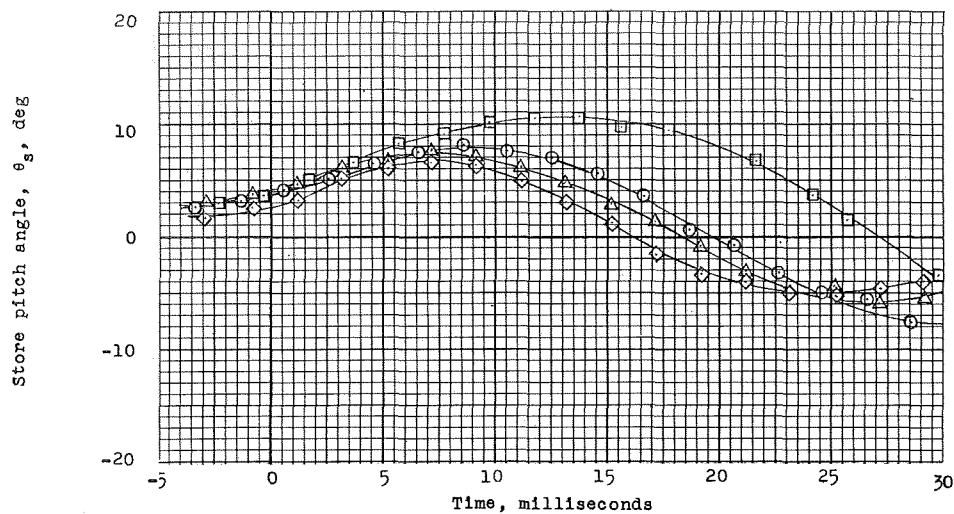


(a) Time history.

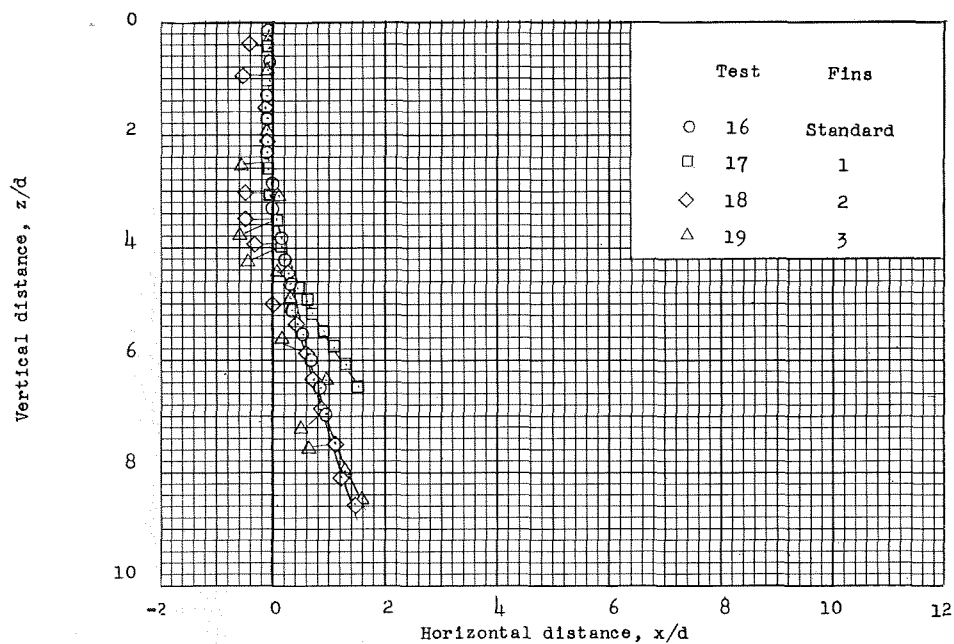


(b) Trajectory.

Figure 18.- Time history and trajectories for streamline store A with fin modifications. $M_0 = 1.39$; $h_p = 3,400$ feet; $\alpha_f = 4^\circ$; and $\dot{z}_0 = 29.5$ feet per second.

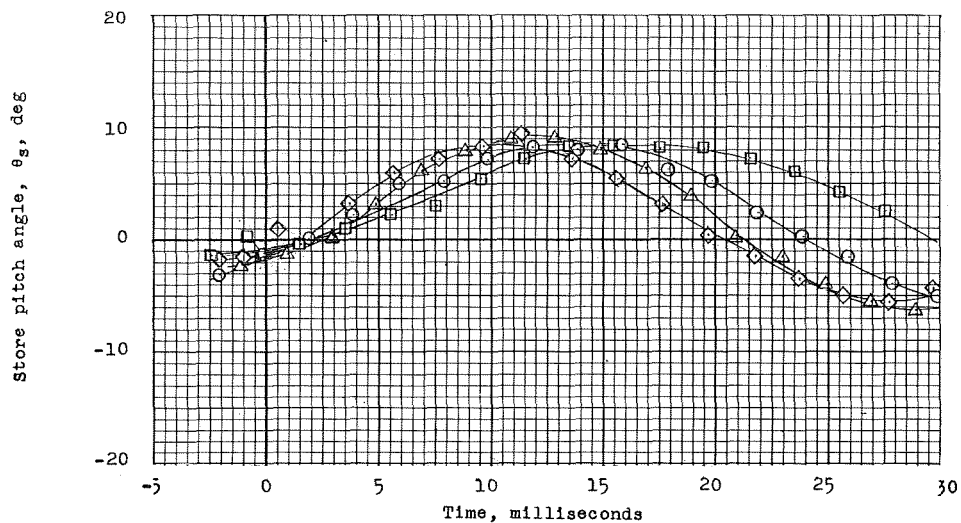


(a) Time history.

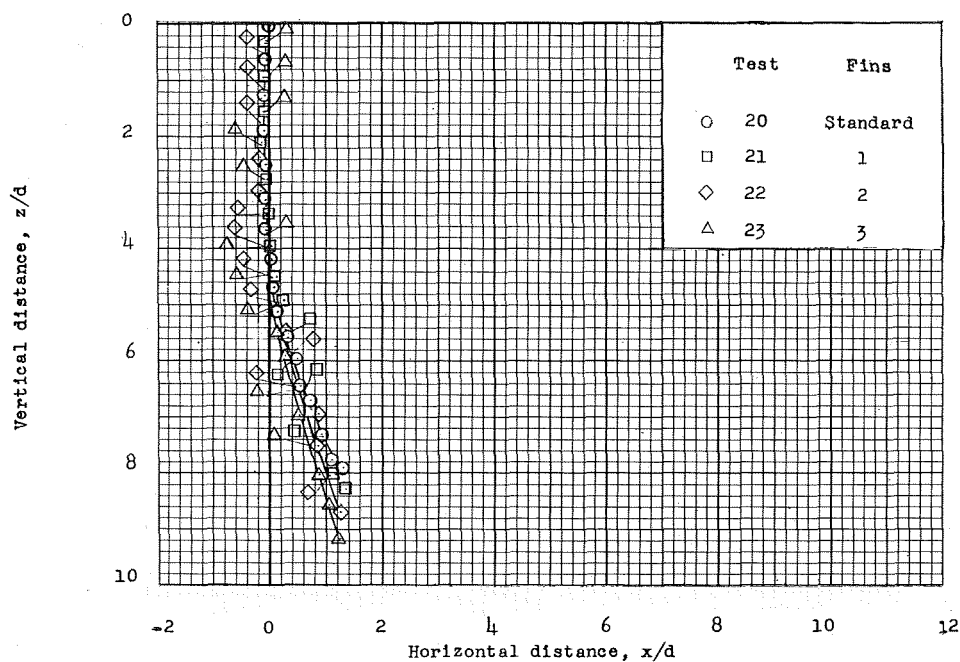


(b) Trajectory.

Figure 19.- Time history and trajectories for streamline store A with fin modifications. $M_0 = 1.98$; $h_p = 29,000$ feet; $\alpha_F = 4^\circ$; $i_0 = 0^\circ$; and $\dot{z}_0 = 29.5$ feet per second.

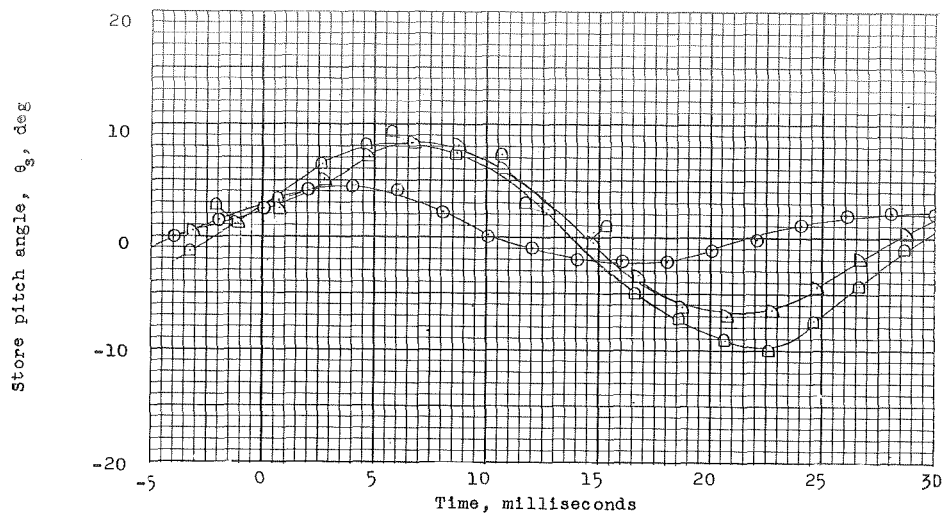


(a) Time history.

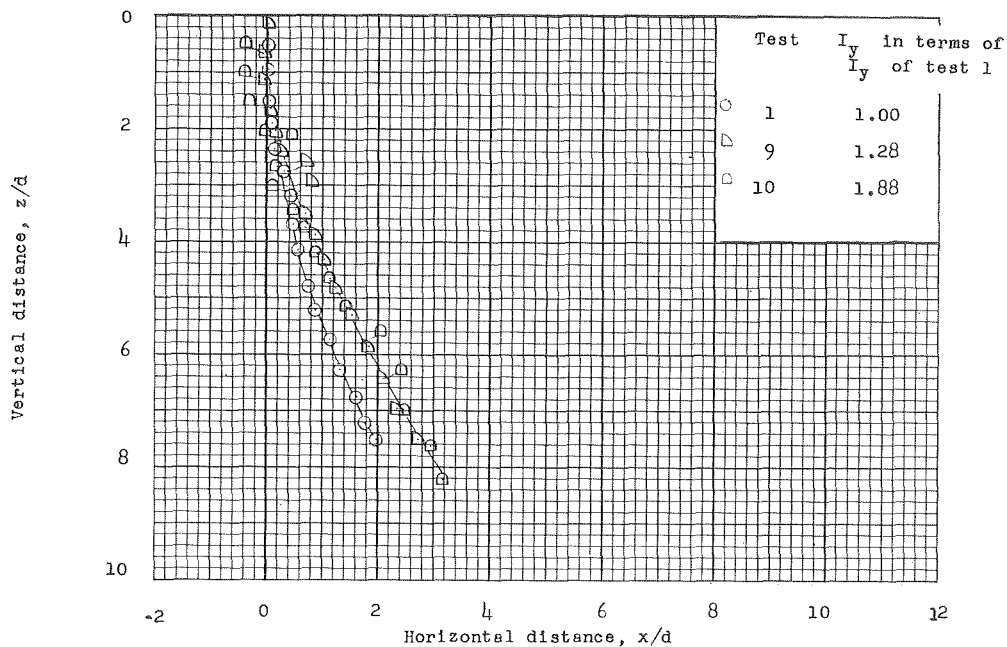


(b) Trajectory.

Figure 20.- Time history and trajectories for streamline store A with fin modifications ejected at a negative incidence angle of $i_0 = -6^\circ$. $M_0 = 1.98$; $h_p = 29,000$ feet; $\alpha_f = 4^\circ$; and $\dot{z}_0 = 32.5$ feet per second.

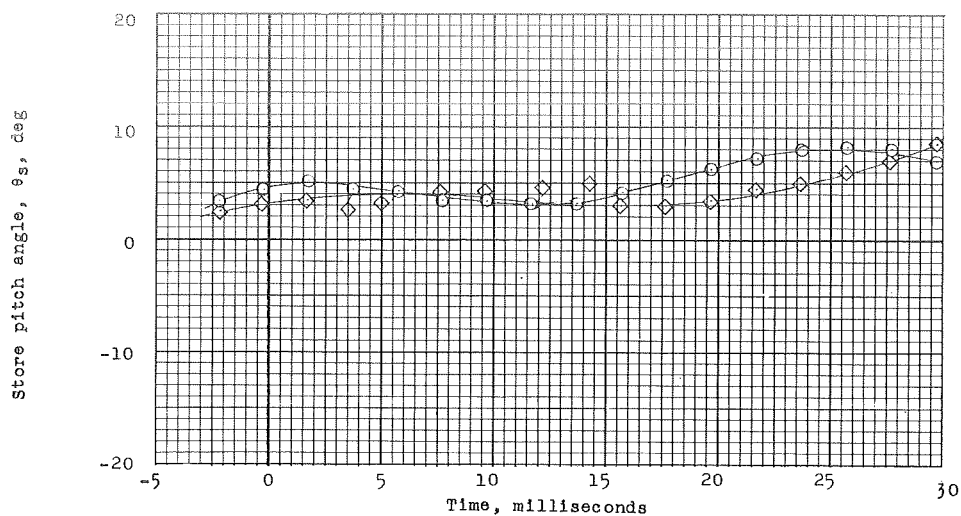


(a) Time history.

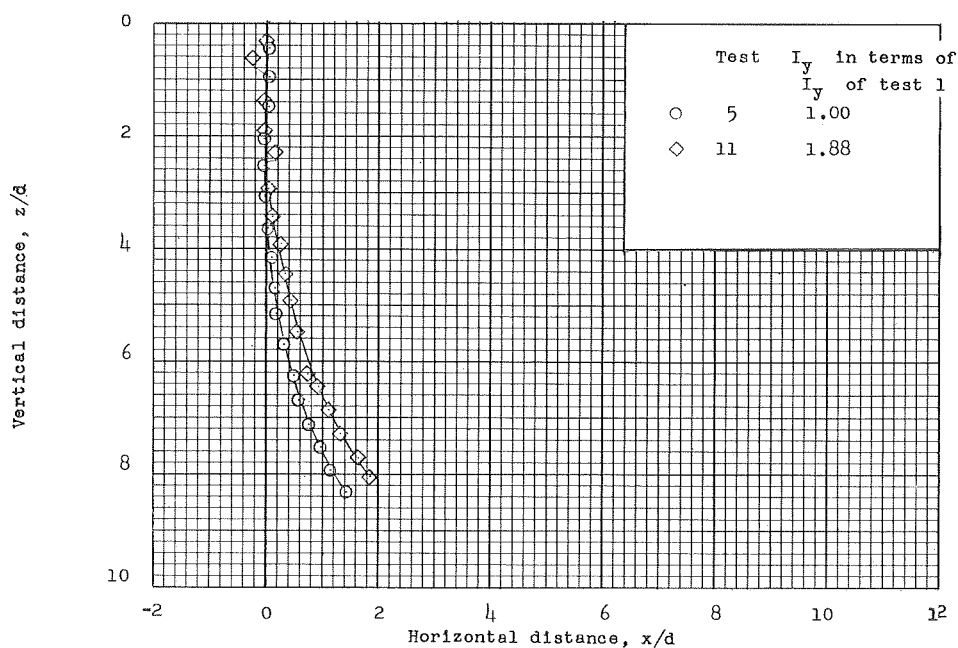


(b) Trajectory.

Figure 21.- Time history and trajectories with inertia changes for streamline store A with standard fins. $M_0 = 1.39$; $h_p = 3,400$ feet; and $\alpha_f = 0^\circ$.

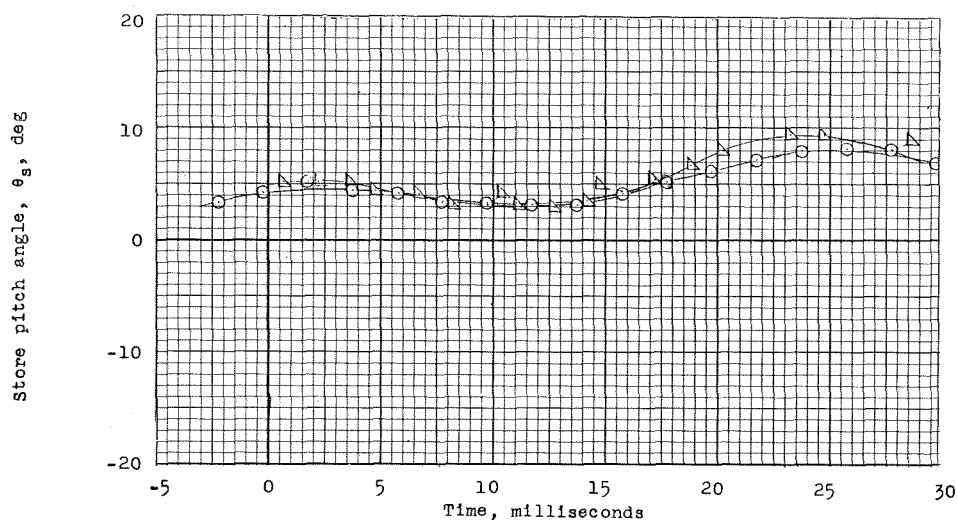


(a) Time history.

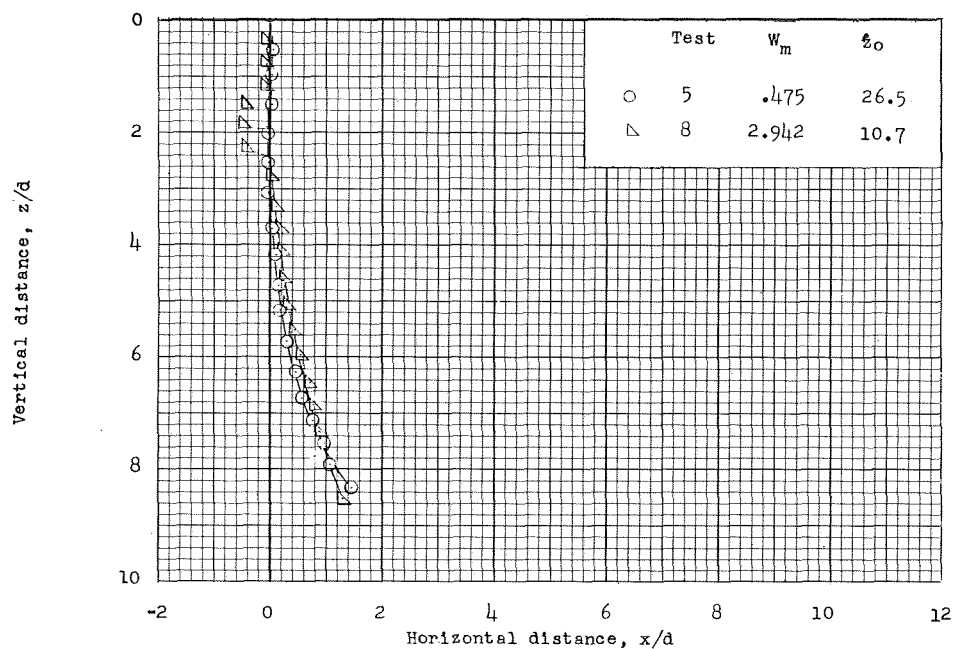


(b) Trajectory.

Figure 22.- Time history and trajectories with an increase in store inertia for streamline store A with standard fins. $M_0 = 1.39$; $h_p = 3,400$ feet; and $\alpha_f = 4^\circ$.

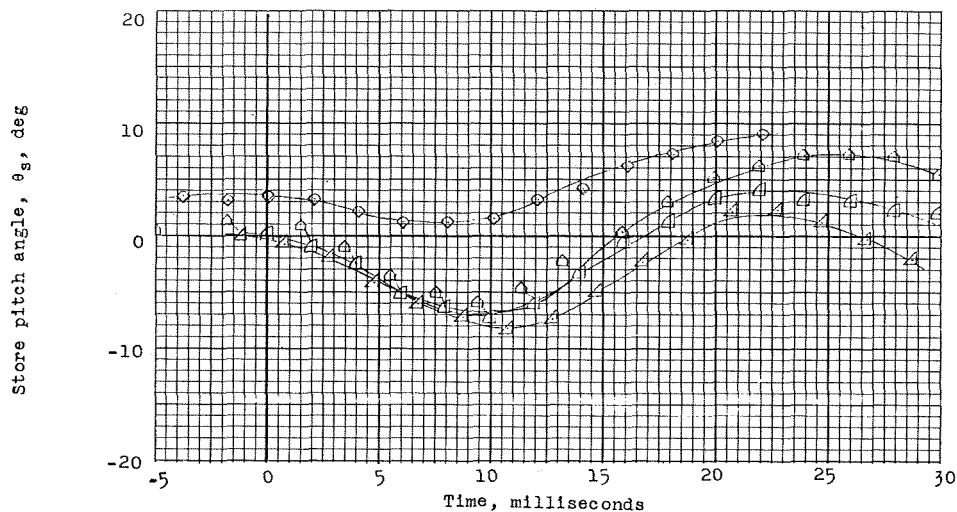


(a) Time history.

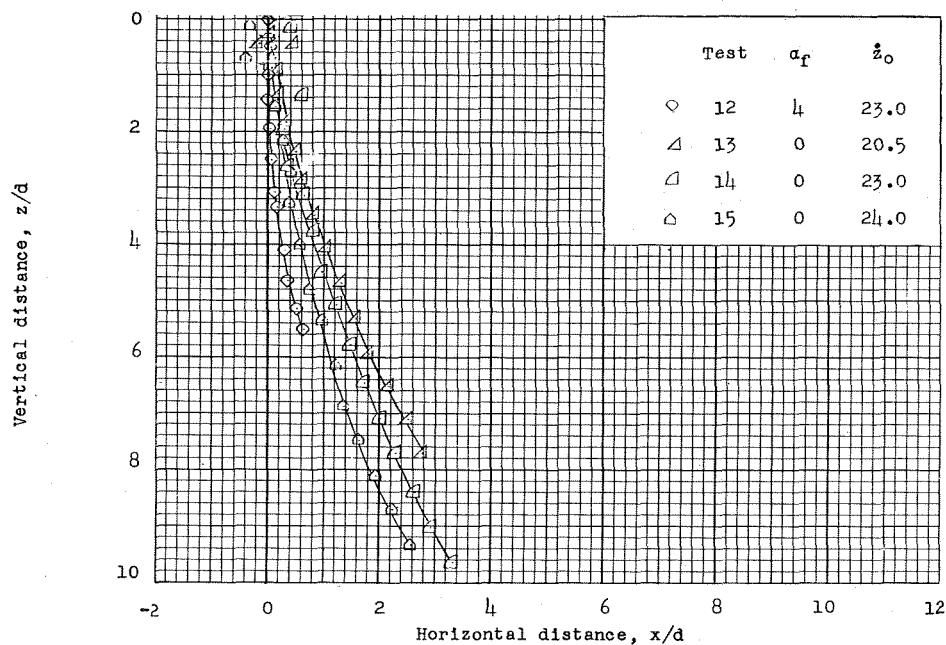


(b) Trajectory.

Figure 23.- Time history and trajectories for streamline store A to check simulation. $M_0 = 1.39$; $h_p = 3,400$ feet; and $\alpha_f = 4^\circ$.

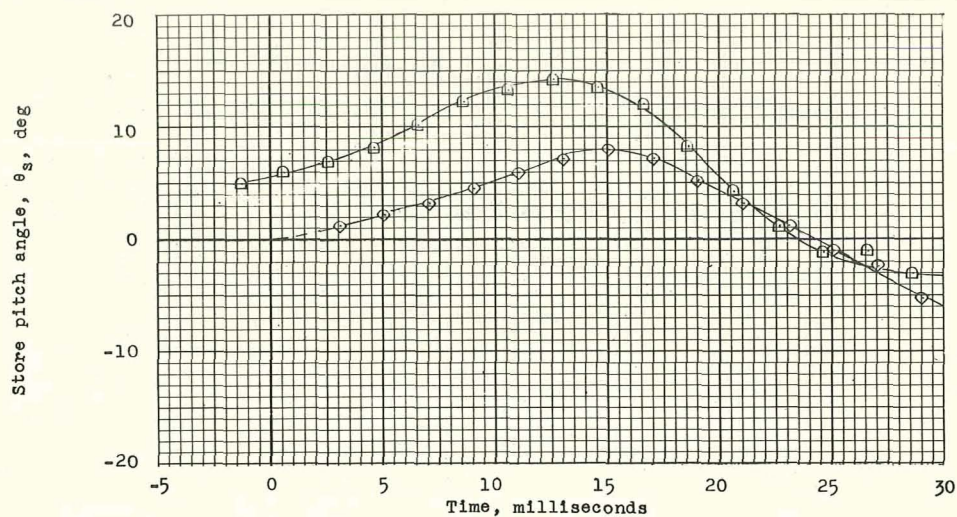


(a) Time history.

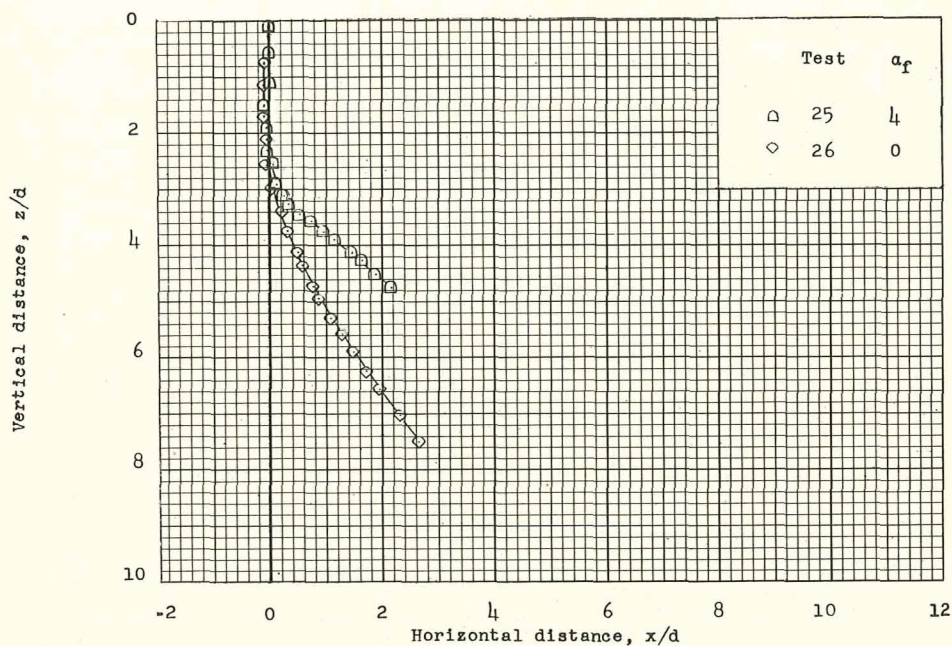


(b) Trajectory.

Figure 24.- Time history and trajectories for streamline store A with standard fins from a semisubmerged position with changes in ejection velocities. $M_0 = 1.39$; $h_p = 34,000$ feet.

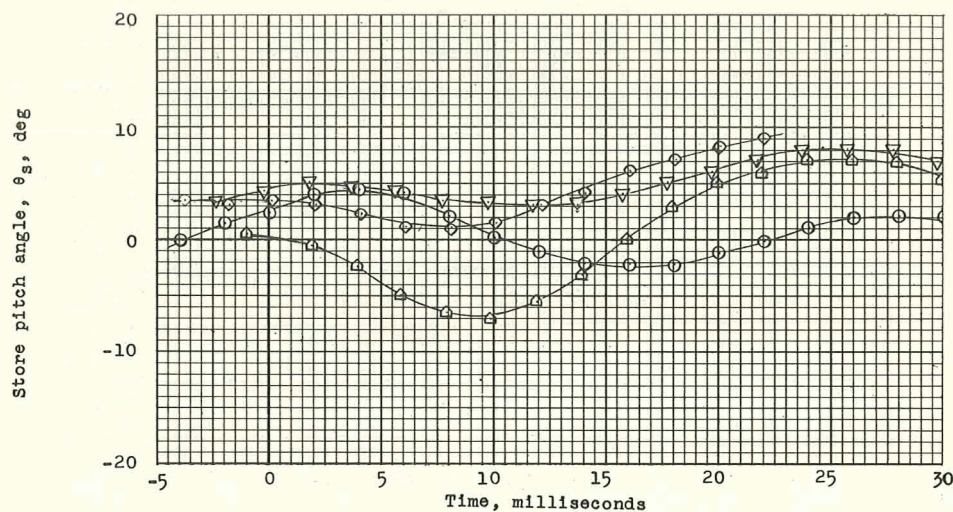


(a) Time history.

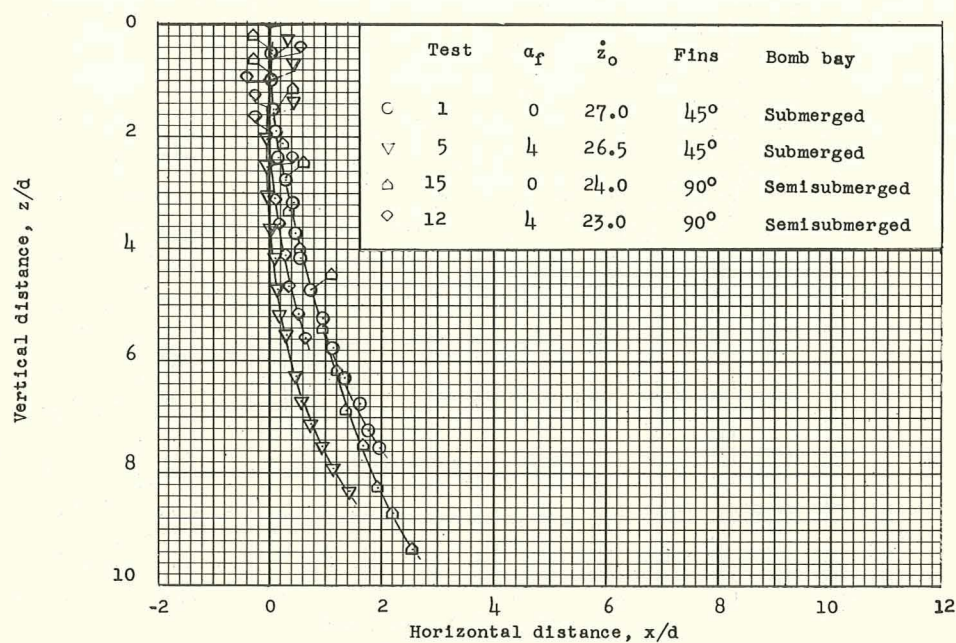


(b) Trajectory.

Figure 25.- Time history and trajectories for streamline store A with standard fins from a semisubmerged position. $M_0 = 1.98$; $h_p = 29,000$ feet; $\alpha_f = 0^\circ$ and $\alpha_f = 4^\circ$; and $\dot{z}_0 = 24.0$ feet per second.

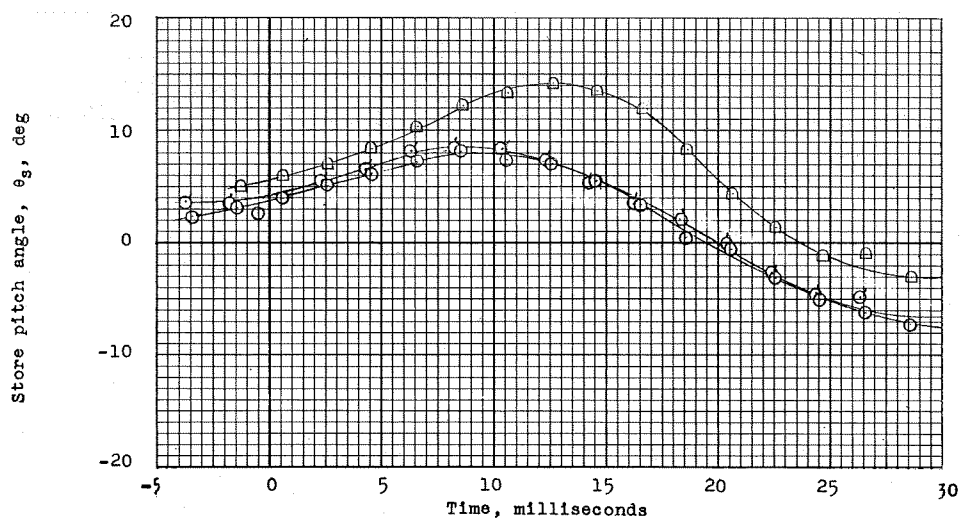


(a) Time history.

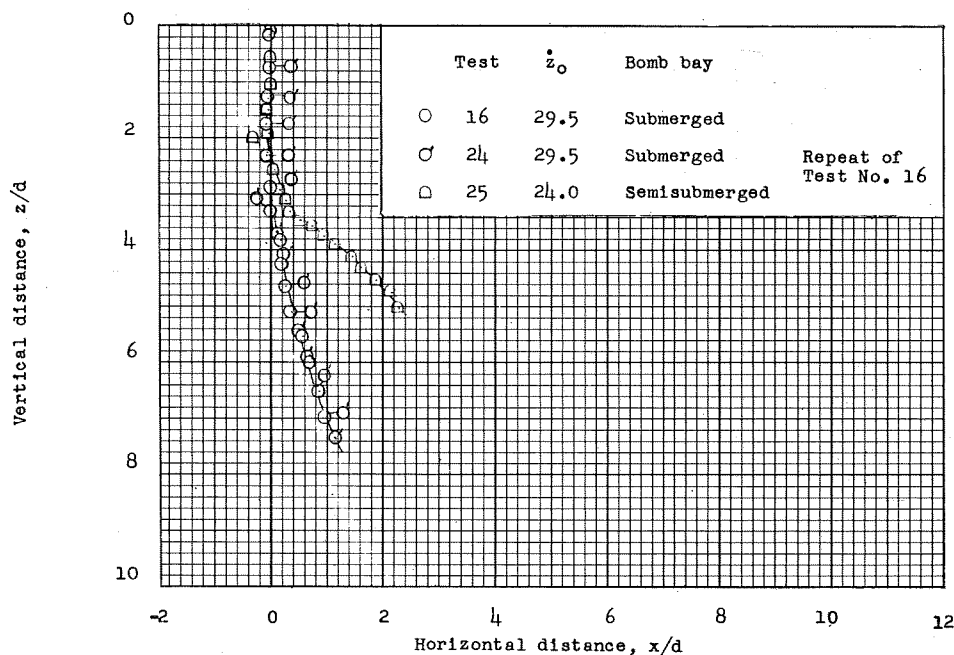


(b) Trajectory.

Figure 26.- Time history and trajectories for streamline store A with standard fins from submerged and semisubmerged positions. $M_0 = 1.39$; $h_p = 3,400$ feet; $\alpha_f = 0^\circ$ and $\alpha_f = 4^\circ$.

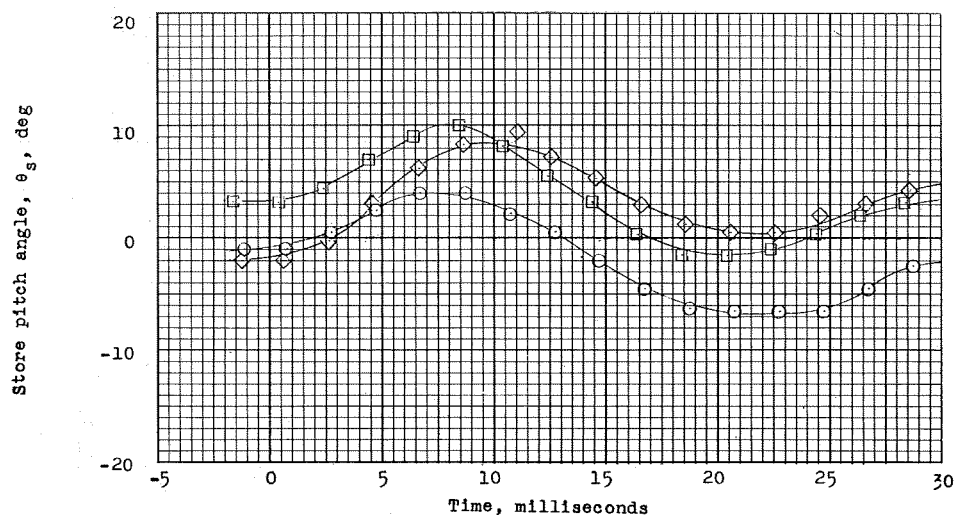


(a) Time history.

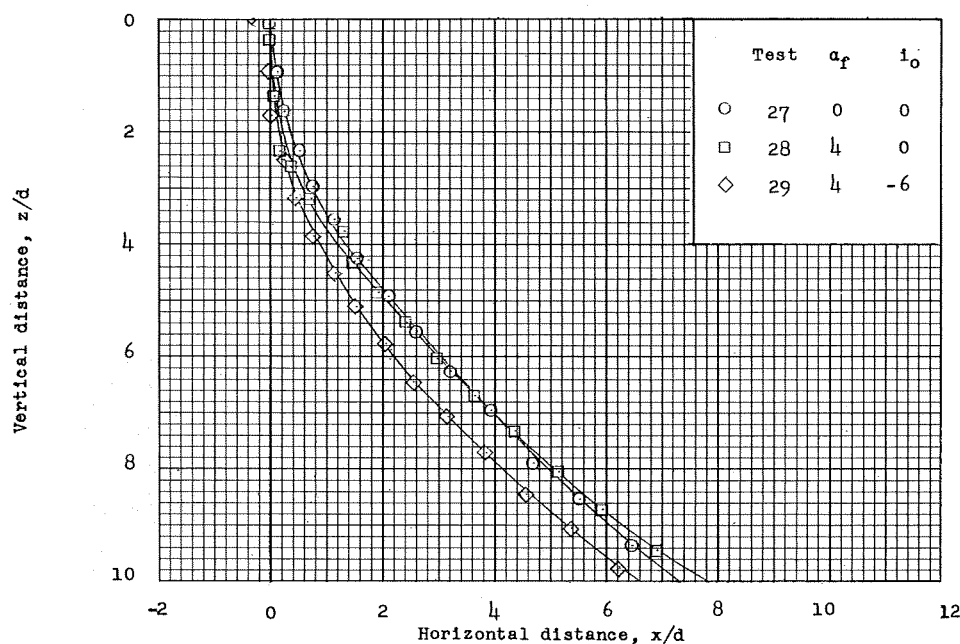


(b) Trajectory.

Figure 27.- Time history and trajectories for streamline store A with standard fins from submerged and semisubmerged positions. $M_0 = 1.98$; $h_p = 29,000$ feet; and $\alpha_f = 4^\circ$.

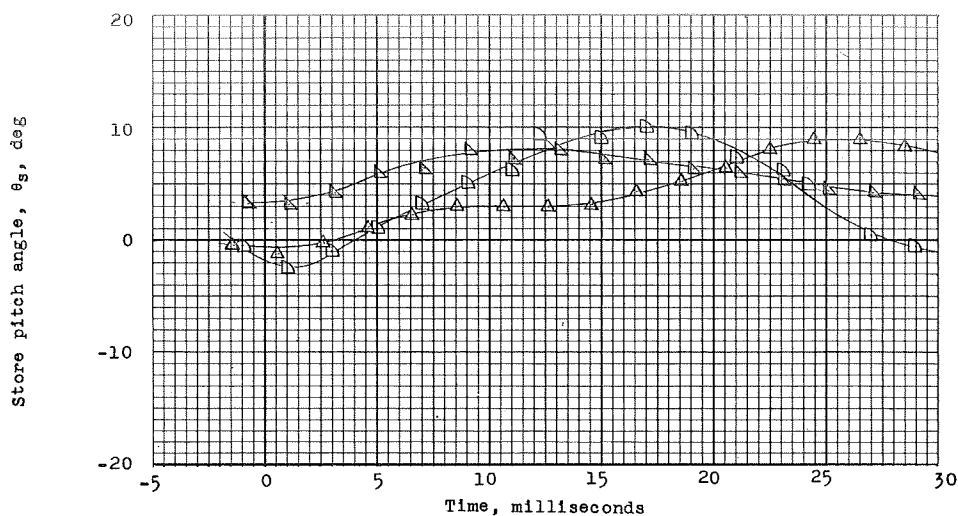


(a) Time history.

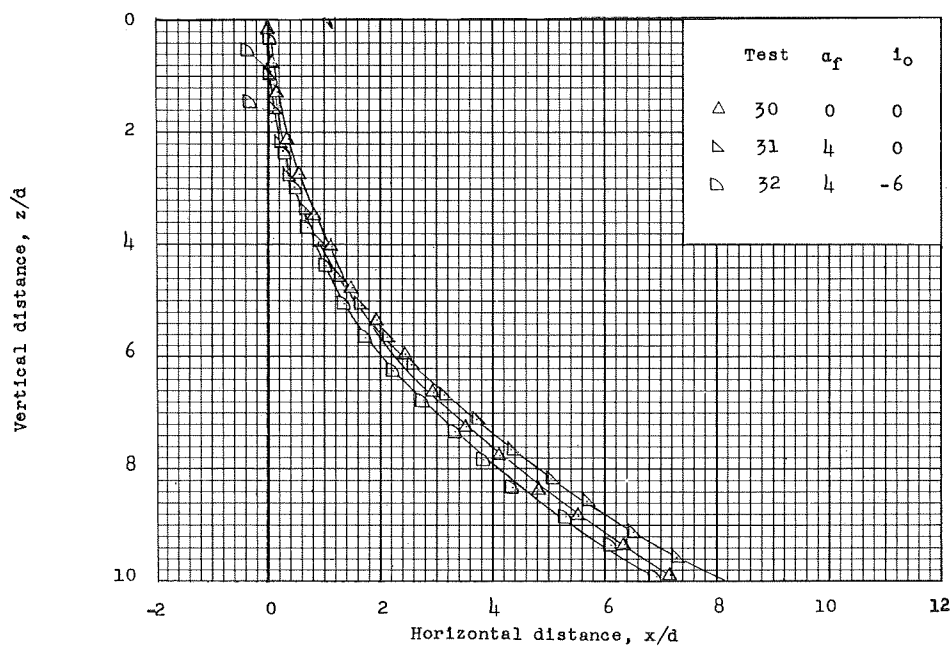


(b) Trajectory.

Figure 28.- Time history and trajectories with changes in fuselage angle of attack for blunt nose store B. $M_0 = 1.39$; $h_p = 3,400$ feet; and $\dot{z}_0 = 31.0$ feet per second.

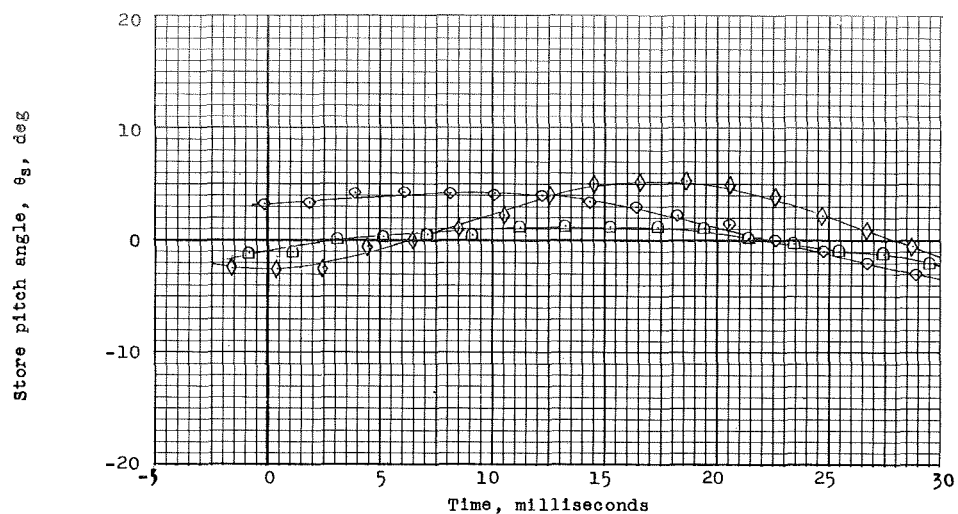


(a) Time history.

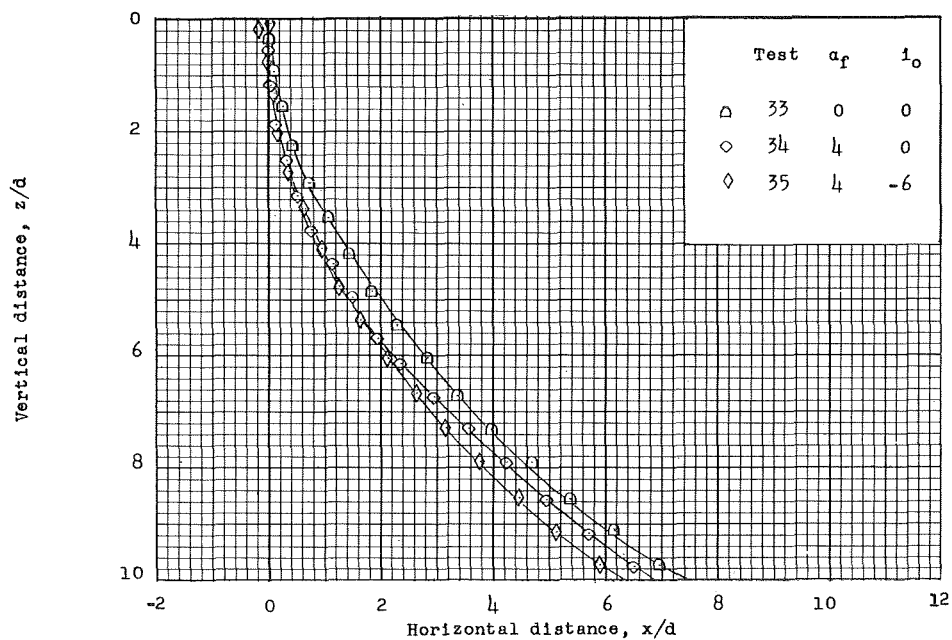


(b) Trajectory.

Figure 29.- Time history and trajectories with changes in fuselage angle of attack for blunt nose store B. $M_0 = 1.60$; $h_p = 16,400$ feet; and $\dot{z}_0 = 29.5$ feet per second.

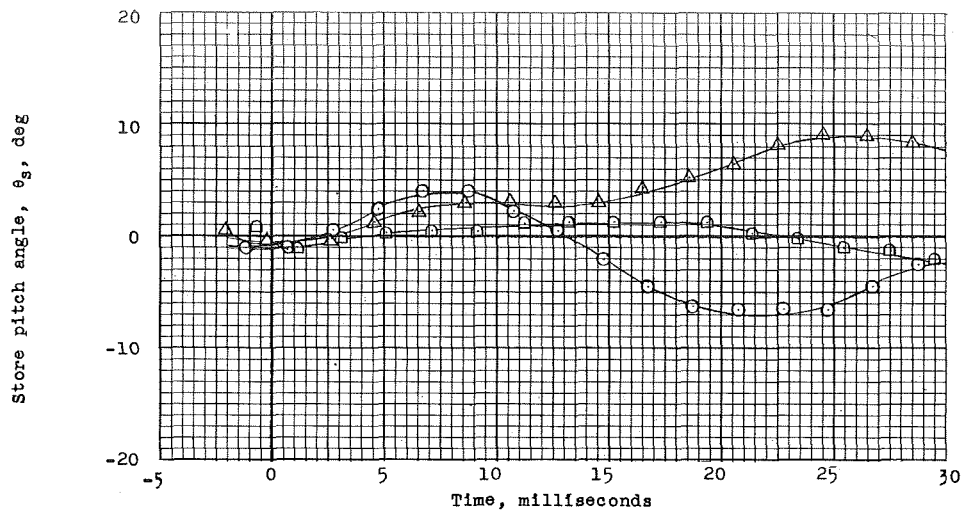


(a) Time history.

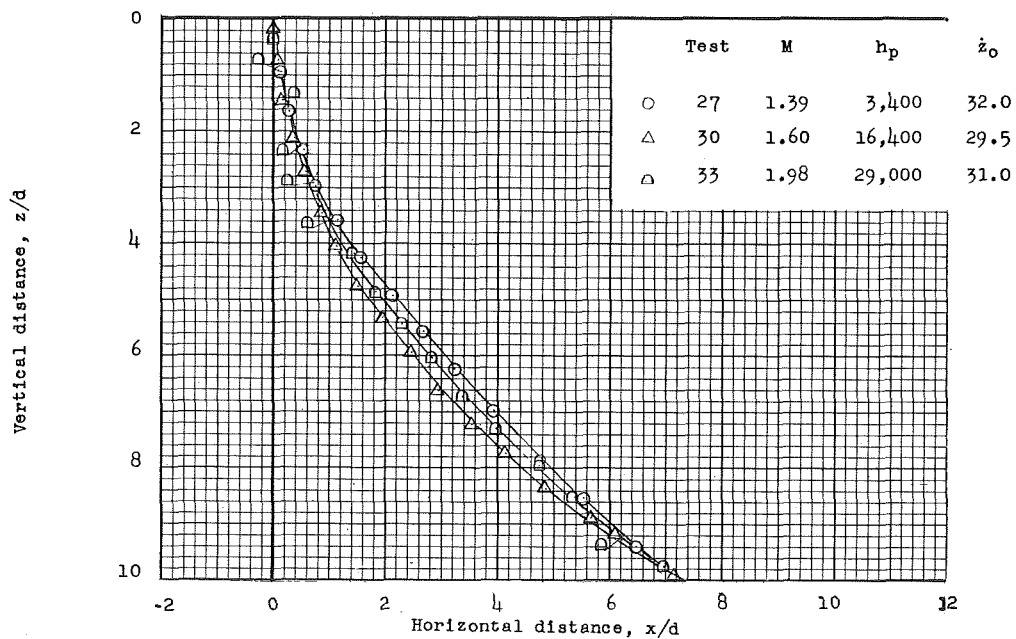


(b) Trajectory.

Figure 30.- Time history and trajectories with changes in fuselage angle of attack for blunt nose store B. $M_0 = 1.98$; $h_p = 29,000$ feet; and $\dot{z}_0 = 30.0$ feet per second.

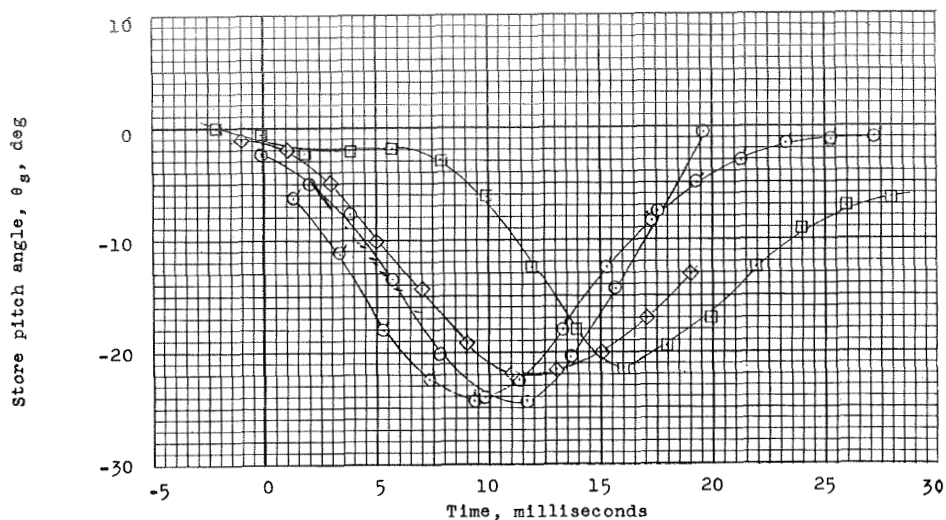


(a) Time history.

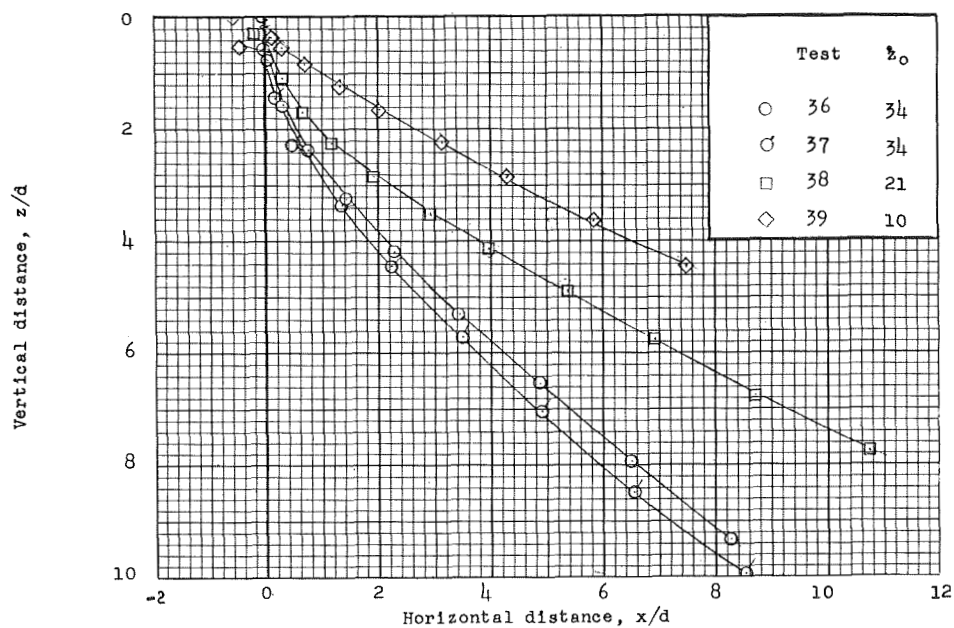


(b) Trajectory.

Figure 31.- Time history and trajectories for blunt nose store B.
 $M_0 = 1.39$, $M_0 = 1.60$, and $M_0 = 1.98$; $h_p = 3,400$ feet,
 $h_p = 16,400$ feet, and $h_p = 29,000$ feet, respectively; and
 $\alpha_f = 0^\circ$.

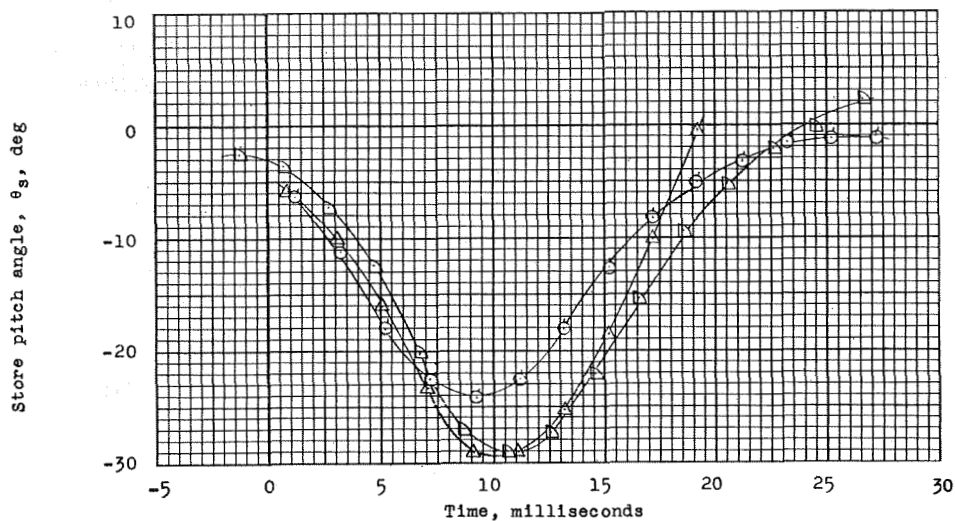


(a) Time history.

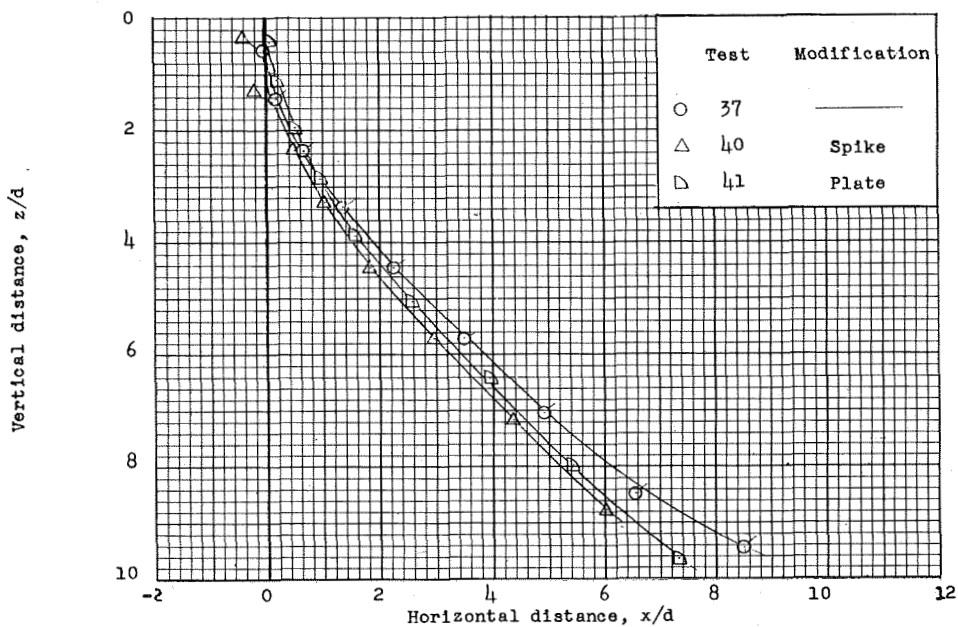


(b) Trajectory.

Figure 32.- Time history and trajectories with changes in ejection velocities for bluff store C. $l/d = 3.75$; $M_0 = 1.39$; $h_p = 3,400$ feet; and $\alpha_f = 0^\circ$.

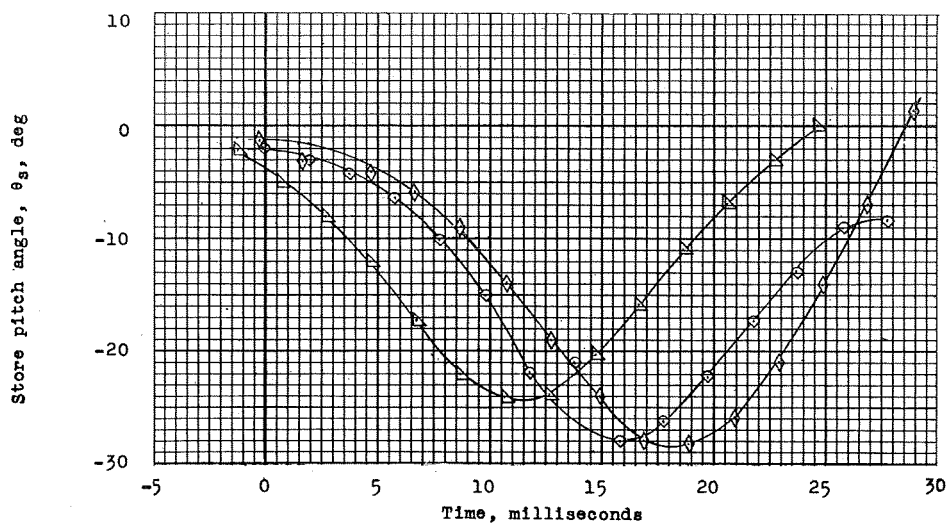


(a) Time history.

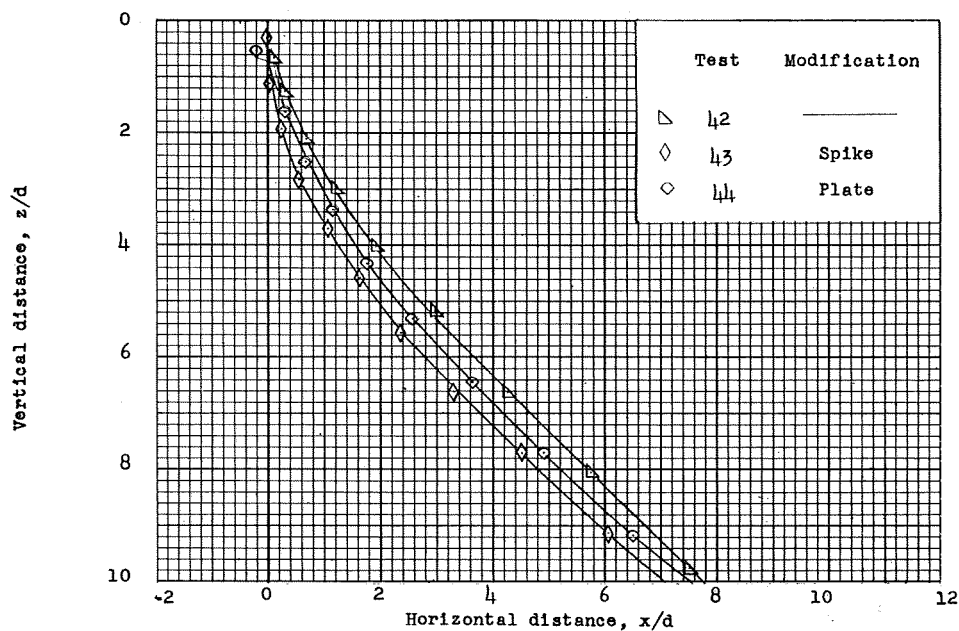


(b) Trajectory.

Figure 33.- Time history and trajectories for bluff store C with nose modifications. $l/d = 3.75$; $M_0 = 1.39$; $h_p = 3,400$ feet; $\dot{z}_0 = 34.0$ feet per second; and $\alpha_f = 0^\circ$.

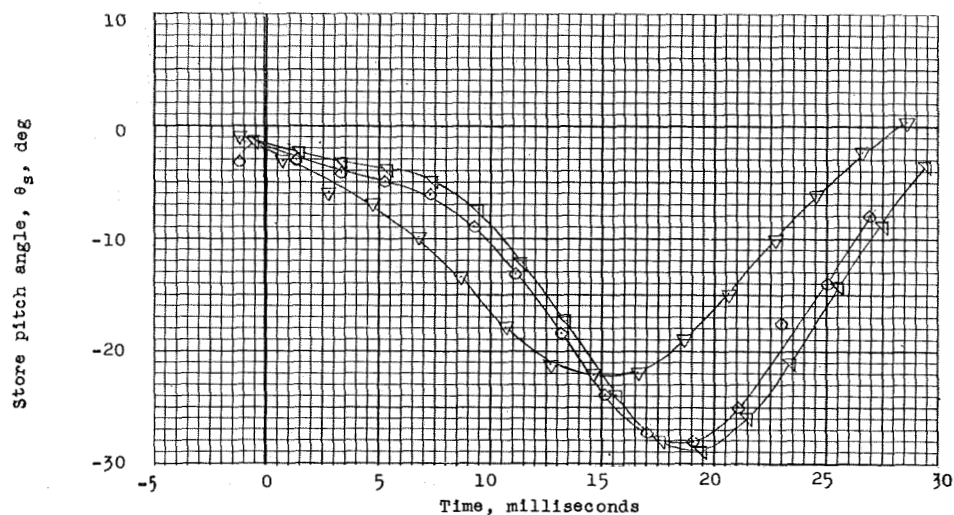


(a) Time history.

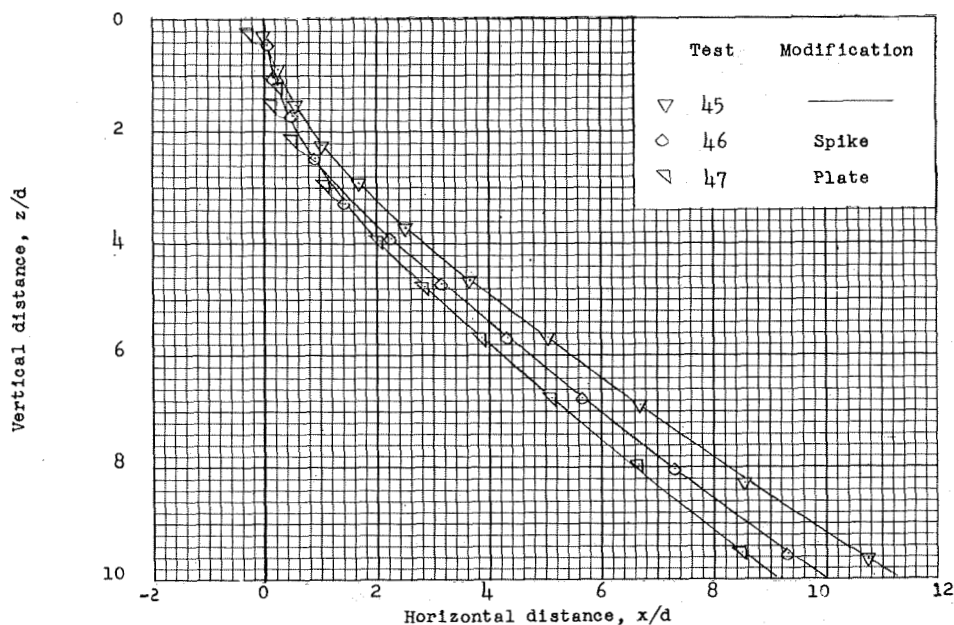


(b) Trajectory.

Figure 34.- Time history and trajectories for bluff store C with nose modifications. $l/d = 4.40$; $M_0 = 1.39$; $h_p = 3,400$ feet; $\dot{z}_0 = 34.0$ feet per second; and $\alpha_f = 0^\circ$.

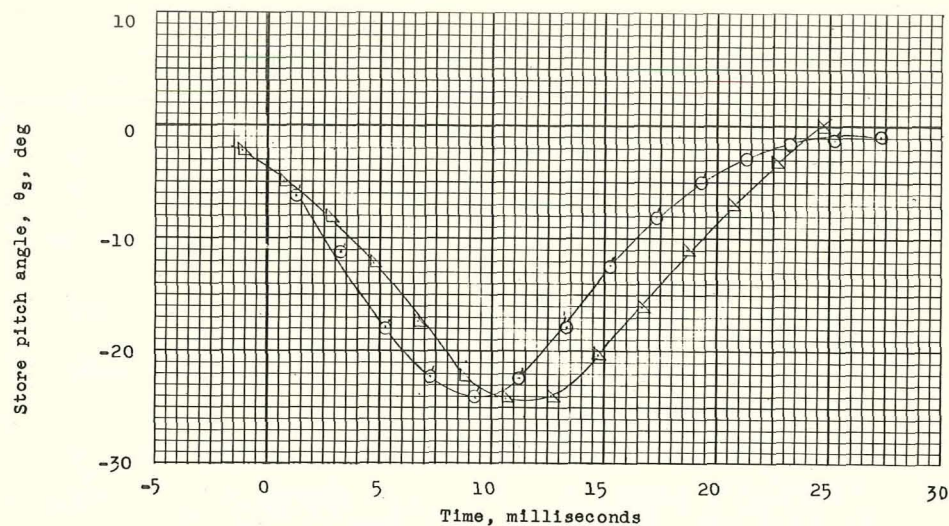


(a) Time history.

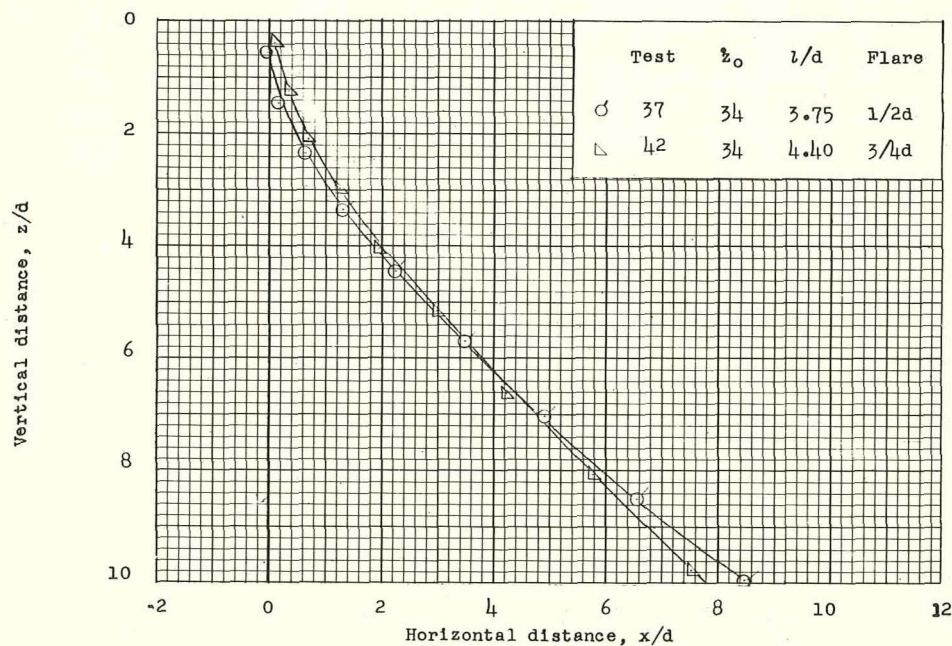


(b) Trajectory.

Figure 35.- Time history and trajectories for bluff store C with nose modifications. $l/d = 4.40$; $M_0 = 1.39$; $h_p = 3,400$ feet; $\dot{z}_0 = 26.0$ feet per second; and $\alpha_F = 0^\circ$.



(a) Time history.



(b) Trajectory.

Figure 36.- Time history and trajectories for bluff store C with changes in fineness ratio. $M_0 = 1.39$; $h_p = 3,400$ feet; and $\alpha_F = 0^\circ$.